IN SEARCH OF SUN: SOLAR PRETREATMENT TO ENHANCE THE BIOMETHANE POTENTIAL OF EMPTY FRUIT BUNCH (EFB) FIBRES

by

JULIA MC GREGOR

in partial fulfillment of the requirements for the degree of

Master of Science
in Environmental Engineering

at the Delft University of Technology,
to be defended publicly on Monday December 16, 2019

Supervisor:	Assis. Prof. dr. ir. Ralph Lindeboom
Thesis Committee :	Prof. dr. ir. Jules van Lier
	Assis. Prof. dr. ir. Ralph Lindeboom
	Assis. Prof. dr. H.Burak Eral
	Ir. Saqr Al-Muraisy

TU Delft Delft University of Technology

SUPERVISORS
Prof. dr. ir. Jules van Lier
Assis. Prof. dr. ir. Ralph Lindeboom
Assis. Prof. dr. H.Burak Eral
Ir. Saqr Al-Muraisy

LOCATION
Delft

THESIS DEFENCE
16 December 2019

ABSTRACT

In the past decades, fossil fuels have become an increasing concern, due them being a non-renewable energy source and due to the environmental concerns related to the production and use of this fuel. This has led to increasingly more research in the value of bio-sourced lignocellulosic biomass such as Empty Fruit Bunch (EFB) fibres from the palm oil industry. EFB fibres are a major by-product of the palm oil industry and globally, over 30 million tons are produced annually. Due to its biomass characteristic, it is a potential source of energy in processes such as anaerobic digestion, however, its complex structure results in poor biological degradation. A pretreatment such as a hydrothermal (HT) pretreatment can be used, to improve the biodegradability, prior to anaerobic digestion; however, this is an energy intensive process and has led to investigating the use of alternative energy sources for the pretreatment such as solar power. The geographical position of Malaysia is beneficial to make use of solar radiation as an alternative energy source. Concentrated Solar Power (CSP) is a technology that is gaining more interest as a way to convert solar radiation into usable energy and in particular the Fresnel lens. This research investigates if a Fresnel lens can be used to improve the biodegradability of the EFB fibres and analysed what effect this pretreatment has on the fibres (in terms of the solar radiation and the duration of exposure). Two conditions are investigated; wet (water and EFB fibre mixture) and dry conditions (dry fibres in an inert environment). These two pretreatments are compared to a conventional HT pretreatment in terms of the biodegradability based on the Biomethane Potential (BMP). From the experimental results, it was found that the Fresnel lens can achieve very high temperatures ($> 400^{o}C$) and possesses fast heating rates resulting in a predominantly photothermal pretreatment. The biodegradability of the EFB fibres (using the Fresnel lens) was significantly improved in comparison to the HT pretreatment under the wet conditions; however, based on the analytical methods used in this research, no conclusive explanation can be given to why the biodegradability increased. Possible explanations are increased available surface area and pore size, which will need to be further researched. The dry condition pretreatment was too inhomogeneous to observe a significant improvement in the biodegradability. However, based on the overall biodegradability and the structural changes observed in the EFB fibres, it is expected that with improved operating conditions that this pretreatment will also improve the biodegradability. Overall, based on this research, the CSP pretreatment has potential to be used as alternative to the conventional HT pretreatment and the surface area for the CSP required by this process is estimated to be 2% of the actual plantation size. Therefore, the CSP pretreatment has potential to be feasible in large-scale, however process efficiency needs to be improved due to the low efficiency of the lens and high energy requirements. Secondly, and most importantly, an economic analysis is crucial to validate the economic feasibility of implementing such a pretreatment.

ACKNOWLEDGEMENTS

Many people have been involved in helping me during the course of this research and this thesis would have not been possible without their help. I would like to take the time and space to thank a few people whose help and contribution were invaluable to the success of this thesis.

Firstly, I would like to thank my supervisor Ralph, who provided continuous support throughout this research. Through the challenges and frustrations of this thesis, he provided invaluable advice, encouragement and was always optimistic. I am grateful to have had Ralph as my main supervisor. I would also like to thank the rest of my committee Jules, Burak and Saqr for their comments, criticism and advice which has helped tremendously to develop this thesis.

I would like to thank Magnolia and Laís, for always being willing to help me in the lab, providing endless advice to improve my research and support through the many challenges. I would not have been able to finish my thesis in 9 months without their help. I would like to thank Chantal for the many training runs that involved endless discussions on my thesis topic, for all your positivity and support through the challenges and for making my stay in Delft so enjoyable. I would also like to thank my friends Didier, Dave, Fabian, Alessandro and the rest of the 'FAC' group for the endless support, thesis discussions, cookie breaks and for making this journey so much more memorable.

Lastly and most importantly I would like to thank my family and Tom, for their incredible love, support and belief in me throughout this journey and for being there for me in all the highs and lows. I especially would like to thank my parents, because I would not be here without them and they have always provided unconditional support for me to pursue my dreams.

CONTENTS

LIST OF FIGURES

LIST OF TABLES

ABBREVIATIONS AND ACRONYMS

AD	Anaerobic Digestion
avg	averaged results
BMP	Biomethane Potential
Control-H	Wet experimental condition untreated sample - HT scale
Control-h	Wet experimental condition untreated sample - PLA scale
CSP	Concentrated Solar Power
CSP-H	CSP wet experimental condition pretreatment - HT scale
CSP-N	CSP dry experimental condition pretreatment - HT scale
CSPL-H	CSP wet experimental condition pretreatment- PLA scale
CSPL-N	CSP dry experimental condition pretreatment- PLA scale
EFB	Empty Fruit Bunch/ Empty Fruit Bunches
FTIR	Fourier Transform Infrared Spectroscopy
HPLC	High-performance liquid chromatography
HT	Hydrothermal pretreatment
IR	Infrared wavelength
IR-H	IR wavelength, wet experimental condition pretreatment
IR-N	IR wavelength, dry experimental condition pretreatment
LCC	Lignin-Carbohydrate Complexes
MF	Mesocarp Fibres
OPF	Oil Palm Fronds
OPL	Oil Palm Leaves
OPT	Oil Palm Trunks
OPW	Oil Palm Waste
PLA	Pulsed Laser Ablation
POME	Palm Oil Mill Effluent
UV	Ultraviolet wavelength
UV-H	UV wavelength, wet experimental condition pretreatment
UV-N	UV wavelength, dry experimental condition pretreatment
VIS	VIS wavelength
VIS-H	VIS wavelength, wet experimental condition pretreatment
VIS-N	VIS wavelength, dry experimental condition pretreatment

1 INTRODUCTION

In the last decades, fossil fuels have become an increased concern, not only due to depletion of this valuable resource but also due to the environmental concerns related to the production and use of this fuel. This is slowly driving the world to use more sustainable forms of energy such as wind, solar and bio-fuels, which has progressively led to more research in the value of bio-sourced lignocellulosic biomass from the agro-industry, such as the palm oil industry. This is mainly due to it being inexpensive, readily available and renewable [Anwar et al., 2014]. In order to make full use of the potential of fuel from lignocellulosic biomass it requires pretreatment to be converted into liquid bio-based energy fuels due to its recalcitrant properties [Anwar et al., 2014].

In particular, the palm oil industry is largely under public scrutiny in the recent years due to its environmental impacts. Globally it is a controversial issue because on the one side, oil palm is a very efficient crop with the highest yields of all the vegetable oils[Ritschel, 2018] . However, on the other, the palm oil industry has resulted in deforestation, biodiversity loss, greenhouse gas emissions and pollution of water resources. Therefore, there is a dire need for improving the sustainability of this industry. Palm Oil Mill Effluent (POME) and Empty Fruit Bunches (EFB) are major by-products of this industry that have potential to be very valuable in terms of energy production due to their organic nature[Ritschel, 2018]. In Malaysia itself, 39% of the world palm oil is produced and world exports account for 44% [MPOC, 2012]. In 2018, around 19.5 million tonnes of crude palm oil were produced in Malaysia alone and for every ton of palm oil produced there are 2.5 tons of POME and 1.5 tons of EFB produced [Chin et al., 2015; Hosseini et al., 2015; MPOB, 2018]. In a study done by Chin et al. [2013], it was estimated that the methane production from POME is about $10 kg/m^3$. The other by-product of this industry, EFB, was usually burnt, however this has been banned due to the air pollution effects. Due to its biomass characteristic it is a potential valuable source of energy too.

EFB is characterised as a non-woody lignocellulosic biomass that primarily consists of cellulose, hemicellulose and lignin. Due to its complex structure of lignin, it is classified as a highly resistant and recalcitrant biomass structure, which means both chemical and biological degradation is difficult [Geng, 2013]. Anaerobic digestion (AD) is defined as the process by which organic material such as lignocellulosic biomass is degraded by microbes in an oxygen free environment [Fitzgerald, 2013]; the resultant products are biogas and a solid digestate. Hydrolysis, is the first step of AD and results in the degradation of macromolecules into compounds such as sugars and long chain fatty acids [Ersahin et al., 2011]. The hydrolysis of solids in AD with suspended organic materials is normally considered to be the rate-limiting step [Pavlostathis and Giraldo-Gomez, 1991]. Therefore, in order to improve the biodegradability of the EFB, pretreatment is essential. The pretreatment would result in the hemicellulose and cellulose components being more accessible to the hydrolysis enzymes in AD and result in reactive cellulosic intermediates [Qian, 2014]. Thereafter, the pretreated biomass could be anaerobically digested, or alternatively, be converted into other high value products such as chemicals or biomaterial. Thus, pretreatment has various applications in the industrial use of lignocellulosic biomass.

Hydrothermal Treatment (HT) is a method that primarily utilizes water either as a liquid or vapour at high temperatures which can efficiently convert biomass

to be more easily digested by enzymes. HT facilitates autohydrolysis reactions with the biomass [Ewanick and Bura, 2010]. In particular, using liquid water has been found to be more environmentally friendly as a phase change is not required and no chemicals are required. A study done by O-Thong et al. [2012], found that hydrothermal pretreating EFB resulted in a 40% increase in the methane production when co-digesting it with POME in comparison to using raw EFB. However, this treatment method requires energy for the heating of the treatment.

Malaysia has potential to make use of solar radiation due to its geographical position. Solar radiation energy in Malaysia ranges from 4-5$kWh/m^2 \cdot day$, which is high when comparing it to the highest solar radiation on earth being up to 6.8$kWh/m^2 \cdot day$ [Arief et al., 2016; Rhino, 2016]. Therefore, using solar power as an energy source in Malaysia is promising. Concentrated Solar Power (CSP) is a technology that is gaining more interest as a way to convert sunlight into usable energy. A CSP system uses either lenses or mirrors in combination with a tracking system to focus a large area of sunlight into a small beam of light [Zhu, 2015]. The main application for this CSP system has been in solar thermal power systems, however solar thermochemical processes are also promising for solar fuel production [Zhang et al., 2013; Chuayboon et al., 2018]. Fresnel lenses have become one of the top contenders in the field of concentrated solar energy applications. This is due to their light-weight and small volume properties, furthermore they are mass produced at a low cost and are able to effectively increase the energy density [Xie et al., 2011].

This research paper investigates whether a Fresnel lens can be used to improve the biodegradability of the EFB fibres. The aim of using this CSP technology is that it would not only provide the necessary energy but that the solar radiation may also influence the pretreatment. Two conditions are investigated; wet (water and EFB fibre mixture) and dry conditions (dry fibres in an inert environment). Dry conditions are investigated as solar gasification is also a promising route for utilising energy from biomass and partial gasification of the fibres could be a potential pretreatment. These two pretreatments are compared to a conventional HT pretreatment in terms of the biodegradability based on the Biomethane Potential (BMP). In order to assess the effect of radiation on the fibres, Pulsed Laser Ablation (PLA) experiments are performed. In the PLA experiments, the effect of ultraviolet (UV), visible (VIS) and infrared radiation (IR) on the EFB fibres are investigated to determine the influence of the three wavelengths on the fibre pretreatment independently.

2 LITERATURE

2.1 PALM OIL WASTE

Oil palm (*Elaeis guineensis*) is grown widely in many tropical regions of South-east Asia, in particular in Malaysia and Indonesia and is mainly used to produce vegetable oil. One of the advantages of oil palm is that it produces the highest oil yield out of all the plant-based oils such as sunflower and rapeseed oil.[Chang, 2014] The palm oil industry also plays an important role in the economy of Malaysia and in 2011 this sector was the fourth largest contributor to Malaysia's economy [May, 2012].

One of the major drawbacks of the palm oil industry is the considerable amount of biomass waste produced in the production of palm oil. Globally, it is estimated that the palm oil industry generates over 190 million tons of waste in the form of liquid and solid residues and only about 10% is utilized commercially for value-added bio-products such as bio-fertilisers [Lee and Ofori-Boateng, 2013]. For a hectare of cultivated land, this industry generates more than 100 tonnes of oil palm waste (OPW) every year [Hosseini et al., 2015; Chin et al., 2015]. The waste includes POME, EFB, Palm Kernel Shell (PKS), Mesocarp Fibre (MF), Oil Palm Trunks (OPT), Oil Palm Leaves (OPL) and Oil Palm Fronds (OPF) [Awalludin et al., 2015]. All this waste has a high fibre content, except for POME.

2.1.1 Empty Fruit Bunch Fibres

EFB is the largest amount of solid waste that is generated during the palm oil production process [Lee and Ofori-Boateng, 2013]. The moisture content of EFB is 60-75% and due to this high water content, EFB is hardly utilized as boiler fuels in palm oil mills [Lee and Ofori-Boateng, 2013; O-Thong et al., 2012]. In the past, the most conventional method for the EFB treatment process was the direct burning of EFB for power and steam utilization in simple incinerators, furthermore the ash was used as a fertiliser for the plantation. This treatment process has now been banned in Malaysia due to the resultant air pollution produced, and no energy was being recovered using this treatment method. [Abdullah and Sulaiman, 2013] Current methods of disposal include using EFB as mulch on the plantation itself or being sold to settlers [Bong et al., 2017; Abdullah and Sulaiman, 2013]. There are contrasting opinions of whether mulching is beneficial to the environment as some plantation owners claim it is beneficial to use as a fertiliser and for soil conditioning; however, it has also been mentioned that the remnant oil on the EFB contributes to environmental pollution, in particular oil spills [Abdullah and Sulaiman, 2013]. However, most of the EFB is dumped in open dump sites and not disposed of [Bong et al., 2017].

EFB is composed of 23.7 – 65% cellulose, 20.6 – 33.5% hemicellulose and 14.1 – 30.5% lignin [Chang, 2014]. Lignin is a complex, three-dimensional, amorphous compound and the product of aromatic alcohols known as monolignols [Janusz et al., 2017]. The complexity and insolubility of lignin results in it being resistant to degradation by most microorganisms. Cellulose is a complex polysaccharides and is formed by long linear chains of D-glucose units that are linked by β-(1,4)-glycosidic bonds [Abhilash and Thomas, 2017; Janusz et al., 2017]. The hydrolysis

of cellulose results in oligosaccharides such as glucose or disaccharides such as cellobiose [Huang and Fu, 2013]. Hemicellulose is similar to cellulose but is made up of smaller chains that have branches with short lateral chains [Abhilash and Thomas, 2017]. Hemicellulose contains multiple types of sugar units, unlike cellulose, and these are linked with a variety of glycosidic bonds in one molecule. Hemicellulose also is linked to cellulose through hydrogen bonds and is covalently bonded with lignin. [Shrotri et al., 2017].

Lignin is linked to carbohydrates by linkages such as benzyl ether and benzyl esters. There are also other chemical bonds such as phenyl glycosidic and acetal linkages that perform the same role of linking lignin with cellulose and hemicellulose; these complex bonds form the lignin-carbohydrate complexes (LCCs) and result in an obstacle in the biodegradation of biomass.[Achyuthan et al., 2010] This complex lignocellulosic composition results in EFB fibres being recalcitrant to bio- and physico-chemical conversions [Geng, 2013]. Therefore, in order to improve the degradation of EFB to convert them into bio-fuels, pretreatments are introduced to break the lignin seal and disrupt the crystalline structure.

2.2 PRETREATMENT METHODS FOR ENHANCED ANAEROBIC DIGESTION

Anaerobic digestion (AD) is defined by four processes, namely: hydrolysis, acidogenesis, acetogenesis and methanogenesis [Zheng et al., 2014]. It is commonly considered that the rate-limiting step in the AD process is methanogenesis; it is believed to have the slowest growth rate and is the most sensitive to changes in the environment. However, in the degradation of recalcitrant solid materials, such as lignocellulosic biomass, hydrolysis is considered to be the rate limiting step [Cirne et al., 2007]. Therefore, a pretreatment step before AD is advised in order to increase the biomass degradation and biogas yield. Different pretreatments have different degrees of impacts on the biodegradability of the lignocellulosic biomass. The pretreatment aims to reduce the structural and compositional barriers of lignocellulosic biomass and to expose the polymer chains of hemicellulose and cellulose to microbial degradation [Alvira et al., 2010]. Furthermore, some methods include the enzymatic hydrolysis of hemicellulose into its sugar components, partial degradation of lignin and hydration of cellulose [Zheng et al., 2014].

2.2.1 Hydrothermal (HT) Pretreatment

In principle, liquid hydrothermal treatments are operated at relatively high temperatures $(160^oC - 240^oC)$ and pressurised to ensure the water remains liquid[Alvira et al., 2010]. Autoionization of the water occurs as a result of the increased temperature and generates hydrogen ions which act as an acid catalyst for the hydrolysis of the lignocellulosic biomass [Garrote et al., 1999]. This results in a slightly acidic liquid hydrolysate. The main objective of liquid hot water hydrothermal treatment is to predominantly solubilise the hemicellulose, resulting in cellulose being more accessible in the AD and to minimise the formation of inhibitors [Alvira et al., 2010]. The hemicellulose polysaccharides are hydrolysed into oligomers and monomers. The correspondent sugars (pentoses and hexoses) can be further dehydrated to produced furfural and hydroxymethylfurfural (HMF), respectively [Zheng et al., 2014]. Usually this occurs under the acidic conditions due to the autoionization of water lowering the pH.

Furfural and HMF are inhibitory substances depending on their concentration for the anaerobic step [Jönsson and Martín, 2016]; therefore, the production of these compounds is an important factor to take into consideration in the pretreatment.

Lignin degradation produces these AD inhibitory phenolic compounds; however, an advantage of liquid hot water is that these products are present in lower concentration than for a steam HT pretreatment [Alvira et al., 2010]. Thus, the risk of degradation inhibition products such as furfural and the condensation and precipitation of lignin compounds is reduced [Zheng et al., 2014]. Furthermore, corrosive-resistant materials are not required for the reactor as no chemicals are used. HT has also been known to be highly effective for increasing the surface area of cellulose (through nonchemical swelling) and increasing access to the cellulose.

2.2.2 Concentrated Solar Power (CSP) Pretreatment

Solar energy is a widely available carbon-neutral energy source that can be used as an energy source for applications such as high-temperature reactions for gasification by using CSP. The working principle of CSP is to concentrate direct beam solar radiation using a combination of mirrors or lenses onto a small area [Bassam et al., 2013]. This concentrated beam is used to produce useful energy such as heat, electricity or fuels using various downstream processing technologies following the concentration of the solar radiation [Lovegrove and Csiro, 2012]. Solar concentrators are classified into two classes based on their optical design and imagining properties: imaging and nonimaging concentrators. Imaging concentrators are generally not ideal while nonimaging devices can be ideal. An ideal concentrator has the potential to approach the thermodynamic limit of concentration based the geometric design; this means that the absorber will either be or exceed the sun's temperature of $5777K$. [Leutz and Suzuki, 2001]

The Fresnel lens

Fresnel lenses are classified as nonimaging devices and have become one of the top contenders in the field of concentrated solar energy applications. This is due to their light-weight and small volume properties, furthermore they are mass produced at a low cost and are able to effectively increase the energy density [Xie et al., 2011]. A Fresnel lens is made up of a chain of refractive prisms that are etched into a surface as seen in Figure 2.1 [Leutz and Suzuki, 2001]. The basic working principle of a linear Fresnel lens is that it refracts the solar radiation to focus onto a point due to the series of concentric circular grooves on the lens [Pham et al., 2017]. This results in a rapid increase in temperature at that concentrated point.

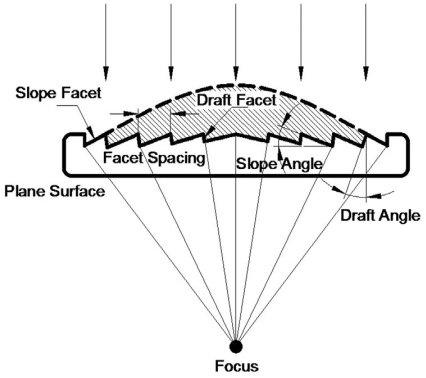

Figure 2.1: Design of a Fresnel lens (Figure obtained from Kumar et al. [2015])

The geometric concentration ratio C and the optical efficiency η are the two common properties that describe solar concentrators [Leutz and Suzuki, 2001]. The concentration ratio, is a ratio of the concentrator (S_1) and radiation receiver (S_2) aperture areas (in m^2). The optical efficiency is defined as the fraction of radiative

energy that is received by the radiation receiver (Φ_2) with respect to to the initial radiative energy input (Φ_1) (in Watt). These two equations are given by

$$C = \frac{S_1}{S_2} \tag{2.1}$$

$$\eta = \frac{\Phi_2}{\Phi_1}, \tag{2.2}$$

respectively. Leutz and Suzuki [2001] describes that the efficiency of the lens is given by the optical concentration ratio and this given by

$$\eta_C = \frac{\frac{\Phi_2}{S_2}}{\frac{\Phi_1}{S_1}} = \eta C \tag{2.3}$$

If there are no optical losses of the lens ($\eta = 1$), then the optical concentration ratio is equal to geometric concentration. The thermodynamic limit of the geometric concentration ratio of a three-dimensional lens was determined to be 43 400 Leutz and Suzuki [2001]. The maximum temperature (assuming no heat loss from the absorber) of an absorber under the sun can be calculated from the actual concentration ratio of the concentrator as follows:

$$T_{abs,max} = T_{sun} \sqrt[4]{\frac{C}{C_{max}}} \tag{2.4}$$

However, in reality there are losses experienced by the lenses such as reflection losses, absorption losses and geometric losses. The material is also an important aspect to consider in the design of the Fresnel lens. The concentration factor for Fresnel lenses usually range from 350 to 500 [Hirn, 2014]. A low cost material that is used for the lens in polymethylmethacrylate (PMMA) and its optical characteristics are very similar to glass [Xie et al., 2011]. A standard PMMA has a high transmission rate over the bandwidth of 350 to about 1100nm, thereafter the transmission rate decreases [Kumar et al., 2015; Leutz and Suzuki, 2001]. A lower bandwidth can be transmitted with a UV-enhanced PMMA lens.

2.2.3 Torrefaction (mild pyrolysis) Pretreatment

Torrefaction, also known as mild pyrolysis, is defined as a thermochemical process that is used to transform biomass into a more energy dense product for further processing such as gasification or in this research for improved anaerobic digestion [Gent et al., 2017; Shankar Tumuluru et al., 2011]. This process occurs in an inert environment and over a relatively low temperature range of $225 - 300^oC$ [Bergman et al., 2005]. It is characterised by low particle heating rates ($< 50^oC/min$), long residence times and the biomass partially decomposes during the process [Bergman and Kiel, 2005]. In general, about 30% of the solid biomass is converted into torrefaction gases and only 10% of the energy is lost with these gases, which results in an energy densification [Bergman et al., 2005].

Mechanism of the torrefaction of biomass

There are various reactions that occur during torrefaction and these can be defined by different reaction pathways [Bergman et al., 2005]. These reaction pathways are grouped in a few main reaction regimes and are given in Figure 2.2. The exact temperatures depend on the type and the properties of the lignocellulosic biomass.

For all three components of lignocellulosic biomass, similar decomposition regimes are identified. The most thermostable of the three components is cellulose, with

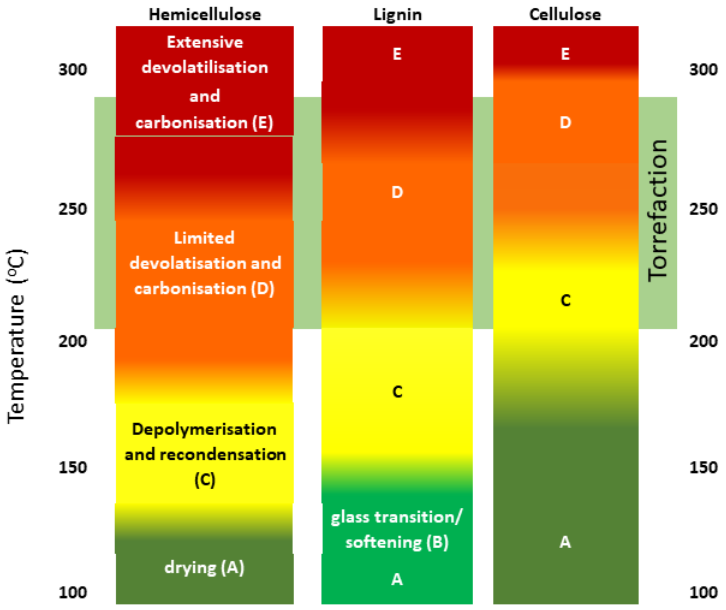

Figure 2.2: Main physico-chemical phenomena during the torrefaction of biomass (adapted from Bergman et al. [2005])

hemicellulose being the most reactive. Physical drying of the biomass occurs in temperature region A. There is also softening of lignin in the glass transition temperature range (B). The glass transition temperature is a temperature range at which amorphous polymers exhibits changes in viscoelastic behaviour [Irvine, 1985]. This results in a decrease in the stiffness of lignin and rubber-like elasticity. Depolymerisation occurs when the temperature is increased to region C, this region is also known as the reactive drying range [Shankar Tumuluru et al., 2011]. Carbon and hydrogen bonds begin to break and the shortened polymers recondense within the solid biomass [Bergman et al., 2005]. Destructive drying (region D) occurs with a further increase in the temperature. This results in limited devolatilisation and carbonisation of the solid structures and polymers formed in region C. A further increase in temperature (region E), results in extensive devolatilisation and carbonisation of the solid structure.

The torrefaction process is also split into a low ($< 250^{o}C$) and high temperature ($> 250^{o}C$) process. In the low temperature process, the mass loss is predominantly due to decomposition of hemicellulose via process D. However, in the high temperature process, lignin and cellulose also contribute to the mass loss through process D. The decomposition reactions for biomass for different temperature ranges is given in Figure 2.3

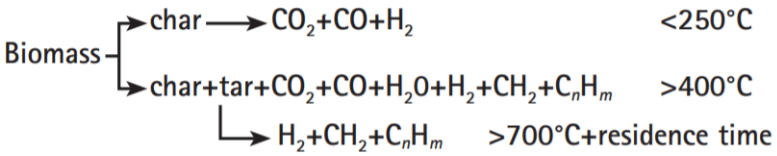

Figure 2.3: Decomposition reactions for biomass over different temperature ranges [Wang et al., 2011]

Torrefaction results in the disruption of the inter- and intramolecular hydrogen bonds, *C-O* and *C-C* bonds [Shankar Tumuluru et al., 2011]. This results in the

formation of compounds such as carboxylic acids, alcohols, hydrophilic extractives and gas such as CO, CO_2, CH_4 and even small traces of H_2. Hemicellulose generally decomposes into light volatiles whilst the degradation of cellulose results in anhydrous cellulose and levoglucosan. The decomposition of lignin results in the production of phenols (due to the cleavage of ether bonds) and converts into char more than hemicellulose and cellulose. The remaining solid biomass is described by Bergman et al. [2005] as "a chaotic structure of the original sugar structures and reaction products". This remaining solid biomass is also hydrophobic due to the loss of the OH functional group [Bergman and Kiel, 2005].

2.3 PULSED LASER ABLATION (PLA)

Pulsed lasers processing of materials is an emerging technology and has the capability to ablate materials precisely with little or no collateral damage [Shirk and Molian, 1998]. Laser ablation can be used for selectively isolating and volatilizing plant tissue within the same plant material. Additionally, the laser results in rapid heating rates at small specific areas resulting in uniform heating [Mukarakate et al., 2011]. This means that the selected area achieves the desired final temperature before sample degradation occurs.

The principle of PLA is that an intense burst of energy is delivered to a sample material by a short laser pulse for the removal of a portion of the material [Russo et al., 2002]. The ablation rate refers to the rate at which this removal is achieved and is affected by the laser wavelength and in general, a shorter laser wavelength results in a higher ablation rate and a lower fractionation. This is because a shorter wavelength has higher photon energy which results in more efficient bond breaking and ionization of the material sample [Russo et al., 2002].

Two different mechanisms can occur depending on the wavelength, these are either thermal (photothermal) and/or non-thermal (photochemical) [Russo et al., 2002]. The thermal mechanism refers to the laser light being transferred into energy and subsequently melting and vaporization of the target material occurs. The photochemical mechanism refers to the breaking of the atomic lattice through inducing ion and atom ejection without the heating effects due to the photon energy being higher than the bonding energy between neighbouring atoms on the material [Russo et al., 2002].

Photochemical reactions are dependant on the bond dissociation energies. Weak bonds have a bond strength of $<3eV \cdot bond^{-1}$, whilst main valence bonds have a bond strength from about 3 to $6eV \cdot bond^{-1}$ [Zumdahl et al., 2016; Ranby and Rabek, 1989]. The photon energy for wavelengths 200nm to 800nm ranges from 6.2 to $1.55eV \cdot photon^{-1}$ respectively. Therefore, theoretically, UV and VIS radiation can cause bond dissociation. However, not all bonds absorb UV and VIS radiation directly, therefore as stated by the Grothus-Draper law (the first law of photochemistry): "Only the light which is absorbed by a molecule can be effective in producing photochemical change in that molecule." UV/visible radiation is only absorbed by chromophores that contain $\pi-$ and/or n-electrons in there structure. Examples of these bonds are C-C, CO and phenyl bonds [Ranby and Rabek, 1989]. The bond energy required to break a C-C bond (the weakest of these three bonds) is $3.6eV$, which is equal to a wavelength of 344nm [Zumdahl et al., 2016].

The intensity of the laser is defined as the optical power per unit area which is transmitted through a surface perpendicular to the propagation direction [Paschotta, 2008]. The optical power of a laser (measured in Watts) is the average power of a pulsed laser. A pulse length can be very short (in magnitude of nanoseconds), which results in very high peak powers but lower average power [Paschotta, 2008]. The intensity could influence the ablation of the material significantly as it can increase

the rate of photochemical reactions and depending on the material also provide enough energy for vaporization and not only melting of the material [Gillner and Gretzki, 2015; Zavala and Ravetta, 2002].

3 RESEARCH QUESTIONS AND HYPOTHESES

3.1 MAIN RESEARCH QUESTION

Does the CSP pretreatment improve the biodegradability of the EFB fibres and is it a potential alternative to a HT pretreatment?

3.2 SPECIFIC RESEARCH QUESTIONS AND HYPOTHESES

1. What temperatures can be achieved by the Fresnel lens at different distances from the centre of the lens for a solar intensity of 1 sun?

   Based on the literature study, the maximum temperature that can be reached from the concentration factor of the Fresnel lens is around 1800K. Therefore, taking into account heat losses, a lower maximum temperature is expected. It is also expected that as the distance from the focus length deviates, the maximum temperature reached will decrease due to a decreased energy density.

2. What are the effects of the CSP pretreatment in comparison to the HT pretreatment on the EFB fibres in terms of the biomethane potential under thermophilic conditions?

   It is expected that the biomethane potential of the EFB fibres is increased due to the CSP pretreatment. The high localised temperatures and photochemical/photothermal effect is expected to increase the biodegradability of the fibres by making cellulose more accessible through lignin and partial hemicellulose degradation. Although, the Fresnel lens has limited transmittance of UV light, it is still expected that this will increase the lignin degradation because lignin has the ability to absorb UV light. Therefore, a a small photochemical effect is still expected due to the absorption of these high energy photons in the bonds, which will result in bond breakage [Datta et al., 2017]. Furthermore, VIS light is also absorbed by chromophores that are present in the lignin structure, which means that these photons will provide additional energy to break lignin bonds and due to the higher percentage of the VIS wavelength in comparison to UV, it is expected the effect will be predominantly photothermal.

3. What are the effects of the exposure time and specific wavelengths in the solar spectrum (UV, VIS, IR) on:

   - The concentration of dissolved lignin in the liquid hydrolysate for the wet conditions?

     It is expected that the UV wavelength has the least effect on the concentration of dissolve lignin. This is because UV is such a small fraction of sunlight and the intensity of this wavelength is low. The IR wavelength, is known for its heating effect; therefore, despite the lower photon energy and the poor absorption of the IR wavelength by the bonds. The increase in the temperature of the water would result in increased lignin degradation [Evstigneyev and Shevchenko, 2019]. However, it is expected that

the VIS wavelength has the greatest effect on the concentration of dissolved lignin. This is mainly due to the higher intensity (in comparison to UV) as a result of the high percentage of VIS light in the solar radiation spectrum and higher photon energy in comparison to the IR wavelength. This means more energy is overall available for bond dissociation. An increase in the duration, is expected to increase the concentration of dissolved lignin, due to an overall higher input of energy.

- The volume and composition of gas produced for the dry experimental conditions?

  It is expected that the UV and VIS wavelength will result in the highest production of gas in terms of the volume. Although, the effect of UV in terms of volume is most likely lower due to low percentage of UV light in the solar spectrum. An increase in the duration is also expected to increase the gas production due to the higher energy input. It is also expected that CO and CO_2 gases will be predominantly produced as these gases are the main gases that are produced in a torrefaction pretreatment.

- The fibre structure for the wet and dry experimental conditions?

  An increase in the exposure duration, is expected to have a more severe effect on bonds and result in increased bond breakages. It is expected that the IR wavelength will have the least effect on the bond breakages. This is because of the lower photon energy and the poor absorption of the IR wavelength by the bonds. Due to the UV wavelength being such a small fraction of the solar radiation, it is expected that the VIS wavelength has the greatest effect on the bond breakages. This is mainly due to the higher intensity as a result of the high percentage of VIS light in the solar radiation spectrum, which means more energy is overall available for bond dissociation.

4 METHODOLOGY

4.1 MATERIALS AND SAMPLING

The EFB samples were harvested in 2016 and collected from a private palm oil mill company,m(SzeTech Engineering Sdn. Bhd., Selangor, Malaysia). The EFB fibres were further processed to reduce the oil content (washed) and were dried and shredded to a fibre size of 1-2 cm. Thereafter, the fibres were shipped to TU Delft, The Netherlands, and then sieved to reduce the dust content. The fibres were stored at 4^oC in a box to ensure the initial properties of the fibres are conserved until they are used for the experiments.

4.2 THERMAL EXPERIMENT

The thermal heating profile of the lens over a period of 10 minutes was measured using a FLIRONE Pro thermal imaging camera. The thermal camera measures a temperature up to 400^oC and has an accuracy of $\pm 3^oC$. A standard unglazed, terracotta tile with dimensions of 24cm x 24 cm x 0.6cm was used. The tile was placed at different distances from the lens (17cm, 20cm, 24cm, 28cm and 30cm). The tile was placed parallel to the lens and the lens was angled to be perpendicular to the solar radiation. The solar intensity at the time of the experiment was determined using an OptiVelox SSO2 solar irradiance measuring device that is linked to an app, SolarTester v1.2. The set-up of the thermal experiment is shown in Figure 4.1.

Figure 4.1: Set up for the thermal experiments using the Fresnel lens

4.3 METHODOLOGY OF PRETREATMENTS

The fibres were treated by either the HT, CSP or PLA pretreatment. Following the pretreatment, the wet experimental condition fibres were filtered from the hydrolysate using a vacuum filtration for the higher volume samples (100ml) and without a vacuum filtration for the 5ml samples. The wet EFB fibres (solid residue) were dried in a 45^oC oven until the mass of the fibres remained constant [Hames et al., 2008]. The EFB fibres and liquid hydrolysate were stored in a 4^oC fridge when they are not being used for further analysis. The experiments were performed in triplicates to improve reproducibility and consistency.

The CSP experiments were compared to the HT pretreatment through a biomethane potential test and by analysing the fibres and hydrolysate. The PLA experiments were used to assess how the solar radiation experiment affects the extent of the pretreatment in terms of lignin degradation, gas production and fibre structure. In order to compare the PLA to the CSP, the same experimental conditions were required. In order to differentiate the two different conditions in the CSP experiments, the pretreatments have been named CSP and CSPL to refer to the HT conditions and PLA conditions (laser scale) respectively. Due to the small diameter of the laser the CSPL experiments were performed in clear glass vials of 15ml with a silicone septum polypropylene screw cap. Whilst, a WECK Glass Ornamental jar (Volume - 0.22 L) was used as a reactor for the comparison of the CSP and the HT experiments. A control was tested for both the dry (raw fibres) and wet conditions (Control-H and control-h), which consisted of an untreated sample that was either flushed with N_2 gas or mixed with water (of the same mass) respectively. Control-H and control-h refer to the controls obtained from the wet experimental conditions for CSP and CSPL respectively. For the dry conditions, the CSP experiments were flushed for 2 min with N_2 and the CSPL (PLA) experiments for 1 min. A summary of the operating conditions for the different experiments is given in Section 4.3.5.

4.3.1 Hydrothermal Pretreatment (HT)

The HT experiments were conducted using a high pressure/ high temperature (HP/HT) commercially available batch type reactor produced by the Parr Instrument Company, USA (Parr – Series 4570 HP/HT reactor). The configuration of the HP/HT batch type reactor is shown in Figure 4.2. The HT experiment was operated

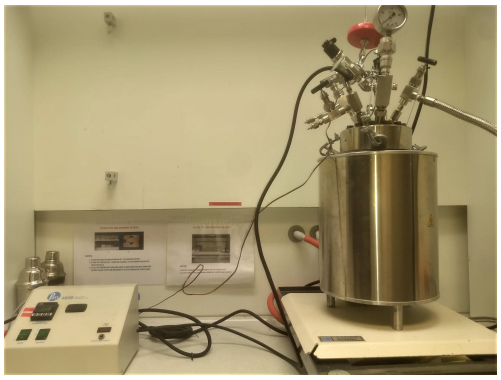

Figure 4.2: Set up of the hydrothermal (HT) reactor

at a temperature of 180^0C with a retention time of 30 minutes as recommended by [Nurdiawati et al., 2015]. The EFB:Water ratio was $1\%_{w/w}$ and an oxygen-free environment was created in the reactor through nitrogen gas sparging for 2min. The product was discharged from the reactor after completion of the pretreatment and once the reactor was depressurised. The EFB residue and hydrolysate analysis is further explained in Section 4.5.

4.3.2 Concentrated Solar Power (CSP)

The solar energy was concentrated using a PMMA Fresnel lens (Hard PMMA Fresnel Lens, MZ-FSXLRHH, Met.Zon, The Netherlands). The Fresnel lens concentrates the solar power at a focal distance of 30cm from the centre of the lens and the dimensions of the Fresnel lens are 27.5cm by 21.2cm. The concentration factor of the lens was assumed to be 400 and the transmission efficiency was estimated to be 50% [Kumar et al., 2015; Hirn, 2014].

Two types of CSP experiments were conducted: CSP, the first set of experiments was operated using the same conditions (in terms of mass and energy input) as the HT experiments, and the second one, CSPL, was operated at a varying energy input on a smaller scale. All the CSP experiments were conducted as batch processes. The set up for the CSPL and CSP experiments is shown in Figure 4.3.

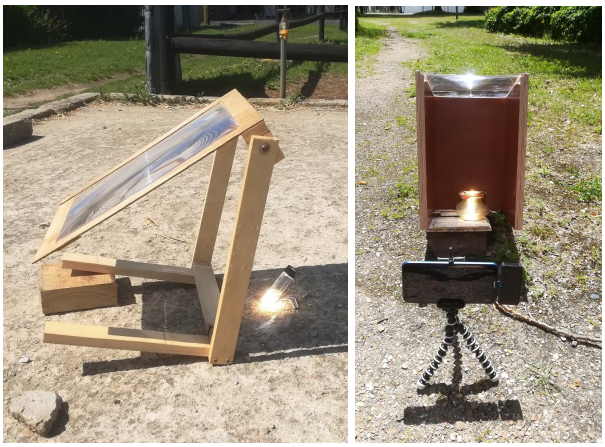

(a) CSPL **(b)** CSP

Figure 4.3: Set up of the CSPL and CSP experiments

The energy input for the CSP experiments was determined from the energy input of the HT experiment (excluding the energy required to maintain it) and was calculated to be 69.2kJ. A more detailed description of the calculations can be found in Section A.1.1. The energy input for the CSPL experiments was based on investigating a pulse duration of 500 to 4500 pulses for the PLA experiments for each wavelength and is further explained in Section 4.3.3. For the CSP and CSPL experiments, the required energy input of the experiment is a function of the time exposed. The duration of the CSP experiments was determined from the solar intensity (at the time of the experiment) and the energy input required. The solar intensity at the time of the experiment was determined using an OptiVelox SSO2 solar irradiance measuring device that is linked to an app, SolarTester v1.2. A more detailed description of the calculations can be found in Section A.1.1 and Section A.1.2. The lens was set up perpendicular to the direction of the solar radiation and the sample was placed 30cm from the centre of the lens. For the CSPL experiments, the bottle was at a 45^0 angle from the ground, to gain the maximum exposure of sunlight.

4.3.3 Pulsed Laser Ablation (PLA) pretreatment

The PLA experiments were performed using a Nd:Yag laser with a repetition rate of 10Hz. Three types of wavelengths were tested, namely: ultraviolet (UV), visible (VIS) and infrared (IR). The corresponding wavelengths are 355, 532 and 1064nm respectively. The laser beam is focused by a 4.5 mm focal length plano-convex lens with average fluence of $8J/cm^2$, mounted on a micrometric translation stage and laser beam diameter of 0.9cm. The pulse duration is on average 7ns (6-8ns) which ensure very fast heating rates and limits secondary reactions [Russo et al., 2002]. The laser beam is focused perpendicular to the surface of the EFB bottle and the EFB bottles were rotated at 4-5RPM using a rotating stand to ensure all the fibres were exposed. The set-up for the PLA experiments is shown in Figure 4.4. The number of pulses (duration of the exposure) were varied from 500 to 4500 with increments of 1000 pulses.

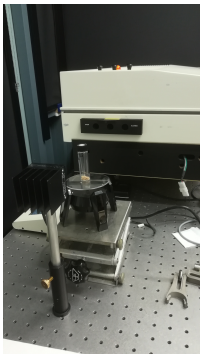

Figure 4.4: Set up of the pulsed laser ablation (PLA) experiments

Energy input for PLA experiments

In order to mimic the Fresnel lens, the intensity of the laser was required to be the same as the intensity of the focal point. The concentration factor of the Fresnel lens was assumed to be 400 with a conservative estimate of efficiency of 50% [Kumar et al., 2015; Hirn, 2014]. The average solar intensity of Malaysia is $824 W/m^2$ [1], which results in an intensity of $165 kW/m^2$ after concentration and taking into account the efficiency. Furthermore, the percentage of UV, VIS, IR for sunlight was taken to be 5, 43 and 52% respectively [NREL, 2009]. This resulted in a concentrated intensity of 8.24, 70.8 and $85.7 kW/m^2$ respectively. The intensity was then translated into a power value using the surface area of the laser beam as the power of the laser is measurable. For the VIS wavelength, the maximum intensity of the laser was less than the calculated intensity from the lens. Therefore, the pulse duration for the VIS wavelength was adjusted according to the theoretical energy input from the theoretical power and desired pulse duration. This means that the number of pulses required for the VIS light were higher in order to ensure the energy input into the system corresponds to the theoretical amount. A more detailed description of the calculations can be found in Section A.1.2. A summary of the energy input for the different PLA experiments is given in Table 4.1 and the CSPL experiment is the sum of the three wavelengths in terms of energy (and intensity).

Table 4.1: Summary of the energy input for the PLA experiments (UV, VIS and IR wavelengths) with respect to number of pulses

Number of Pulses	Energy input (kJ)			
	UV	VIS	IR	CSPL
500	0.026	0.23	0.27	0.52
1500	0.079	0.68	0.82	1.6
2500	0.13	1.1	1.4	2.6
3500	0.18	1.6	1.9	3.7
4500	0.24	2.0	2.5	4.7

4.3.4 Higher Energy CSP experiments

Due to the CSPL and PLA experiments not providing conclusive results on the extent of the fibre pretreament for the wet conditions, three additional experiments were performed to gain a better understanding of the solar radiation. In the first set of experiments (CSPL-HE), a higher energy input was tested for the CSPL experiments. The second set of experiments (CSPL-LIG) was run using pure lignin alkali powder (CAS 8068-05-1) with the same energy input as CSPL-HE. The mass

1 This data was obtained from the NASA Langley Research Center (LaRC) POWER Project funded through the NASA Earth Science/Applied Science Program.

of lignin for the CSPL-LIG experiment was based on the mass of lignin in 50mg of fibre [Chang, 2014]. Lastly, the degradation of dissolved lignin was investigated (CSPL-LIGD). This was done by saturating water with EFB fibres and after 12 hours, the subsequent filtered liquid was exposed to the solar radiation using the Fresnel lens. The energy input for all three of these experiments ranged from 5kJ to 20kJ, with an increment of 5kJ. This energy input is higher than theoretical amount of 3.4kJ (Section A.1.1) that would be required to heat up (not maintain) the PLA size samples to 180^0C under HT conditions.

4.3.5 Overview of experimental conditions

An overview of the experimental conditions for the different pretreatment experiments is given in Table 4.2.

Table 4.2: Overview of experimental conditions

Pretreatment	Component	Mass (g)	Volume of water (ml)	Energy input (kJ)/ time (min)
HT	EFB	1	100	30 minutes
CSP-H/N	EFB	1	100	69 kJ
CSPL-H/N	EFB	0.05	5	0.5 - 4.7 kJ (500 - 4500 pulses)
UV-H/N	EFB	0.05	5	0.02 - 0.2 kJ (500 - 4500 pulses)
VIS-H/N	EFB	0.05	5	0.2 - 2.0 kJ (500 - 4500 pulses)
IR-H/N	EFB	0.05	5	0.2 - 2.5 kJ (500 - 4500 pulses)
CSPL-HE	EFB	0.05	5	5-20 kJ
CSPL-LIG	Lignin	0.011	5	5-20 kJ
CSPL-LIGD	Dissolved lignin	-	5	5-20 kJ

4.4 BIOMETHANE POTENTIAL TEST (BMP)

The BMP test was performed on the pretreated fibres obtained from the HT and CSP experiments, as well as raw fibres as reference point for the pretreatments. In order to produce BMP tests results that are validated and that are comparable to other BMP tests, certain elements were considered in the procedure. These elements were obtained from an article written by Holliger et al. [2016] on the standardization of BMP tests.

The thermophilic (55^0C) batch reactions were performed using an Automatic Methane Potential Test System (AMPTS) II supplied by Bioprocess Control (Sweden) and the AMPTS manual was followed in the preparation of the BMP tests. The inoculum to substrate ratio (ISR) of VS was 2:1 and as the different conditions of fibres had different VS contents, the inoculum volume was kept constant in all the samples Table A.5.

For the validation of the BMP test results it is necessary that a positive control is run for the validation of the gas measurement procedure [Holliger et al., 2016]. The positive control was prepared using microcrystalline cellulose (CAS 9004-34-6) as the substrate. In order to determine the endogenous methane production (blanks), a negative control was prepared from inoculum only. The total average methane yield for each substrate was calculated using a method described by

Hafner [2019] and the biodegradability of the different substrates was determined. The biodegradability of the pretreatments and control is defined as the ratio of the average methane yield and the theoretical methane potential (in $NL_{CH4}/kgVS$). The theoretical methane potential at STP was determined from the Buswell's equation. A detailed description of the calculation of the BMP, biodegradability and error analysis can be found in Section A.2.2.

4.5 POST CHARACTERIZATION

4.5.1 Liquid hydrolysate analysis - UV-VIS spectrophotometer

The liquid hydrolysate was analysed using an UV-VIS spectrophotometer to determine the lignin concentration. The UV-VIS spectra were recorded with a GENESYS 10S UV-VIS spectrophotometer in a wavelength range of 190-450nm using a spectral resolution of 1nm and quartz glass cuvettes. A lignin calibration curve was developed using concentrations of dissolved alkali lignin from 0.5mg/l to 12.5mg/l. The alkali lignin was dissolved using a solution of 0.035M of $NaOH$ to develop the lignin calibration curve and the lignin peak was recorded at a wavelength of 212nm [Lee et al., 2013]. The experimental samples were diluted using the same 0.035M NaOH solution. The dilutions ranged from 1:10 to 1:46 to ensure the absorbance measurement was below 1 Au.

4.5.2 Fibre analysis using FTIR

The fibres were analysed using a Fourier Transform Infrared (FTIR) spectroscopy. This analysis is used to determine the chemical properties of a material. The FTIR machine is a Perkin Elmer FTIR with a ZnSe ATR crystal. A wavelength range of 600 to 4000cm^{-1} was scanned and each sample was scanned 10 times to reduce the noise in the sample.The FTIR analysis method was development based on a method described by Sim et al. [2012] for lignocellulosic biomass and which was originally described in a previous paper by the same author to analyse edible oils [Sim and Ting, 2012]. The FTIR results were normalised to ensure that the absorbance at wavelength 4000cm^{-1} was zero and then a baseline correction was performed using an asymmetric least square smoothing algorithm in Python 3.6. This method is a combination of using a Whittaker smoother and asymmetric least squares to correct the signal [Eilers and Boelens, 2005]. There are three parameters that can be varied: p for asymmetry, λ for smoothness and the number of iterations to perform. The suggested range for the first two parameters is $0.001 \leq p \leq 0.1$ (for signals with positive peaks) and $10^2 \leq \lambda \leq 10^9$, however there are exceptions and visual inspection is often sufficient enough to find suitable parameter values. For the FTIR spectrum results from these experiments the values of the parameters can be found in Table A.6 (Section A.3).

The baseline corrected spectra were then subjected to a peak detection algorithm to identify the absorption peaks. This was done to identify which peaks were present in the raw fibres and in the wet experimental conditions control group (Control-H and control-h) and subsequently if there were any new peaks identified in the pretreated fibres. The second derivative spectrum was then calculated using a Savitzky-Golay algorithm for all the samples for a better comparison of the absorption peaks. An advantage of the second derivative is that baseline errors are removed in the differentiation [Rieppo et al., 2012]. The disadvantage of the second derivative is that it causes significant loss in signal-to-noise ratio; however, this loss is minimised when using smoothing techniques which is included in the Savitzky-Golay algorithm.

This algorithm is based on least-squares polynomial smoothing [Schafer, 2011]. The second derivative was calculated using the Savitzky-Golay filter in Python 3.6, and the window size and polynomial order were chosen to reduce the noise but still ensure the adsorption peaks are observed. A window size of 27 and polynomial order of 3 was found to be suitable. In order to compare the second derivative spectra, an independent T-test was performed on the different pretreatments in comparison to the controls at each of the peaks identified to determine any significant changes in the peak. A more detailed explanation of the method and developed code can be found in Section A.3

4.5.3 Gas analysis - Micro Gas Chromatography

Micro Gas Chromatography (GC) was used to analyse the gas produced in the CSP-L and PLA experiments from the dry experimental conditions experiments. An Agilent Micro GC (490) was used to analyse the gas and the column was calibrated to measure syngas (H_2, CO_2, CO, CH_4, O_2 and N_2). The gas samples were analysed within 24 hours of the experiments and were analysed when the samples were at room temperature (20^o) and atmospheric pressure.

5 RESULTS: CSP, AN ALTERNATIVE PRETREATMENT METHOD?

5.1 THERMAL ANALYSIS OF THE FRESNEL LENS

The temperature profile of the Fresnel lens at different distances from the centre of the lens to the center of the concentration point was analysed using a thermal camera (FLIR One Pro Series). The results are given in Figure 5.1. The conditions under which the temperature profile was obtained is given in Table 5.1.

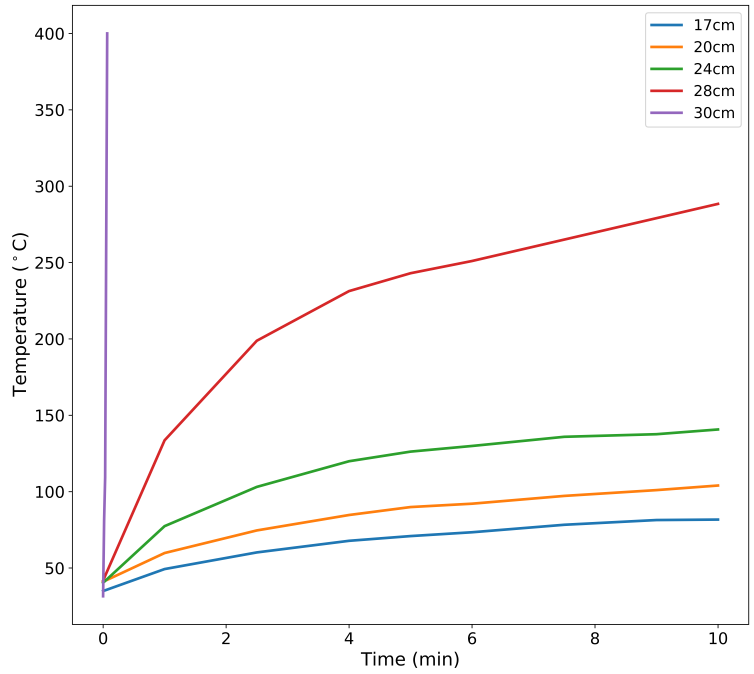

Figure 5.1: Temperature profile over time for the Fresnel lens at different distances from the lens

Table 5.1: Experimental conditions for the thermal experiments

Distance from lens (cm)	17	20	24	28	30
Intensity (Q) W/m^2	1100	1100	1120	1100	1100
Azimuth angle (^{o})	33	33	32	34	34
Area of light (cm^2)	140	93.5	45.5	19.5	0.8
Energy density (kW/m^2)	4.6	6.9	14.3	32.9	800

From these experiments, it was also observed that the concentration factor was under estimated and that the actual concentration factor at the focal distance is around 700, almost double than originally thought. As the distance from the lens increases towards the focal point of 30cm, the gradient of the temperature increases from $11^oC/min$ to $5500^oC/min$. For distances 17, 20 and 24cm, the rate of temperature increase decreases over time and is less than $3^oC/min$ at 10 minutes. From Figure 5.2, it is observed that there is a temperature gradient in the focus area; this

means there is an uneven distribution of temperature, with the hottest point being the centre. This is as a result of the decrease energy density as the distance towards the lens decreases (Table 5.1). The rate of temperature increase at 28cm is higher than for the other three distances. Increasing the distance by 2cm from 28cm to the focal length of 30cm, resulted in the temperature reaching 400^oC in 5 seconds. This because the concentration factor increases exponentially. The energy density increased from $32.9kW/m^2$ to $800kW/m^2$, by increasing the distance from the lens from 28cm to 30cm (Table 5.1). Due to the limitation of the thermal camera in terms of temperature of 400^oC, higher temperatures can not be recorded at a the focal length of $30cm$.

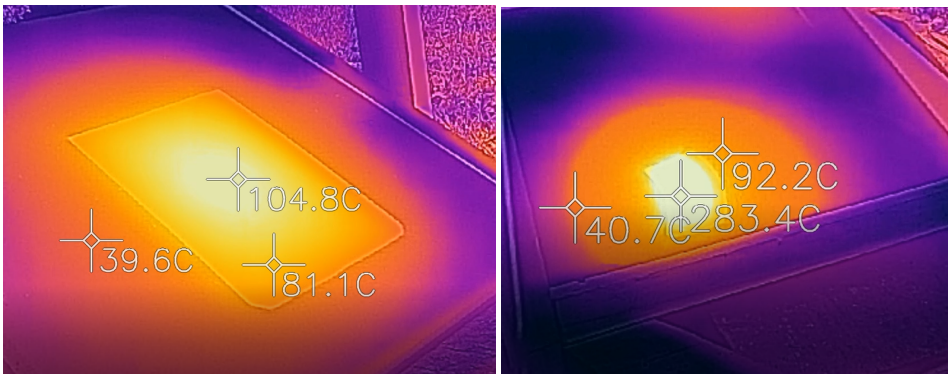

(a) 20cm **(b)** 28cm

Figure 5.2: FLIR Images of the thermal analysis after 10 minutes for distances 20 and 28cm

5.2 BIOCHEMICAL ANALYSIS

This section discusses the results from the BMP test performed and the analysis of the liquid hydrolysate from the CSP pretreated fibres (wet experimental conditions) and the HT pretreatment.

5.2.1 Biomethane Potential Test (BMP)

The total average yield of methane from the substrates was used to compare the effectiveness of the different pretreatments. The cumulative methane production for the BMP over the first 19 days is given in Figure 5.3. Unfortunately, due to a technical issue the plot is unable to give the results for the entire duration of the BMP (total of 27 days). The methane production for the $CSP-N3$ experiment and the three blanks (inoculum only) continued to produce methane gas beyond the time line of the plot. The average total yield of methane (NL) produced per kilogram of VS in the substrate for the different pretreatments, raw fibres and positive control is given in Figure 5.4 and Table 5.2. The biodegradability of the substrates were also compared and the results are also given in Table 5.2.

According to Holliger et al. [2016], certain requirements need to be fulfilled in order to validate the BMP test results. These criteria involve the RSD of the controls, the substrate and the endogenous activity of the blanks. The methane production of the positive control (cellulose) is required to be between 85 and 100% of the theoretical amount (biodegradability) and the RSD is required to be $< 5\%$. For heterogeneous substrates, the RSD is required to be $< 10\%$.

From Figure 5.3, it is observed that endogenous activity is very high. The methane production should be below 20% of the total methane production (inoculum and substrate). The inoculum for this BMP was obtained from Wabico B.V., Waalwijk,

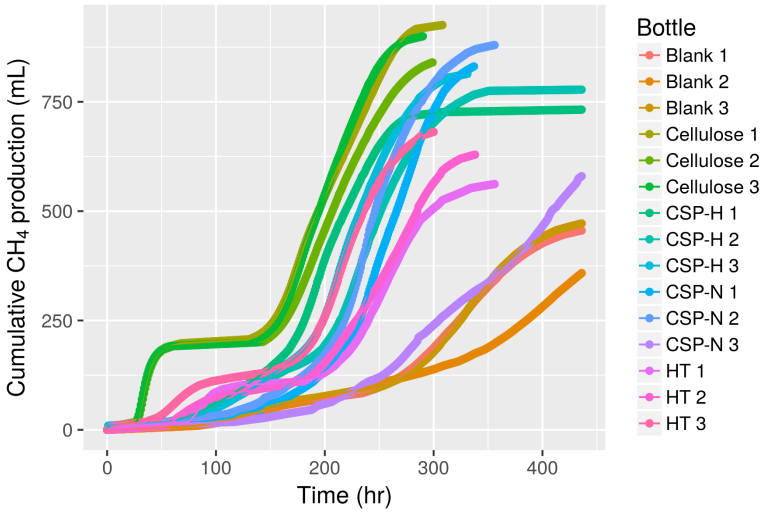

Figure 5.3: Cumulative methane yield expressed in ml obtained during the batch anaerobic digestion of the three different pretreatments (HT, CSP-H and CSP-N), positive control (cellulose) and negative control (inoculum only) for the first 19 days (Generated from the Online Biogas App (OBA) developed by Hafner et al. [2018])

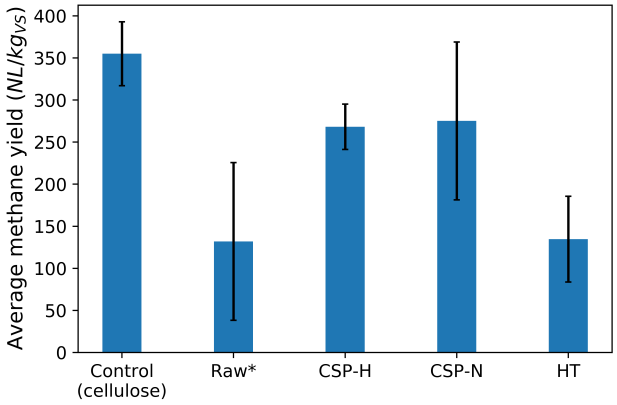

Figure 5.4: Average methane yield of the different pretreatments, Raw*[1], EFB fibres and control.

[1] Results calculated from a second BMP test that was run at the same time, same pH range of 7 - 8.5 and using the same inoculum

The Netherlands. The characteristics of this inoculum is that this inoculum is used to process substrates from egg factories and slaughter houses. The possible reasons for the high methane production is that this is a new inoculum and ideal incubation is not yet known. Therefore, the incubation phase was not long enough to ensure low endogenous activity.

The cellulose biodegradability is within the required range, however the RSD is 10.7%, which is too high (Table 5.2). The possible reasons for this is that methane production of the inoculum was high, in comparison the the total production of gas on the BMP. The methane production of the inoculum was $462 \pm 10.8 Nml$ which is half of the final methane production for cellulose. The VS of cellulose was determined to be $0.84 g/g$ and this is unusually low. This could be due the cellulose not being fresh.

Furthermore, the RSD error for the pretreatments and raw fibres is also high, with the lowest being the CSP-H pretreatment with a 10.0% error. This is on the

Table 5.2: The average total yield of methane (NL) produced per kilogram of VS and biodegradability of the pretreatments determined from the theoretical yield of methane.

	Average BMP yield (NL_{CH4}/kg_{VS})	Relative standard deviation (RSD) %	Theoretical methane yield (NL_{CH4}/kg_{VS})	Biodegradability
Positive control (cellulose)	355 ± 38.0	10.7	415	$85.6 \pm 8.85\%$
Raw*[1]	132 ± 93.7	71.0	484	$27.2 \pm 19.1\%$
CSP-H	268 ± 26.9	10.0	484	$55.4 \pm 5.14\%$
CSP-N	275 ± 93.8	34.1	484	$56.8 \pm 19.3\%$
HT	135 ± 50.9	37.7	484	$27.8 \pm 10.3\%$

[1] Results calculated from a second BMP test that was run at the same time, same pH range of 7 - 8.5 and using the same inoculum

limit of the RSD requirement for a heterogeneous substrate. The high error is most likely as a result of two reasons, one being the high endogenous activity. The second reason is that the methane yield is influenced by the high heterogeneity of the EFB fibres. EFBs are made up of a stalk and spikelets, and stalk fibres have been found to be less recalcitrant than spikelets [Reneta Nafu et al., 2015]. Therefore, this could influence the biodegradability. In the CSP-N experiments, the extent of the pretreatment varied amongst the fibres. This was evident due to some fibres being more blackened in colour than others and is as a result of the area of substrate was larger than the focal area of the lens. Therefore, to ensure homogeneity in the BMP experiment, an attempt was made to ensure that three triplicates contained an even ratio of both blackened and not fully blackened fibres (by mass). However, the extent of pretreatment could still vary in particular for the non-blackened fibres as the full extent of the pretreatment is not necessarily visible to the naked eye. This is most likely the reason for the high standard deviation in the CSP-N methane yield.

Despite the high RSD, in comparing the biodegradability of the different pretreatments, it was found that the BMP yield for the CSP-H pretreatment was significantly different to the HT pretreatment ($p < 0.05$) and in comparison to the raw fibres, the p-value was determined to be 0.07. The biodegradability for the CSP-H pretreatment is almost double than that of the HT. Although, the CSP-N pretreatment has a high RSD, the average biodegradability is similar to the CSP-H pretreatment. It was also observed that the HT pretreatment was not significantly different from the raw fibres. There are two possible reasons for this. The first being, that the raw fibres were preprocessed before being sent to The Netherlands. The full extent of this preprocessing is not known, however, the fibres were dried and mechanically shredded. This could have an influence on the biodegradability as the fibre structure could be weakened through the heating process and a shredding process generally increases the surface area and can expose hemicellulose and cellulose resulting in a high BMP yield for the raw. In addition to this, a study done by Fernández-Cegrí et al. [2012], found that the methane yield of the sunflower oil cake solid fibres decreased with an increase in the HT temperature (in a temperature range of 100 to 200^0C). The possible reason for this was that at an increasing temperature a higher portion of the soluble compounds were dissolved in the liquid hydrolysate. In this paper, it was also observed that the methane yield increased initially at a HT temperature of 100^0C and then decreased, most likely due to the presence of inhibitors. This could be the reason why the HT pretreatment did not increase the methane yield as only the fibres were tested.

In comparing the HT pretreatment and the raw fibres to studies done in literature, it was found that the BMP yield of this research was lower. In a study done by O-Thong et al. [2012], it was found that BMP yield (under thermophilic conditions) for raw EFB fibres was 202 and 153 NL_{CH4}/kg_{VS} (based on an initial VS loading of 20 and 40g_{VS}/L respectively). The same study also investigated a hydrothermal pretreatment and the BMP yield was 208 NL_{CH4}/kg_{VS} for a loading rate of 39g_{VS}/L. The BMP of the fibres increased with the hydrothermal pretreatment, however, it was mentioned in the methodology that both the liquid hydrolysate and EFB fibres were used in the BMP. Furthermore, the particle size of the EFB used in this study was 5mm or less. This is smaller than the particle size used in this current research, which is 1 to 2cm. This means that the accessible surface area available is smaller and the porosity is also lower for this current research. In addition, to having a larger particle size, this current research also only investigated the BMP from the fibres, not the liquid hydrolysate. The BMP results for the CSP-H and CSP-N, were both higher than the raw and HT pretreatment BMP from the study done by O-Thong et al. [2012].

Another study, done by Kim et al. [2013] found that the BMP yield (under mesophilic conditions) for untreated, raw EFB fibres was 264NL_{CH4}/kg_{VS}. This is higher than the raw EFB fibres BMP for both the study done by O-Thong et al. [2012] and this current research study for the raw EFB fibres. The CSP-H and CSP-N methane yield was also only slightly higher than the untreated, raw from that study. One of the reasons could be that these raw EFB fibres were ground to an even smaller particle size. The fibres were ground into a fine powder of less than 1mm in size [Kim et al., 2013].

5.2.2 Analysis of the liquid hydrolysate

The dissolved lignin concentration and the chemical oxygen demand (COD) of the liquid hydrolysate for the pretreatments were analysed and are given in Table 5.3. The Control-H refers to an untreated sample to observe the changes in the COD and dissolved lignin concentration of the hydrolysate by merely mixing the EFB fibres with water.

Table 5.3: COD and lignin concentration of the liquid hydrolysate for the CSP and HT pretreatments

Pretreatment	COD (mg/L)	Dissolved lignin concentration ($mg/L.g_{EFB}$)
Control-H	170 ± 8.6	48.7 ± 10.1
CSP-H	210 ± 6.0	55.4 ± 15.0
HT	4100 ± 1100	354 ± 131

The HT pretreatment had the highest concentration in terms of COD and dissolved lignin concentration, more than 10 times the amount of COD and more than 5 times the dissolved lignin concentration, in comparison to the CSP pretreatment. The reason being is that more than 40% of the fibres by mass completely dissolved into the hydrolysate. For the CSP experiments (Control-H and CSP-H) only about 10% of the fibres dissolved (by mass). From the Control-H results, it is observed that the COD and lignin concentration increased in the liquid merely by the addition of the EFB fibres to distilled water. There is a slight increase in both the COD and lignin concentration after exposing the fibres (CSP-H) to the solar pretreatment. The average COD increases by 36mg/L and however the increase in dissolved lignin concentration is not statistical significant.

6 RESULTS: DEEPENING THE UNDERSTANDING OF THE INFLUENCE OF THE SOLAR SPECTRUM ON THE EFB FIBRES

6.1 FTIR METHOD DEVELOPMENT FOR THE STRUCTURAL ANALYSIS OF EFB FIBRES

The structure of the EFB fibres and lignin powder were analysed using a peak detection and comparison method developed in Python 3.6 that processed the data that was obtained from the FTIR analysis. The developed method was based on a FTIR analysis method developed by Sim et al. [2012], for the computational analysis of lignocellulosic fibres. The functions of this method is that the peaks are identified and are compared (by the second derivative) using a t-test analysis.

In order to identify the main peaks in the FTIR spectrum of the samples, a smoothing and baseline correction is first implemented. Thereafter, a peak identification function is implemented, to determine the wavenumbers of the peaks. These identified peaks are then manually compared to peaks observed in literature. This is necessary because one of the limitations of this peak identification function is that it is sensitive to noise and although extensive smoothing will decrease the noise, it may also smooth small peaks that show significant changes in the structure. The second reason this was done, is to only compare the bands commonly associated with lignin, hemicellulose and cellulose. For this research, the peaks for both the raw fibres and control fibres (Control-H and control-h) were identified separately.

For the comparison of the treated and untreated, a t-test was used to compare the second derivative for each peak identified (in the raw and the control fibres), as this minimises the baseline error. A limitation of using the second derivative is that small peak shifts are not identified as being significantly different when comparing treated and untreated fibres, however these can be visually identified or identified by comparing the actual absorbance data and not the second derivative. A more detailed explanation of the development of the FTIR analysis method and implementation is given in Section A.3.

6.2 STRUCTURAL ANALYSIS OF THE PRETREATMENTS

6.2.1 Structural analysis of the CSP pretreatments

The pretreated and raw fibres that were test in the BMP experiment were analysed using FTIR (prior to the BMP) to observe if there were any structural bond changes due to the pretreatments. The analysis of the FTIR results can be quite complex as there is often an overlap in peaks for lignin, hemicellulose and cellulose. The trends of three components are not necessarily equal, therefore it is difficult to make an accurate conclusion of what influenced the bond change. Therefore, the focus of this analysis is mainly limited to peaks that are of a result of one of the three components. There are exceptions, which is as a result of one peak representing the bonding of two components.

The CSP-N pretreatment was compared to the raw fibres (Figure 6.1), whilst the HT and CSP-H fibres were compared to the Control-H (Figure 6.2). The Control-H refers to the sample that consisted of the same mass of fibres and volume of water but was untreated. The vertical lines identify the main band assignments that were used to compare these pretreatment methods, these were determined from a combination of literature data and a peak analysis of the FTIR results. A complete list of the adsorption peaks that showed a significant change is given in Appendix B (Table B.1, Section B.1.1).

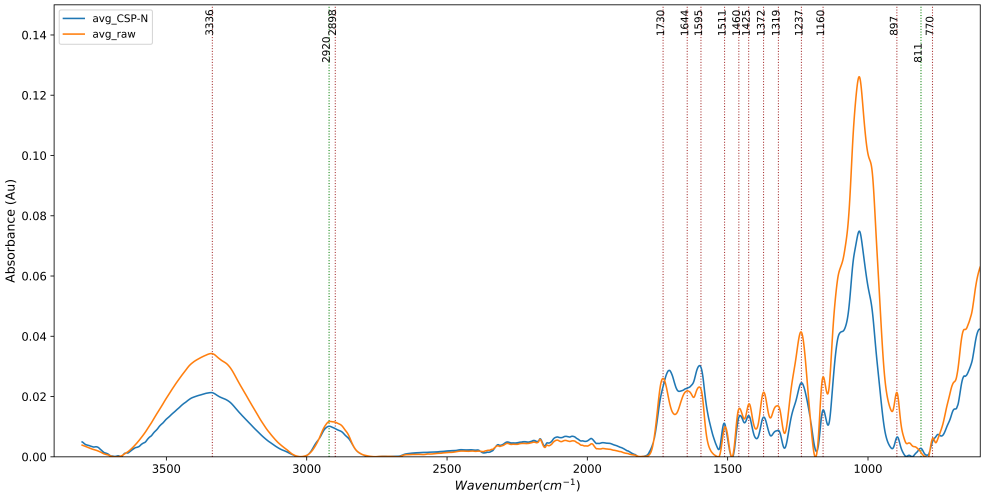

Figure 6.1: FTIR analysis of the EFB fibres for the CSP-N pretreatment and the raw fibres (averaged results)

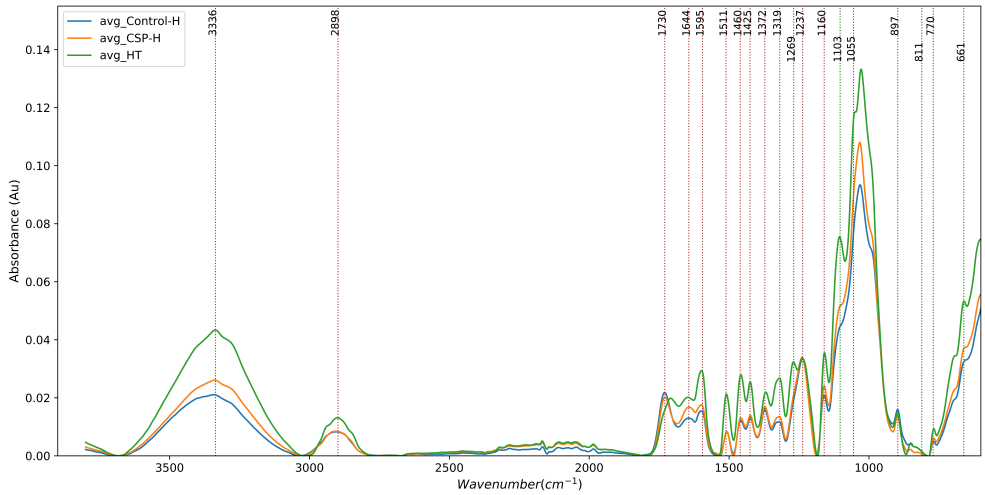

Figure 6.2: FTIR analysis of the EFB fibres for the CSP-H, HT and Control-H pretreatments (averaged results)

From the dry experimental conditions it was observed that significant changes in the functional groups were observed for the CSP-N pretreatment in comparison to the raw fibres (Figure 6.1). Structural changes were observed for cellulose after this pretreatment. This is observed by a clear decrease in the absorption for the peak at $897cm^{-1}$ due to the partial degradation of the β-(1,4)-glycosidic bonds in cellulose [Ishola et al., 2012]. Wavenumbers around $2900cm^{-1}$ are associated with the asymmetrical stretching of $-CH$ bond and wavenumbers around $3340cm^{-1}$ are associated with $-OH$ stretching and corresponds to all three components [Coates, 2006; Shi and Li, 2012; Lu et al., 2017]. There was a shift in the peak observed from

wavenumber $2898cm^{-1}$ to $2920cm^{-1}$ for the CSP-N pretreatment. This shift could indicate the weakening of the hydrogen bonds as this is the associated trend for blue shifts of OH bonded $-CH$ bonds [Selvam et al., 2010]. A red shift refers to a downward shift in the wavenumber and a blue sift refers to an upward shift in the wavenumber.

From the wet experimental conditions, significant changes were only observed for the HT pretreatment in comparison to the Control-H fibres. New absorption peaks are observed at wavenumbers 692, 1055, 1103 and $1269cm^{-1}$. The wavenumber, $692cm^{-1}$ is associated with cellulose and absorption peak at wavenumber $1103cm^{-1}$ is a typical characteristic of cellulose [Faix and Böttcher, 1992]. The appearance of both these peaks indicates more cellulose is exposed due to partial degradation of lignin and hemicellulose [He et al., 2008; Faix and Böttcher, 1992]. Absorption peak $1050cm^{-1}$, is associated with both cellulose and hemicellulose, this could mean both cellulose and hemicellulose are exposed due to partial degradation of lignin [Shi and Li, 2012].

The wavenumber $1160cm^{-1}$ is associated with the C-O-C vibration of glycosidic linkages of cellulose and hemicellulose [Shi and Li, 2012]. Both hemicellulose and cellulose are linked with glycosidic bonds. Cellulose is only linked with β-(1,4)-glycosidic bonds (observed at wavenumber $897cm^{-1}$), whilst hemicellulose contains a variety of glycosidic bonds in one molecule [Shrotri et al., 2017]. Therefore, an increased adsorption for the HT pretreatment indicates increased exposure of these two components most likely as a result of partial lignin degradation.

For both the CSP-N and HT, similar peak changes were observed for the LCC bonds. As mentioned in the literature study (Section 2.1.1), LCCs are complex bonds that hinder the biodegradation of lignocellulosic biomass. Changes in the LCCs linkages could mean that more cellulose is exposed and available for biodegradation [He et al., 2008]. Wavenumbers that are associated with these LCCs bonds are 1237, 1269 and $1730cm^{-1}$ [Coates, 2006; Ishola et al., 2012; Lu et al., 2017]. Wavenumbers 1237 and $1269cm^{-1}$ are associated to the C-O stretching of ether bonds. There is a decrease in the absorption at wavenumber $1237cm^{-1}$ for the CSP-N pretreatment (Figure 6.1) and this could be as a result of damage to these ether bonds linking lignin and hemicellulose. There is a red shift for the peak observed at wavenumber $1730cm^{-1}$ for both the HT and CSP-N pretreatment. The absorption peak at $1730cm^{-1}$ is associated with the C=O stretching of ester bonds. This shift is an indicator of damage to the ester bonds in the LCCs caused by deacetylation during the thermal treatment [He et al., 2008; Xu et al., 2006]. For the HT pretreatment there is a reduction in this peak, which was also observed by Tjeerdsma and Militz [2005] in a study done on the chemical changes in hydrothermally treated wood.

In the region of wavenumbers 1300 to $1511cm^{-1}$, it is observed that there is an increase in the absorption for wavenumbers 1319, 1425, 1460 and $1511cm^{-1}$ for the HT pretreatment. Wavenumbers 1425 and $1511cm^{-1}$ are associated to the C=C stretching vibrations of the aromatic rings in lignin [Ishola et al., 2012; Shi et al., 2012]. The reason for the enhancement of these bands could be as result of the accumulation of condensed, degraded polysaccharides and breakage of lignin [He et al., 2008]. This results in the original network structure to change from a three-dimensional structure to a linear structure [He et al., 2008]. However, $1425cm^{-1}$ is also assigned to CH_2 scissors vibrations in cellulose and $1460cm^{-1}$ is assigned to both lignin and cellulose, therefore an increase could be as a result of cellulose being more exposed due to the HT pretreatment. There was a decrease in the absorption for CSP-N at wavenumber $1372cm^{-1}$ which indicates partial degradation of cellulose and hemicellulose as this peak is assigned to the $-CH$ deformations in cellulose and hemicellulose. For the CSP-N pretreatment, it is observed that the peak at $1644cm^{-1}$ is flattened and this wavenumber is associated with the C=O stretching vibration in the conjugated carbonyl group of lignin [Coates, 2006; Shi et al., 2012].

Carbonyl groups mainly exist as side chains for lignin and disappearance of this peak indicates degradation of these side chains [He et al., 2008].

6.2.2 Structural analysis of the influence of the solar spectrum on the heterogeneous fibres and homogeneous lignin for the wet experiments

Low Exposure Time

The results from the FTIR analysis of the wet experiments for the CSPL-H and PLA experiments for the maximum number of pulses (4500 pulses) are given in Figure 6.3. The red dashed lines indicate the identified absorbance peaks in control-h where as the green dashed lines indicate a new absorbance peak that was not observed in the control-h.

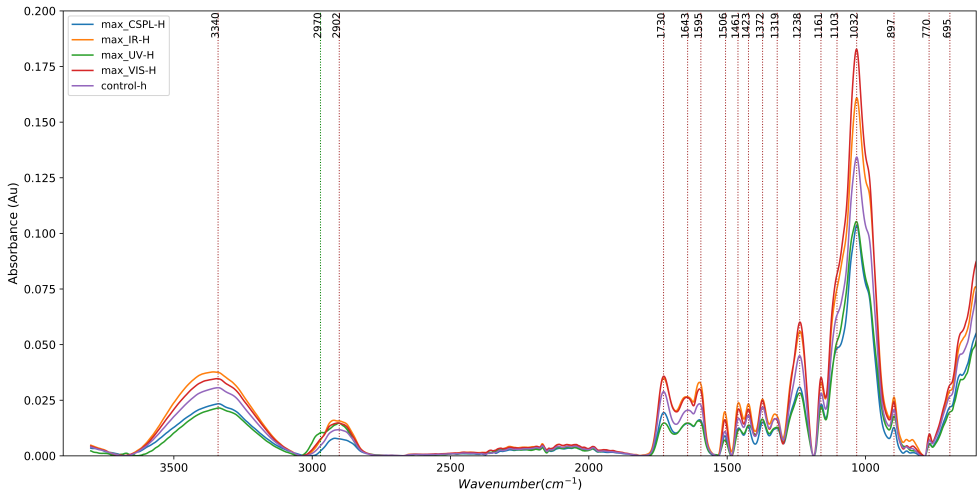

Figure 6.3: FTIR analysis of the EFB fibres for the CSPL-H, UV-H, VIS-H, IR-H and control-h pretreatments (averaged results)

A complete analysis of the structural changes can be found in Section B.1, Appendix B. The main observation from this analysis is that although changes are observed in the absorbance peaks for both the PLA experiments and the CSPL-H experiments there is no clear trend. The absorbance increased for the VIS-H and IR-H experiments and decreased for the UV-H and CSPL-H experiments. The CSPL-H pretreatment had a higher energy input than the other three pretreatments and the least significant changes were observed for this pretreatment (based on the T-test analysis). For the UV-H, the changes in the lignin structure are observed for pulses 2500 and 4000 and for CSPL-H at pulse durations of 500 and 2500. For VIS-H and IR-H, only significant changes were observed for 4500 pulses.

High Exposure Time

As a result of no clear trend being observed for the PLA experiments and CSPL-H experiments, further CSP experiments (CSPL-HE) were conducted at a higher energy input of 5kJ to 20kJ. The theoretical amount of energy input needed for the same experiments to mimic the HT pretreatment is 3.46kJ. An FTIR analysis was also performed on the fibres from the CSPL-HE experiments and the results are given in Figure 6.4. The legend labelling refers to the energy input of the pretreatment. A complete list of the significant changes observed in comparing the second derivative results for the four conditions to the untreated blank fibres (control-h) and the respective functional groups is given in Table B.3 (Appendix B).

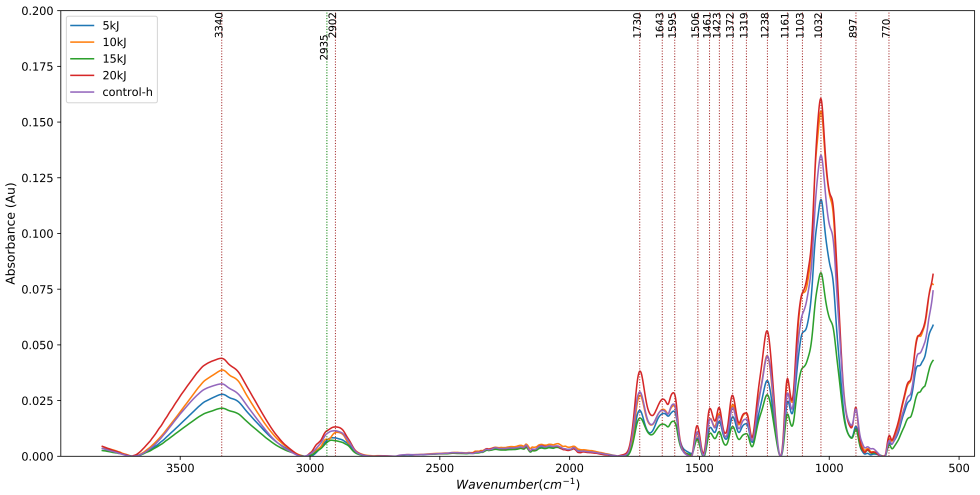

Figure 6.4: FTIR analysis of the EFB fibres for the CSP-HE pretreatments and control pretreatments (averaged results for all energy inputs)

Based on the detailed analysis of the FTIR results, no clear trend observed in the FTIR analysis when comparing it to the untreated blank fibres for the higher energy input. A more detailed explanation of the observations can be found in Section B.1.

Homogeneous lignin

The structural changes of the homogeneous lignin experiments (CSPL-LIG) were also analysed using the FTIR method developed. Based on this analysis, no clear trend was observed and no structural changes were observed for the lignin powder (Figure B.5, Section B.1).

6.2.3 Structural analysis of the influence of the solar spectrum on the heterogeneous fibres for the dry experiments

The results from the FTIR analysis of the wet experiments for the CSPL-H and PLA experiments for the maximum number of pulses (4500) are given in Figure 6.5. The red dashed lines indicate the identified absorbance peaks where visual changes were observed. The green dashed lines indicate a new absorbance peak that was not observed in the raw fibres. A complete list of significant changes observed in comparing the second derivative results for the four pretreatments to the raw fibres and the respective functional groups is given in Table B.4 (Section B.1).

Based on the FTIR analysis, it is observed that there are some visible changes in the absorbance peaks for the CSPL-N pretreatment and for the VIS-N pretreatment, in comparison to the raw fibres (Figure 6.5). For both CSPL-N and VIS-N, there is a red shift in the wavenumber from 1730 to 1704 and $1720cm^{-1}$ respectively. Wavenumber $1730cm^{-1}$ is associated with the $C{=}O$ stretching of ester bonds [Coates, 2006; Ishola et al., 2012]. As mentioned in Section 2.1.1, lignin is linked to carbohydrates by linkage such as benzyl ether and benzyl esters [Achyuthan et al., 2010]. This shift could indicate damage to the ester bonds in the LCCs. The peak height also increased for both these pretreatments which indicates an increase in the presence of these carboxylic bonds. Carboxylic bonds are produced during delignification due the oxidation of the carbonyl and hydroxyl groups [Xu et al., 2006]. Therefore, this increase in the absorption peak could be as a result of delignification in both the CSPL-N and VIS-N pretreatment.

Other wavenumbers that are associated with these LCCs bonds are 1237 and $1269cm^{-1}$. Wavenumbers 1239 and $1269cm^{-1}$ are associated to the C-O stretching

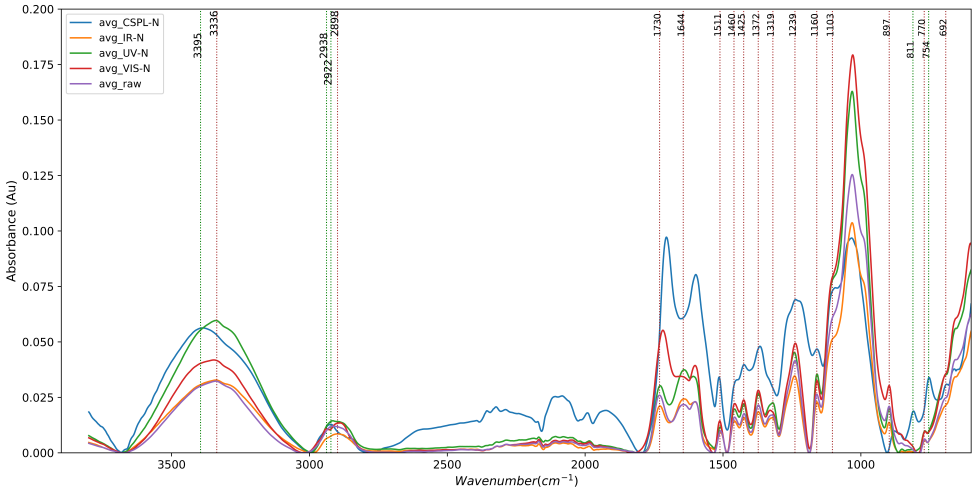

Figure 6.5: FTIR analysis of the EFB fibres for the CSPL-N, UV-N, VIS-N, IR-N and raw pretreatments (averaged results)

of ether bonds [Coates, 2006; Lu et al., 2017]. For the pretreatment of CSPL-N, changes are observed in the peak at wavenumber $1239cm^{-1}$ and $1269cm^{-1}$ (changes for wavenumber $1269cm^{-1}$ are observed from the second derivative analysis - Table B.4). The absorption peak at wavenumber $1239cm^{-1}$ is no longer as prominent, this could be as a result of damage to these ether bonds linking lignin and carbohydrate. Changes in the LCCs linkages could mean that more cellulose is exposed and available for biodegradation for both the CSPL-N and VIS-N pretreatment.

Although, there is some appeared flattening of the peak at wavenumber $1644cm^{-1}$ for VIS-N (Figure 6.5), no significant change was observed when comparing the second derivative spectra. Two new prominent peaks are observed at $754cm^{-1}$ and $811cm^{-1}$ after the CSPL-N pretreatment and a significant difference was also observed for wavenumber $811cm^{-1}$ for UV-N and VIS-N. Both these peaks are associated with CH bending for cellulose [Coates, 2006; Ishola et al., 2012], indicating more cellulose is exposed for the CSPL-N pretreatment. The absorption peak at $897cm^{-1}$ is no longer observed for the CSPL-N pretreatment and this band is associated with the β-(1,4)-glycosidic linkages and breakage degree of intramolecular bonds [He et al., 2008]. Therefore, the disappearance of this band is as result of the partial degradation of cellulose and breakage of the linkages in cellulose.

As mentioned in Section 6.2.1, wavenumber $1160cm^{-1}$ is associated with the C-O-C vibration of glycosidic linkages of hemicellulose and cellulose. The prominent peak observed in the raw fibre is flattened for the CSPL-N pretreatment. This indicates the breakage of these linkages and partial degradation of both hemicellulose and cellulose.

The lignin associated peak $1511cm^{-1}$, is observed to have an increased absorbance intensity for the CSPL-N pretreatment. This wavenumber is associated to the C=C stretching vibrations of the aromatic rings in lignin. The reason for the enhancement of these bands is most likely due to increase in the aromatic fraction of lignin due to degradation of hemicellulose [Park et al., 2013]. Wavenumber $1595cm^{-1}$ is also associated with the aromatic rings of lignin and the absorption of this peak increased significantly . This increased absorption could indicate an increased amount condensed guaiacyl units are present as a result of the accumulation of condensed degraded polysaccharides and breakage of lignin [Park et al., 2013].

In comparing the FTIR analysis for the different pulse durations, only the VIS-N and CSPL-N showed significant changes in the structure below 4500 pulses (Figure B.6 to Figure B.9, Section B.1.5). For the VIS-N experiments, the main changes that were observed were for the wavenumber $1730cm^{-1}$ and the severity of the

LCCs bond breakages increased with an increase in pulse duration. Similarly, for the CSPL-N experiment an increase in the pulse duration, increased the structural changes to the EFB fibres. Specifically, the LCCs and the lignin structure (aromatic ring vibrations) were affected.

The results from this research were compared to a study done by Park et al. [2013] which investigated the transformation of lignocellulosic biomass during torrefaction (without using sunlight). The difference between the study and this research is that the temperature was controlled and the duration was varied. Whilst, for this research, the temperature was dependent on the duration of exposure. However, similar changes were still observed in the FTIR analysis; a shift in the absorption peak around $1730cm^{-1}$, an increase in the absorption peak at $1595cm^{-1}$ and changes to the aromatic skeletal vibrations in lignin were observed. The study investigated three different treatment severities and the trend of these observations is the same as the trend observed in the CSPL-N and VIS-N pretreatments (with respect to duration). From this study, it was also observed that structural changes are mainly observed at a higher severity (for the 'severely torrified biomass') and in particular, CSPL-N pretreatment from a pulse duration of 2500 can be classified as severe based on the relative changes observed from the study.

6.3 BIOCHEMICAL ANALYSIS OF THE HETEROGENEOUS FIBRES

The dry and wet experimental conditions were also analysed in terms of the gas production and dissolved lignin concentration in the liquid hydrolysate respectively.

6.3.1 Analysis of the gas production in the dry experimental conditions

The gas that was produced in the PLA and CSPL experiments was analysed in terms of the composition and the resultant volume of gas that was produced. The volume of gas produced was determined from the composition of the gas and the volume of the vial (excluding the mass of fibres in the vial).

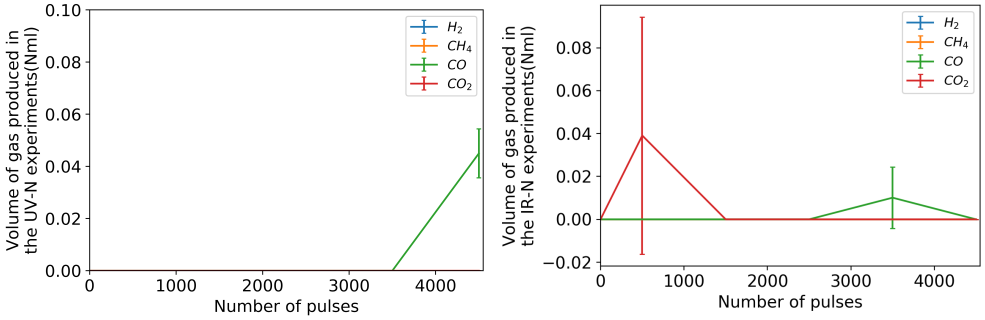

(a) UV-N **(b)** IR-N

Figure 6.6: Average volume of gas produced (Nml) for the UV-N and IR-N experiments

Gas was not produced for all the pulses durations investigated for the IR-N and UV-N PLA experiments. In the IR-N experiments it was observed that for 500 pulses, 0.11Nml of carbon dioxide (CO_2) was produced and for the 3500 pulses, 0.03Nml of carbon monoxide (CO) (Figure 6.6b). However, this gas was only produced for one of the triplicates for both pulse durations and no other gas production was detected for the other three pulse durations. This indicates that although the gas production is inconsistent, gas is produced under specific conditions. An

improvement in the set-up could result in more consistent gas production; for example, exposing a smaller number of fibres, to ensure that the fibres are adequately exposed. Another possible reason for the lack of gas production could be due to fibre structure, as mentioned in Section 4.1 and Section 5.2.1, the fibres are heterogeneous. Therefore, it could mean that the structure of some are more weakened than others and more hemicellulose is exposed. This compound is more volatile of the three and the IR wavelength may be more effective in partially degrading this component. Based on the inconsistency of the gas production, no conclusion can be made on the overall effect of the IR wavelength on the production of gas.

For the UV-N experiments, $0.045 \pm 0.009 Nml$ of CO gas was produced at the maximum number of pulses observed (4500 pulses) Figure 6.6a. All three triplicates produced CO gas; therefore, it could be that the energy input in the system at less than 4500 pulses is insufficient to result in gas production. The energy input at 4500 pulses is 0.24kJ (Table 4.1). The reason for this being so low is because there is only 5% of the UV wavelength in the solar spectrum. Therefore, an increase in the energy beyond 4500 pulses could potentially result in increased gas production, for not only CO gas but also the other torrefaction gases (CO_2, H_2, CH_4) could be expected.

The VIS-N and CSPL-N experiments produced gas for all five pulse durations investigated and the results are given in Figure 6.7. The CSPL-N experiment is the combination of all three wavelengths (UV, VIS and IR) and replicates the combined energy input of the three PLA experiments.

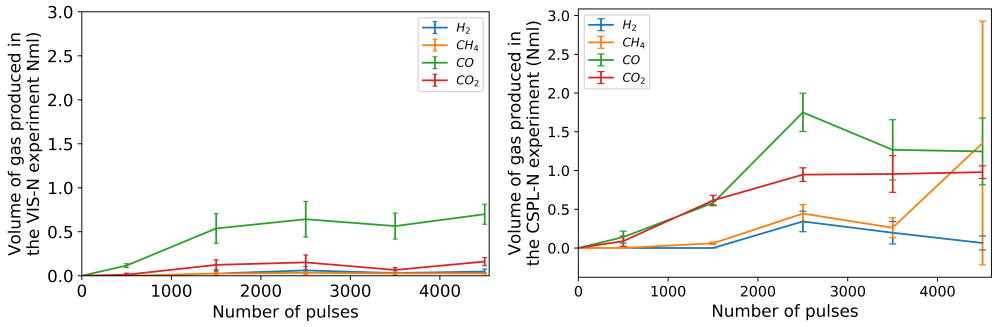

(a) VIS-N **(b)** CSPL-N

Figure 6.7: Average volume of gas produced (in Nml) for the VIS-N and CSPL-N experiments

Initially, only a small volume of CO and CO_2 gas (0.12 ± 0.021 and $0.012 \pm 0.019 Nml$ respectively) is produced for the VIS-N experiments. This increases to a maximum volume of $0.69 \pm 0.11 Nml$ and $0.16 \pm 0.046 Nml$ respectively as the number of pulses increases to 4500. H_2 and CH_4 are both produced from 1500 pulses onwards. The maximum volume of H_2 and CH_4 produced is at 2500 pulses and this is $0.061 \pm 0.045 Nml$ and $0.033 \pm 0.018 Nml$ respectively. Based on the standard deviation for H_2 and CH_4, the gas production did not significantly increase from pulses 1500 to 4500. The same is observed for production of CO and CO_2. This could be due to only a very small fraction of the fibres being exposed to the laser beam due to its small diameter.

Similarly, to the VIS-N experiments, CO and CO_2 are the first two gases to be produced at 500 pulses for the CSPL-N experiments (Figure 6.7b). As the number of pulses increase, CH_4 gas is produced from 1500 pulses onwards and H_2 from 2500 pulses onwards. The volume of H_2 produced decreases after 2500 pulses and based on the data of the triplicates, H_2 gas is only produced in two of the triplicates for 3500 pulses and one of the triplicates for 4500 pulses. This could be due possible side reactions of H_2 such as the carbon hydrogenation reaction that produces CH_4 from H_2 [Uddin et al., 2014].

The gas production, is influenced by factors such as the wavelength, the absorption mechanisms of a specific wavelength, the photon energy, the pulse duration and the power [Brown and Arnold, 2010]. The absorption depth of a material differs depending on its properties and the wavelength, for lignocellulosic biomass this is unknown. This can influence the amount of energy that is transferred to the molecules for the different wavelengths. Therefore, there are quite a few factors that influence the gas production from the different wavelengths. Although, it is difficult to pinpoint which factor influenced the variation in the production of gas, the main aim was to determine the influence of the different wavelengths in the same composition as sunlight. As the energy input for the four experiments differed, in order to eliminate this factor, the experiments were compared in terms of the total volume of gas produced per kJ of energy input (for the different pulse durations). The results are given in Figure 6.8.

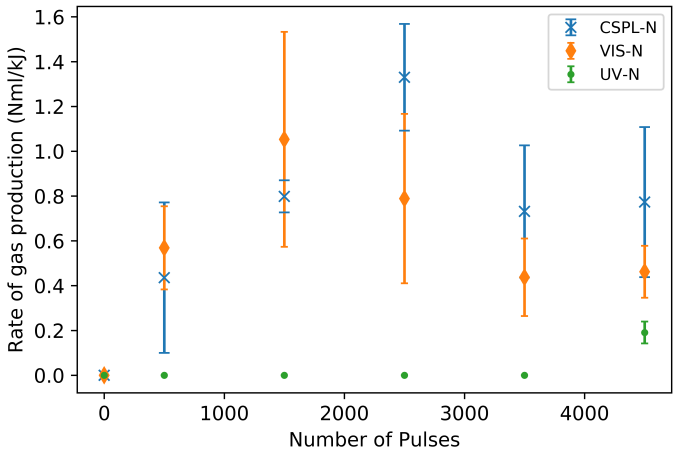

Figure 6.8: Comparison of the rate of gas production (Nml/kJ) for the different pulse durations for the PLA (UV-N, VIS-N, IR-N) and CSP-N experiments

As mentioned previously, IR-N produced no significant volume of gas. This is despite the energy input of the IR-N experiments being slightly higher than that of the VIS-N experiments (Table 4.1) and the intensity of the IR being the highest of the three wavelengths. The photon energy of IR light is lower than that of the visible and UV wavelength, due to the inverse relationship between the wavelength and energy of photon [Lindon et al., 2016]. Therefore, the lack of gas production could be due to the lower photon energy and the poor absorption providing insufficient energy to break the bonds [Garrison and Srinivasan, 1985]. In general, if the energy is insufficient to break the bond it is essentially absorbed into the molecules as heat. This type of response is called a photothermal response and when sufficient energy is absorbed (resulting in a high enough temperature) to break the bonds, gas will be produced [Brown and Arnold, 2010]. However, during the process of accumulating sufficient energy to be able to break one particular bond, energy is also lost to other parts of the sample through vibrational energy transfers. In addition to improving the set up, the lack of gas production could be due to the poor absorption of this wavelength. Therefore, a longer pulse duration may result in more consistent gas production from the IR-N experiments.

Gas is produced for the VIS-N experiments already from 500 pulses (Figure 6.7a) and this is most likely due to a combination of the higher photon energy and higher absorption of this wavelength in comparison to IR, resulting in increased heating rates. The initial rate of gas production of UV (at 4500 pulses) is lower than the rate of gas production for the VIS-N experiments for all pulses durations. The VIS-N experiments also produces CO_2 for an energy input of around 0.2kJ whilst UV-N only produces CO at this energy input (4500 pulses for UV-N and 500 pulses for VIS-

N). The two factors that most likely could have influenced this are the absorption properties of the wavelength and the higher power input of the VIS-N experiments.

In comparing the rate of gas production of the VIS-N experiments to the CSPL-N experiments, it is observed that the rates are similar. This means that although only 43% of the energy input in the CSPL-N experiment is due to the VIS wavelength, it still had the same rate of gas production. Therefore, the entire wavelength spectrum contributes to the gas production despite only VIS light producing gas in the PLA experiments. This means that the photothermal effect is most likely the biggest contributor to the gas production. The rate of gas production for the CSPL-N experiments continues to increase after 1500 pulses but this is most likely due to the limitation of the laser beam diameter which is smaller than that of the CSP focal point. Therefore, more fibres are being exposed to the solar light in the CSPL-N experiments. The decrease in the rate for both these experiments is due to a plateau being reached in the gas production.

The duration of the VIS-N and CSPL-N experiments were not the same, the CSPL-N experiment was significantly shorter with the 4500 pulses duration being equivalent to about $1.5min$ (at an intensity of $1000W/m^2$). In contrast, the 4500 pulses in the VIS experiment are equivalent to about $11.5min$. This is due to the difference in focus area size and resulting in the laser having a much lower power output, for the same intensity.

The Fresnel lens results in a larger focal area than the laser. Therefore, with the higher energy input, a larger radius of high temperatures is achieved in the CSPL-N. This results in the larger volume of gas produced. Although the standard deviations are high, the average rate of gas production for the CSPL-N experiment is slightly lower. This is expected as the energy is distributed over a larger surface area. The main limitation of the gas production is the mass of fibre available to be treated.

The composition of the gas produced for the four experiments was also compared. The gas composition of the VIS-N and CSPL-N experiments over the number of pulses investigated is given in Figure 6.9.

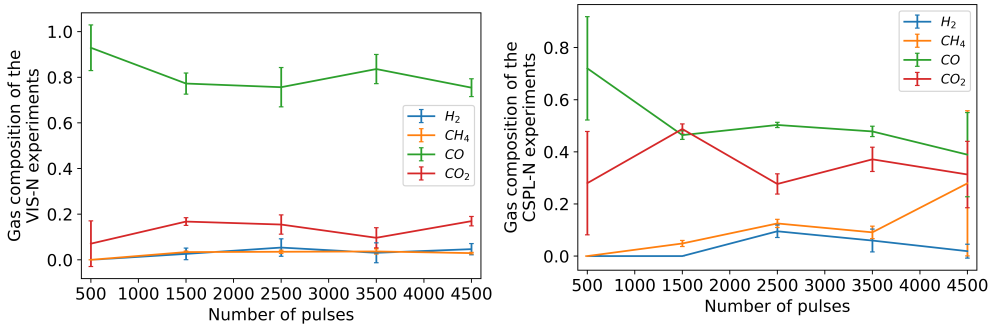

(a) VIS-N **(b)** CSPL-N

Figure 6.9: Comparison of the average gas composition over the pulses duration investigated for the VIS-N and CSPL-N experiments

For the VIS-N experiments, the fraction of CO produced was more than 0.75 for all pulses and the fraction of CO stabilised to about 0.78 from 1500 pulses onwards. The same is observed for the other gases (CO_2, CH_4 and H_2) which results in a stable gas composition from pulses 1500 to 4500. This is because the volume of gas does not increase significantly after 1500 pulses. This is also supported by the fact that there is not a significant change in mass of the fibres over this pulse range as can be seen in Section B.2.2 (Figure B.10). The CSPL-N experiments had a higher fraction of CO_2 in comparison to the VIS-N experiments. This could be as a result of the higher heating rate and the higher energy input of these experiments resulting in higher local temperatures.

6.3.2 Analysis of the liquid hydrolysate for the wet experimental conditions

Low exposure time

The liquid hydrolysate from the PLA and CSPL-H experiments was analysed in terms of the dissolved lignin concentration and the results are given in Figure 6.10.

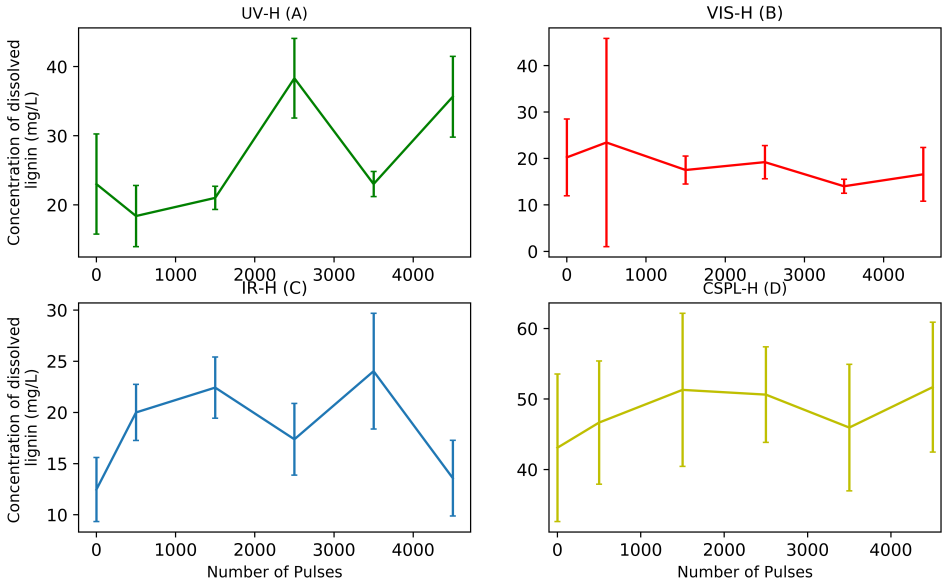

Figure 6.10: Concentration of dissolved lignin in the PLA and CSPL-H experiments for the different pulse durations (A: UV-H, B: VIS-H, C: IR-H and D: CSPL-H)

The peak observed in the UV-VIS spectrophotometer corresponds to the aromatic ring of the lignin structure and the unsaturated carbon bonds [Ohnishi et al., 1989]. From Figure 6.10, it is observed that the concentration of dissolved lignin for the untreated experiments ranges from $12.5 \pm 3.1 mg/L$ to $43 \pm 10.5 mg/L$. This means that a small concentration of lignin dissolved without any pretreatment. From the IR-H (C) pretreatment results it can be observed that the concentration of lignin increases from $12.5 \pm 3.1 mg/L$ to a maximum of $24 \pm 5.7 mg/L$ at 3500 pulses and then decreases again to $13.6 \pm 13.7 mg/L$. Based on a T-test analysis, pulses 2500 and 4500 were not significantly different from the untreated lignin concentration. A similar increasing and decreasing trend is observed for the UV-H (A) experiment. Although, in this experiment, the lignin concentration increase is greater than for the IR-H experiments. The dissolved lignin concentration increases from $23 \pm 7.2 mg/L$ to $38 \pm 1.8 mg/L$ for 2500 pulses and at 4500 pulses an increase is also observed. However, for 3500 pulses no increase in the concentration of lignin is observed in comparison to the untreated control.

There are a few possible reasons for this, the variation in the concentration could be due to the limitation of this experiment. The area of the laser beam is very small, which means not all fibres are exposed to the laser beam and the pretreatment is very localised. The variations in the structure of the fibre in terms of thickness and size could also influence the concentration of dissolved lignin. It was originally thought that this increase and subsequent decrease could be as a result of competing reactions and that the dissolved lignin was being further degraded due to the photochemical reactivity of lignin [Opsahl and Benner, 1998]. However, based on the result of the CSP lignin degradation experiments, no decrease in the concentration of dissolved lignin was observed Section B.2.3.

For both the VIS-H (B) and CSPL-H (D), no clear trend in the increase in the concentration of dissolved lignin with increasing number of pulses was observed. The standard deviation for the concentration of lignin in the VIS-H experiments

was the lowest out of all four experiments (with the exception of 500 pulses). The average concentration of dissolved lignin for the CSPL-H experiments increased by about $7mg/L$/L as the number of pulses increases (with the exception of 3500 pulses). However, the standard deviation is high therefore no significant difference is observed.

Although significant increases in the dissolved lignin concentration were observed for the IR-H and UV-H experiments for some pulse durations and the average concentration of the CSPL-H increased, a clear conclusion on the influences of each wavelength on the lignin concentration can not be made. This variation indicates that these two wavelengths most likely do influence the lignin degradation however the results are not reproducible. The CSPL-H results also showed a high standard deviation, but the overall average did increase.

High Exposure Time

The dissolved lignin concentration for the higher exposure time experiment (CSPL-HE) was analysed and the results are given in Figure 6.11.

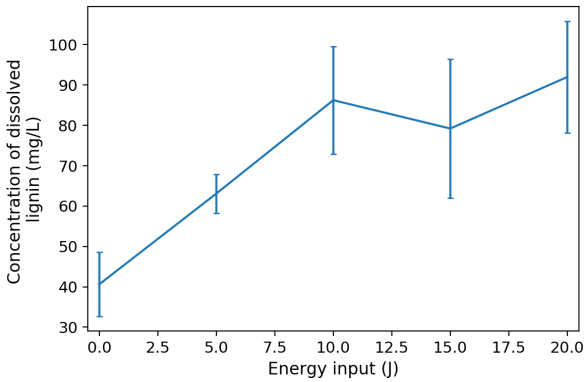

Figure 6.11: Concentration of dissolved lignin in the CSPL-HE experiments

From Figure 6.11, it is observed that the concentration of dissolved lignin increases, with the increasing energy input. Initially, there is steep increase in the concentration and from 10kJ onwards, a fairly stable concentration of dissolved lignin. The average concentration of dissolved lignin after 10kJ was about $86mg/L$. The dissolved lignin concentration from the fibres (CSPL-HE) doubled with an energy input of 10kJ (from $41 \pm 8mg/L$ to $86 \pm 13.3mg/L$) (Figure 6.11). The standard deviation for 15kJ is high ($17.2mg/L$), so no significant difference is observed between this condition and 5kJ. The high variation could be related the high variance in the fibre structure. Both the 10kJ and 20kJ conditions show a significant increase in the concentration in relation to the 5kJ condition.

In addition to the UV-VIS spectrophotometer analysis, the concentration of sugars was analysed using HPLC machine of the blank and the maximum energy input of 20kJ hydrolysate to obtain an indication of the sugar content in the liquid hydrolysate. Glucose was the only sugar present and it was found that the concentration of glucose increased from $61.6 \pm 1.68mg/L$ to $71.4 \pm 3.8mg/L$. This is an indication of the solubilisation of hemicellulose from the fibres due to CSPL-HE pretreatment.

6.4 BIOCHEMICAL ANALYSIS OF THE HOMOGENEOUS COMPOUND, LIGNIN

6.4.1 Analysis of the dissolved lignin concentration for the wet experimental conditions

The dissolved lignin concentration for the homogeneous compound, lignin, under wet experimental conditions was analysed and the results are given in Figure 6.11.

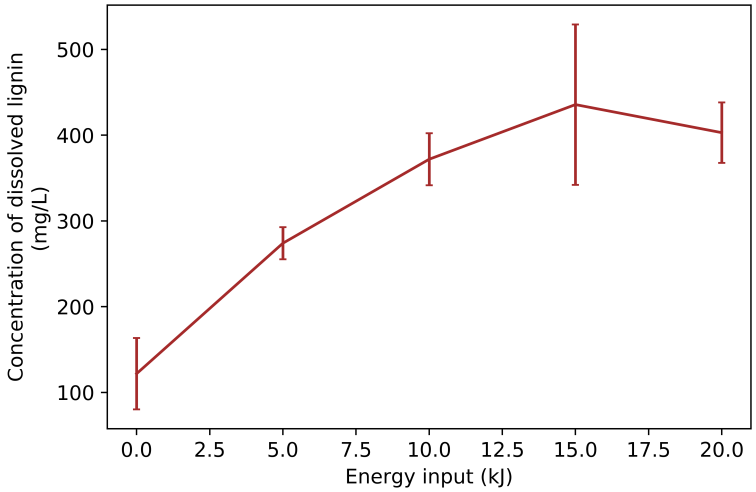

Figure 6.12: Concentration of dissolved lignin in the CSPL-LIG experiments

A similar trend is observed for homogeneous lignin as for the heterogeneous fibres at a higher exposure time. From the pure lignin experiment (CSPL-LIG) in Figure 6.12, the initial concentration of dissolved lignin in the untreated sample was $122 mg/L$ and this increased to a maximum of $435 \pm 93.5 mg/L$. The standard deviation for the concentration of dissolved lignin is more than double than that of the other pulse durations. Despite this high standard deviation, from the other energy inputs (that have a lower standard deviation) it can be observed that gradient decreases with increasing energy input after 5kJ. Therefore, the lignin concentration appears to stabilise after 10kJ to about 400mg/L despite the maximum possible concentration of dissolved lignin (based on the initial mass) being 2 200mg/L.

In an experiment done by Bobleter [1994], it was observed in the degradation of isolated lignin (Willstatter lignin) at $304^{o}C$ that initially an increasing amount of lignin degradation products dissolved. However, the reaction curve levelled of after 10 min, with only 36% of the lignin being dissolved. The reason for this was the recondensation of dissolved products as lignin degraded compounds have a high chemical reactivity. The percentage of how much lignin dissolved increased when the samples were washed with an acetone-water mixture; this could explain why a plateau was reached by both the CSPL-HE (Figure 6.11) and CSPL-LIG.

6.5 VISUAL OBSERVATIONS OF THE WET EXPERIMENTAL CONDITIONS

The CSPL and PLA experiments were visually observed to determine if there any specific observations that can be made from the experiments. For both the heterogeneous fibres and homogeneous lignin, observations were made in how the solution of EFB fibres or pure lignin 'boils'. These observations were made for an energy in-

put of 3.4kJ and higher and a time-lapse photo series of this is given in Figure 6.13. The time-lapse photo series was taken after the experiment was conducted, the observations from during the experiment were intenser.

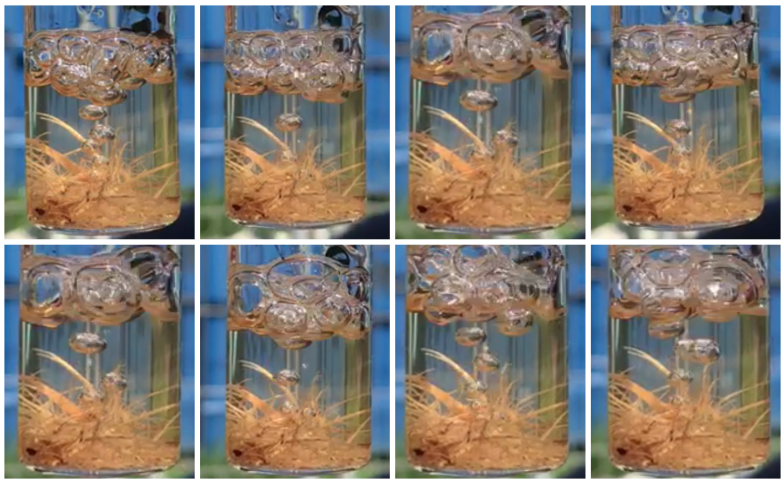

Figure 6.13: Time-lapse photo series of the 'boiling' of the EFB fibre and water mixture

It is noticed that the water does not boil but that the bubbles originate out of the fibres themselves. This could be as a result of the evaporation of the water in the fibres themselves due to the high local point temperature of the Fresnel lens. The same was observed for pure lignin powder and the moisture content of the EFB fibres and the pure lignin powder is 11% and 5% respectively. One of the possible reasons that the water does not boil, is that energy absorbed by the water is less than the energy absorbed by the fibres. Water primarily absorbs the IR wavelength, whilst compounds in EFB have absorption properties for both the UV and VIS wavelength [Wozniak and Dera, 2007; Ranby and Rabek, 1989]. Therefore, the fibres could be heated to a higher temperature than the surrounding water due to a higher photon energy input resulting in the free water evaporating. This evaporation of free water could increase the surface area available and pore size of the fibres which is beneficial for the hydrolysis process [Sanders, 2001; Gomide et al., 2019].

7 DISCUSSION

The Fresnel lens is able to achieve a range of different temperatures, depending on the operating distance from the lens. In particular around the focal length, higher point temperatures are reached than the operational temperature of the HT pretreatment. From the literature study, Section 2.2.2, the maximum temperature reached by the lens (at the focal point) is dependent on the concentration factor. For the same concentration factor, a larger lens will results in a large focal area, but the energy density will be the same. From the dry experiment results (CSPL-N experiments), it was observed that the pretreatment was considered 'severe' and results in more of a treatment than pretreatment. This is supported by the high temperature ($> 400^0C$) reached by the lens at the focal point in a very short time frame. Ideally, the temperature range for the torrefaction should range between $225 - 300^0C$, therefore operating at a point closer to the lens will result in a less severe pretreatment and a lower heating rate. This will also limit the amount of cellulose that will be devolatilised and carbonised, which is beneficial for biogas production.

Based on the BMP test for the wet experimental conditions, it is observed that the CSP-H pretreatment was effective in improving the biodegradability in comparison to the HT pretreatment. In the results from the liquid hydrolysate, it is observed that more lignin and hemicellulose (in the form of glucose, Section B.2.1) has been degraded for the HT pretreatment then the CSP-H pretreatment. This is supported by the structural changes observed in the HT fibres. The HT pretreatment resulted in partial degradation of hemicellulose, partial breakage of the LCCs and exposed cellulose. Based on the studies mentioned in Section 5.2.1, the analysis of the liquid hydrolysate supports the HT BMP result and that the more easily degradable compounds are in the liquid and not in the fibres. This BMP test used only the treated EFB fibres, whilst in literature studies, the combination of the partially hydrolysed EFB fibres and liquid hydrolysate resulted in an improved BMP.

In contrast to the HT pretreatment, for the CSP-H no significant changes were observed in the structure of the fibres and no significant increase in the concentration of dissolved lignin or hemicellulose (in the form of glucose, Section B.2.1). In both the low energy and high energy input CSPL experiments, no significant structural changes in the treated fibres were observed, despite the dissolved lignin concentration of high energy input (CSPL-HE) increasing significantly. A similar observation was made in the experiments pretreating pure lignin powder. This could mean that the bond changes are not severe enough to observe significant structural changes, which is also observed in other studies, for example a study mentioned previously by Park et al. [2013] on the torrefaction of biomass, mentioned that changes were mainly observed in the severe torrefaction pretreatment.

The biodegradability of the CSP-H pretreatment can not be explained based on the FTIR results and analysis of the liquid hydrolysate no clear explanation can be given. There are a few possible reasons that could potentially explain this. Based on the lack of chemical changes and the 'bubbling' of the gas from the EFB fibres it could indicate that the overall changes are more physical than chemical changes. Possible physical changes could be an increase in the surface area or pore size due to the evaporation of the free water in the fibres or cellulose swelling. An increased surface area and pore size improves the hydrolysis of the EFB fibres and subsequently improves the BMP [Sanders, 2001; Gomide et al., 2019]. The high

BMP of the raw fibres obtained in study done by [Kim et al., 2013] also show that the biodegradability increases with an increase in surface area. Lignin is also highly reactive, which results in recondensation lignin and it could be that this structure could be more easily degraded than the original lignin structure in an anaerobic digestion.

Based on the BMP test for the dry experimental conditions, the high RSD of the CSP-N experiment indicates an inhomogeneous pretreatment. The area of exposed fibres was limited due to the small focal area of the lens, resulting in this inhomogeneity. This inhomogeneity could be improved and better controlled if the pretreatment is operated at a point closer to the lens as this would result in better temperature control and a higher surface area of exposure.

For the PLA and CSPL-N experiments, it is observed that the results from the GC analysis coincide with the FTIR analysis. The VIS-N and CSPL-N experiments produced gas for all five pulse durations. The energy input for the VIS-N experiments was significantly higher than the UV-N experiments, which is the most likely reason that that the UV wavelength had only a very small impact on the gas production in the pulse duration investigated. The VIS-N and CSPL-N pretreatment resulted in the partial degradation of the LCCs and, for CSPL-N, more cellulose was exposed after the pretreatment. Furthermore, CO_2 and CO gas is produced from the cracking and reforming of the carboxyl functional groups and this corresponds to the bond changes that were observed for the VIS-N and CSPL-N [Shen et al., 2010].In terms of understanding the influence of the solar spectrum, a direct interaction between the visible wavelength and the gas production is observed. In the CSPL-N experiments, it is observed that the entire spectrum influences the gas production and it is difficult to reproduce this using the three different wavelengths individually.

For the dry experimental conditions, an increase in energy resulted in increased production of gas. In the wet experimental conditions it was expected that there would be increased lignin degradation as a result of the photochemical reactions due to the exposure to the UV and the VIS wavelength. However, lignin degradation was only observed at an overall higher energy input. Based on the analysis of the PLA and CSPL experiments and the observed transmission of the lens (> 350) [Kumar et al., 2015; Leutz and Suzuki, 2001], it is most likely that the predominant effect of the solar radiation is photothermal. A wavelength of 344nm or less is needed to break the bond energy of weakest bonds and this slightly out of the range [Zumdahl et al., 2016]. It is possible that there could photochemical reactions, however this will be difficult to test. The FTIR method developed was able to identify the structural changes observed in the dry experimental conditions and the HT pretreatment. For the wet experimental conditions, the results indicate that the changes in the fibre structure are less severe and could be more physical.

8 CONCLUSION AND OUTLOOK

8.1 CONCLUSION

The conclusion for the specific research questions are given as follows:

1. What temperatures can be achieved by the Fresnel lens at different distances from the centre of the lens for a solar intensity of 1 sun?

   The Fresnel lens is able to reach higher temperatures ($> 400^oC$) than the HT pretreatment in a localised point at the focal point with a surface area of . The temperature achieved by the receiving body is dependent on the concentration factor (assuming the efficiency is equal) and not on the surface area of the lens, therefore a higher concentration factor will result in high temperatures. However, increasing the surface area of the lens will result in a larger focal area, for the same concentration factor. The heating rate at the focal point is significantly higher than at operating at a distance closer to the lens.

2. What are the effects of the CSP pretreatment in comparison to the HT pretreatment in terms of the BMP under thermophilic conditions?

   Under the wet experimental condition, the CSP pretreatment (CSP-H) significantly improved the BMP of the EFB fibres. This is most likely predominantly due to a photothermal effect. Although, there might be a small contribution due to the photochemical effect, but this is difficult to test. The RSD was high for the dry experimental condition, therefore despite the BMP potential being almost double than that of the HT pretreatment, no significant improvement was observed.

3. What are the effects of the exposure time and specific wavelengths in the solar spectrum (UV, VIS, IR) on:
   - The concentration of dissolved lignin in the liquid hydrolysate for the wet conditions?

     No clear conclusion can be made on the influence of the individual wavelengths on the dissolved lignin concentration for the pulse duration investigated. However, based on the results it was observed that the UV and IR wavelength most likely have the biggest influence on the concentration of dissolved lignin. This is because no clear trend was observed in the dissolved lignin concentration and the standard deviation overlapped.
   - The volume and composition of gas produced for the dry experimental conditions?

     It is observed that for the duration analysed, that the VIS wavelength has the greatest influence in terms of the wavelength. However, based on the CSPL experiments, it was concluded that gas production is predominantly due to the photothermal effect of the solar radiation as an increase in the energy increased the gas production at the same rate.

     An increase in the duration of the experiments, only initially increased the volume of gas produced. This was due to limitations in the laser light

area and the mass of sample available. In terms of the gas production, the high heating rate and intensity of the CSPL experiments resulted in a higher fraction of CO_2 in comparison to the VIS-N experiments. Only a very small fraction of H_2 and CH_4 gas were produced for both the VIS-N and CSPL-N experiments. One drawback of this small-scale experiment, is that the torrefaction of EFB fibres in the CSPL-N experiment resulted in the complete charring of the fibres and resulting in a too severe pretreatment. Operating at a distance closer to the lens could pretreat the fibres without charring them completely.

- The fibre structure for the wet and dry condition?

  Clear changes in the fibre structure were only observed in the dry experimental conditions. There were bond breakages observed for the UV and VIS wavelength, with the VIS wavelength showing the greatest change in the chemical structure. An increase in the duration resulted in more severe bond changes due to a increased energy input. No significant changes in the fibre structure were observed for the wet experimental conditions.

This leads to the overall research question and conclusion:

Does the CSP pretreatment improve the biodegradability of the EFB fibres and is it a potential alternative to a HT pretreatment?

The CSP pretreatment does significantly improve the biodegradability of the EFB fibres for the wet experimental conditions. There is a high likelihood that the dry experimental conditions are able to significantly improve the biodegradability if the treatment severity is better controlled. The methodology used in this research did not successfully explain how the wet experimental conditions improved the biodegradability of the EFB fibres. In addition to this, that the three individual wavelengths experiments did not accurately model the effect of the entire spectrum, and that the entire spectrum contributes to the pretreatment. Overall, it can be concluded that the CSP pretreatment is a potential alternative to a HT pretreatment, however further research is required to gain a better understanding of the pretreatment and to use it to its full potential.

8.2 FUTURE IMPLEMENTATION

The CSP pretreatment shows potential to be used as an alternative to the HT pretreatment.However, an important factor to take in consideration is how can this pretreatment be implemented in large scale and most importantly, for a CSP system,what is the required surface area needed, in terms of the Fresnel lens, to implement this pretreatment. The area of solar power required by the CSP system will ultimately lead to how it will be designed.

Based on a back-of-the-envelope calculation for a 1000 hectare of oil palm (Section B.3), about 13 metric tons of EFB are produced per day, this requires a Fresnel lens surface area of 14ha to pretreat the fibres in a continuous process (in the rainy season) [Woittiez et al., 2017]. This is roughly 1.5% of the total area required by the oil palm plantation,which is a very small fraction of the plantation. This was calculated using a solid concentration of $1\%_{w/w}$ and the high water content requires most of the energy. If the pretreatment is as effective at a higher solid concentration; for example $10\%_{w/w}$ then the required surface area required would decrease to 1.5 hectares.

Specific research needs to be addressed to reduce the amount of water used in the pretreatment and reduce the energy losses in both the concentration of the

energy and from the reactor vial. The most important factor to take in consideration with respect to the future implementation of this process is the economic cost and benefit. This leads to the overall conclusion of the future implementation of the pretreatment has potential to be feasible but optimisation of the pretreatment is required to decrease the amount of solar energy needed and an economic analysis is crucial to validate this feasibility.

8.3 EXPERIMENTAL RECOMMENDATIONS

This research was a preliminary study in investigating the potential of CSP to be used as a pretreatment for EFB fibres and although effort was made to minimise the error and ensure reliable results, further research is required to address some of the shortcomings of this research and limitations of this research.

Based on the results of this thesis, a clear understanding of how the CSP pretreatment under wet experimental conditions improves the biodegradability was not achieved. Possible explanations were increased pore size, increased surface area available and a weakened structure of recondensed lignin. It is recommended that further research involves investigating the pore size and surface area available, and this can be done by using the BET (Brunauer, Emmett and Teller) Method [Naderi, 2015].

Furthermore, a SEM (Scanning electron microscopy) analysis may give further insight on how the morphology of the surface of the treated and untreated EFB fibres compare [Kim et al., 2012]. Another analysis that would give insight in the composition of the fibres and possible explain why the HT pretreatment did not improve the biodegradability is a compositional analysis to investigate the percentage of lignin, hemicellulose and cellulose. In addition to this, the thermal camera was not very sensitive to determine a heating profile inside the vials, however, this temperature profile would be able to give more insight on what temperatures are achieved on the surface of the fibres. This could assist in determining the mechanism of pretreatment.

For the dry experimental conditions, it was observed that the severity of the pretreatment was difficult to control, due to the high temperatures reached by the Fresnel lens, operating at distances closer to lens could improve the results. Furthermore, based on the rapid heating rate of the Fresnel lens, there is potential for the lens to be used for a pyrolysis treatment, this would need to be further investigated.

Specifically with respect to the experimental results, there are some improvements necessary. The RSD for the BMP rest was above the required limit in order to conform with the standard. Therefore, it is suggested that this experiment is repeated to improve the reliability of the BMP result. This research was also limited to a simple CSP set-up with uninsulated vials and assumptions were made on the energy input and the efficiency of the lens. In addition to this, the experimental results for the dissolved lignin concentration were not conclusive and the standard deviation was high.

Therefore, the following recommendations are proposed to improve the experimental design:

- improve the Fresnel frame set-up to ensure more consistency amongst the different conditions. In particular for the large vials used as the sunlight is at an angle to the surface of the earth, therefore, optimal exposure is difficult.
- following on from the previous point, it is recommended to perform the experiments in a solar simulator to achieve better consistency and control of the exposure, or using vials that do not require the fibres to be exposed through the top but at a similar angle to the sun.

- using insulated vials, to decrease heat loss of the system, which in turn could improve the pretreatment results.
- perform the PLA experiments with less fibres to increase the exposure of the fibres to the laser.
- increase the pulse duration of the PLA experiments to determine if there is a clear trend for the wet experimental conditions and determine the influence of the UV and IR wavelength on the fibres in the dry experimental conditions.

BIBLIOGRAPHY

Abdullah, N. and Sulaiman, F. (2013). The oil palm wastes in malaysia. In *Biomass Now-Sustainable Growth and Use*. IntechOpen.

Abhilash, M. and Thomas, D. (2017). Biopolymers for biocomposites and chemical sensor applications. In *Biopolymer Composites in Electronics*, pages 405–435. Elsevier.

Achyuthan, K. E., Achyuthan, A. M., Adams, P. D., Dirk, S. M., Harper, J. C., Simmons, B. A., and Singh, A. K. (2010). Supramolecular self-assembled chaos: polyphenolic lignin's barrier to cost-effective lignocellulosic biofuels. *Molecules*, 15(12):8641–8688.

Alvira, P., Tomás-Pejó, E., Ballesteros, M., and Negro, M. (2010). Pretreatment technologies for an efficient bioethanol production process based on enzymatic hydrolysis: a review. *Bioresource technology*, 101(13):4851–4861.

Anwar, Z., Gulfraz, M., and Irshad, M. (2014). Agro-industrial lignocellulosic biomass a key to unlock the future bio-energy: a brief review. *Journal of radiation research and applied sciences*, 7(2):163–173.

Arief, Y. Z., Aziz, N. A., Aziz, P. A., and Wahid, S. (2016). Evaluation of solar energy potential in malaysia. *Trends in Bioinformatics*, 9(2):35–43.

Awalludin, M. F., Sulaiman, O., Hashim, R., and Nadhari, W. N. A. W. (2015). An overview of the oil palm industry in malaysia and its waste utilization through thermochemical conversion, specifically via liquefaction. *Renewable and Sustainable Energy Reviews*, 50:1469–1484.

Bassam, N. E., Maegaard, P., and Schlichting, M. L. (2013). Chapter seven - solar energy. In Bassam, N. E., Maegaard, P., and Schlichting, M. L., editors, *Distributed Renewable Energies for Off-Grid Communities*, pages 91 – 109. Elsevier.

Bergman, P. C., Boersma, A., Zwart, R., and Kiel, J. (2005). Torrefaction for biomass co-firing in existing coal-fired power stations. *Energy Centre of Netherlands, Report No. ECN-C-05-013*.

Bergman, P. C. and Kiel, J. H. (2005). Torrefaction for biomass upgrading. In *Proc. 14th European Biomass Conference, Paris, France*, volume 2005, pages 17–21.

Bobleter, O. (1994). Hydrothermal degradation of polymers derived from plants. *Progress in polymer science*, 19(5):797–841.

Bong, C. P.-C., Goh, R. K. Y., Lim, J.-S., Ho, W. S., Lee, C.-T., Hashim, H., Mansor, N. N. A., Ho, C. S., Ramli, A. R., and Takeshi, F. (2017). Towards low carbon society in iskandar malaysia: Implementation and feasibility of community organic waste composting. *Journal of Environmental Management*, 203:679–687.

Brown, M. S. and Arnold, C. B. (2010). Fundamentals of laser-material interaction and application to multiscale surface modification. In *Laser precision microfabrication*, pages 91–120. Springer.

Chang, S. H. (2014). An overview of empty fruit bunch from oil palm as feedstock for bio-oil production. *Biomass and Bioenergy*, 62:174–181.

Chin, M. J., Poh, P. E., Tey, B. T., Chan, E. S., and Chin, K. L. (2013). Biogas from palm oil mill effluent (pome): Opportunities and challenges from malaysia's perspective. *Renewable and Sustainable Energy Reviews*, 26:717–726.

Chin, S. X., Chia, C. H., Zakaria, S., Fang, Z., and Ahmad, S. (2015). Ball milling pretreatment and diluted acid hydrolysis of oil palm empty fruit bunch (efb) fibres for the production of levulinic acid. *Journal of the Taiwan Institute of Chemical Engineers*, 52:85–92.

Chuayboon, S., Abanades, S., and Rodat, S. (2018). Comprehensive performance assessment of a continuous solar-driven biomass gasifier. *Fuel Processing Technology*, 182:1–14.

Cirne, D., Lehtomäki, A., Björnsson, L., and Blackall, L. (2007). Hydrolysis and microbial community analyses in two-stage anaerobic digestion of energy crops. *Journal of Applied Microbiology*, 103(3):516–527.

Coates, J. (2006). Interpretation of infrared spectra, a practical approach. *Encyclopedia of analytical chemistry: applications, theory and instrumentation*.

Datta, R., Kelkar, A., Baraniya, D., Molaei, A., Moulick, A., Meena, R. S., and Formanek, P. (2017). Enzymatic degradation of lignin in soil: a review. *Sustainability*, 9(7):1163.

Eilers, P. H. and Boelens, H. F. (2005). Baseline correction with asymmetric least squares smoothing. *Leiden University Medical Centre Report*, 1(1):5.

Ersahin, M. E., Ozgun, H., Dereli, R. K., and Ozturk, I. (2011). Anaerobic treatment of industrial effluents: an overview of applications. *Waste water-treatment and reutilization*, pages 9–13.

Evstigneyev, E. I. and Shevchenko, S. M. (2019). Structure, chemical reactivity and solubility of lignin: a fresh look. *Wood science and technology*, 53(1):7–47.

Ewanick, S. and Bura, R. (2010). Hydrothermal pretreatment of lignocellulosic biomass. In *Bioalcohol production*, pages 3–23. Elsevier.

Fackler, K., Stevanic, J. S., Ters, T., Hinterstoisser, B., Schwanninger, M., and Salmén, L. (2010). Localisation and characterisation of incipient brown-rot decay within spruce wood cell walls using ft-ir imaging microscopy. *Enzyme and microbial technology*, 47(6):257–267.

Faix, O. and Böttcher, J. (1992). The influence of particle size and concentration in transmission and diffuse reflectance spectroscopy of wood. *Holz als Roh-und Werkstoff*, 50(6):221–226.

Fernández-Cegrí, V., De la Rubia, M. Á., Raposo, F., and Borja, R. (2012). Effect of hydrothermal pretreatment of sunflower oil cake on biomethane potential focusing on fibre composition. *Bioresource technology*, 123:424–429.

Fitzgerald, G. (2013). Pre-processing and treatment of municipal solid waste (msw) prior to incineration. In *Waste to Energy Conversion Technology*, pages 55–71. Elsevier.

Garrison, B. J. and Srinivasan, R. (1985). Laser ablation of organic polymers: microscopic models for photochemical and thermal processes. *Journal of Applied Physics*, 57(8):2909–2914.

Garrote, G., Dominguez, H., and Parajo, J. (1999). Hydrothermal processing of lignocellulosic materials. *European Journal of Wood and Wood Products*, 57(3):191–202.

Geng, A. (2013). Conversion of oil palm empty fruit bunch to biofuels. In *Liquid, gaseous and solid biofuels-conversion techniques*. IntechOpen.

Gent, S., Twedt, M., Gerometta, C., and Almberg, E. (2017). Fundamental theories of torrefaction by thermochemical conversion. *Theoretical and Applied Aspects of Biomass Torrefaction*, page 41–75.

Gillner, A. and Gretzki, P. (2015). Laser micro-structuring.

Gomide, F. T. F., da Silva, A. S., da Silva Bon, E. P., and Alves, T. L. M. (2019). Modification of microcrystalline cellulose structural properties by ball-milling and ionic liquid treatments and their correlation to enzymatic hydrolysis rate and yield. *Cellulose*, 26(12):7323–7335.

Hafner, S. D. (2019). Calculation of biochemical methane potential (bmp).

Hafner, S. D., Koch, K., Carrere, H., Astals, S., Weinrich, S., and Rennuit, C. (2018). Software for biogas research: Tools for measurement and prediction of methane production. *SoftwareX*, 7:205–210.

Hames, B., Ruiz, R., Scarlata, C., Sluiter, A., Sluiter, J., Templeton, D., et al. (2008). Preparation of samples for compositional analysis. *Laboratory Analytical Procedure (LAP)*, 1617.

He, Y., Pang, Y., Liu, Y., Li, X., and Wang, K. (2008). Physicochemical characterization of rice straw pretreated with sodium hydroxide in the solid state for enhancing biogas production. *Energy & Fuels*, 22(4):2775–2781.

Hirn, G. (2014). Energy from a thousand suns.

Holliger, C., Alves, M., Andrade, D., Angelidaki, I., Astals, S., Baier, U., Bougrier, C., Buffière, P., Carballa, M., and De Wilde, V. (2016). Towards a standardization of biomethane potential tests. *Water Science and technology*, 74(11):2515–2522.

Hosseini, S. E., Bagheri, G., Wahid, M. A., and Saat, A. (2015). Clean fuel, clean energy conversion technology: Experimental and numerical investigation of palm oil mill effluent biogas flameless combustion. *BioResources*, 10(4):6597–6609.

Huang, Y.-B. and Fu, Y. (2013). Hydrolysis of cellulose to glucose by solid acid catalysts. *Green Chemistry*, 15(5):1095–1111.

Irvine, G. (1985). The significance of the glass transition of lignin in thermomechanical pulping. *Wood science and technology*, 19(2):139–149.

Ishola, M., Millati, R., Syamsiah, S., Cahyanto, M., Niklasson, C., Taherzadeh, M., et al. (2012). Structural changes of oil palm empty fruit bunch (opefb) after fungal and phosphoric acid pretreatment. *Molecules*, 17(12):14995–15012.

Janusz, G., Pawlik, A., Sulej, J., Świderska-Burek, U., Jarosz-Wilkołazka, A., and Paszczyński, A. (2017). Lignin degradation: microorganisms, enzymes involved, genomes analysis and evolution. *FEMS microbiology reviews*, 41(6):941–962.

Jönsson, L. J. and Martín, C. (2016). Pretreatment of lignocellulose: formation of inhibitory by-products and strategies for minimizing their effects. *Bioresource technology*, 199:103–112.

Kim, S., Park, J. M., Seo, J.-W., and Kim, C. H. (2012). Sequential acid-/alkali-pretreatment of empty palm fruit bunch fiber. *Bioresource technology*, 109:229–233.

Kim, S.-H., Choi, S.-M., Ju, H.-J., and Jung, J.-Y. (2013). Mesophilic co-digestion of palm oil mill effluent and empty fruit bunches. *Environmental technology*, 34(13-14):2163–2170.

Kumar, V., Shrivastava, R., and Untawale, S. (2015). Fresnel lens: a promising alternative of reflectors in concentrated solar power. *Renewable and Sustainable Energy Reviews*, 44:376–390.

Lee, K. T. and Ofori-Boateng, C. (2013). Oil palm biomass as feedstock for biofuel production. In *Sustainability of biofuel production from oil palm biomass*, pages 77–106. Springer.

Lee, R. A., Bédard, C., Berberi, V., Beauchet, R., and Lavoie, J.-M. (2013). Uv–vis as quantification tool for solubilized lignin following a single-shot steam process. *Bioresource technology*, 144:658–663.

Leutz, R. and Suzuki, A. (2001). *Nonimaging Fresnel lenses: Design and performance of solar concentrators*. Springer.

Lindon, J. C., Tranter, G. E., and Koppenaal, D. (2016). *Encyclopedia of spectroscopy and spectrometry*. Academic Press.

Lovegrove, K. and Csiro, W. S. (2012). Introduction to concentrating solar power (csp) technology. In *Concentrating Solar Power Technology*, pages 3–15. Elsevier.

Lu, Y., Lu, Y.-C., Hu, H.-Q., Xie, F.-J., Wei, X.-Y., and Fan, X. (2017). Structural characterization of lignin and its degradation products with spectroscopic methods. *Journal of Spectroscopy*, 2017.

May, C. Y. (2012). Malaysia: economic transformation advances oil palm industry.

MPOB, M. P. O. B. (2018). Production of crude palm oil for the month of december 2018.

MPOC (2012). Malaysian palm oil industry, malaysian palm oil council.

Mukarakate, C., Scheer, A. M., Robichaud, D. J., Jarvis, M. W., David, D. E., Ellison, G. B., Nimlos, M. R., and Davis, M. F. (2011). Laser ablation with resonance-enhanced multiphoton ionization time-of-flight mass spectrometry for determining aromatic lignin volatilization products from biomass. *Review of Scientific Instruments*, 82(3):033104.

Naderi, M. (2015). Surface area: Brunauer–emmett–teller (bet). In *Progress in filtration and separation*, pages 585–608. Elsevier.

NREL, T. E. (2009). Reference air mass 1.5 spectra.

Nurdiawati, A., Novianti, S., Zaini, I. N., Nakhshinieva, B., Sumida, H., Takahashi, F., and Yoshikawa, K. (2015). Evaluation of hydrothermal treatment of empty fruit bunch for solid fuel and liquid organic fertilizer co-production. *Energy Procedia*, 79:226–232.

Nyakuma, B. B., Johari, A., Ahmad, A., and Abdullah, T. A. T. (2014). Comparative analysis of the calorific fuel properties of empty fruit bunch fiber and briquette. *Energy Procedia*, 52:466–473.

O-Thong, S., Boe, K., and Angelidaki, I. (2012). Thermophilic anaerobic co-digestion of oil palm empty fruit bunches with palm oil mill effluent for efficient biogas production. *Applied Energy*, 93:648–654.

Ohnishi, H., Matsumura, M., Tsubomura, H., and Iwasaki, M. (1989). Bleaching of lignin solution by a photocatalyzed reaction on semiconductor photocatalysts. *Industrial & Engineering Chemistry Research*, 28(6):719–724.

Opsahl, S. and Benner, R. (1998). Photochemical reactivity of dissolved lignin in river and ocean waters. *Limnology and Oceanography*, 43(6):1297–1304.

Park, J., Meng, J., Lim, K. H., Rojas, O. J., and Park, S. (2013). Transformation of lignocellulosic biomass during torrefaction. *Journal of Analytical and Applied Pyrolysis*, 100:199–206.

Paschotta, R. (2008). *Encyclopedia of laser physics and technology*, volume 1. Wiley-vch Berlin.

Pavlostathis, S. G. and Giraldo-Gomez, E. (1991). Kinetics of anaerobic treatment. *Water science and technology*, 24(8):35–59.

Pham, T., Vu, N., and Shin, S. (2017). Daylighting system based on novel design of linear fresnel lens. *Buildings*, 7(4):92.

Qian, E. W. (2014). Chapter 7 pretreatment and saccharification of lignocellulosic biomass.

Ranby, B. and Rabek, J. F. (1989). 12 - photodegradation of polymer materials. In Allen, G. and Bevington, J. C., editors, *Comprehensive Polymer Science and Supplements*, pages 253 – 283. Pergamon, Amsterdam.

Reneta Nafu, Y., Foba-Tendo, J., Njeugna, E., Oliver, G., and Omar Cooke, K. (2015). Extraction and characterization of fibres from the stalk and spikelets of empty fruit bunch. *Journal of Applied Chemistry*, 2015.

Rhino, G. E. (2016). Annual solar irradiance, intermittency and annual variations.

Rieppo, L., Saarakkala, S., Närhi, T., Helminen, H., Jurvelin, J., and Rieppo, J. (2012). Application of second derivative spectroscopy for increasing molecular specificity of fourier transform infrared spectroscopic imaging of articular cartilage. *Osteoarthritis and cartilage*, 20(5):451–459.

Ritschel, C. (2018). The reasons why palm oil is so controversial.

Russo, R. E., Mao, X., Liu, H., Gonzalez, J., and Mao, S. S. (2002). Laser ablation in analytical chemistry—a review. *Talanta*, 57(3):425–451.

Sanders, W. T. M. (2001). *Anaerobic hydrolysis during digestion of complex substrates*.

Sandler, S. I. (2017). *Chemical, biochemical, and engineering thermodynamics*. John Wiley & Sons.

Schafer, R. W. (2011). What is a savitzky-golay filter? [lecture notes]. *IEEE Signal Processing Magazine*, 28(4):111–117.

Selvam, L., Chen, F., and Wang, F. (2010). Solvent effects on blue shifted improper hydrogen bond of cho in deoxycytidine isomers. *Chemical physics letters*, 500(4-6):327–333.

Shankar Tumuluru, J., Sokhansanj, S., Hess, J. R., Wright, C. T., and Boardman, R. D. (2011). A review on biomass torrefaction process and product properties for energy applications. *Industrial Biotechnology*, 7(5):384–401.

Shen, D., Gu, S., and Bridgwater, A. V. (2010). Study on the pyrolytic behaviour of xylan-based hemicellulose using tg–ftir and py–gc–ftir. *Journal of analytical and applied pyrolysis*, 87(2):199–206.

Shi, J. and Li, J. (2012). Metabolites and chemical group changes in the wood-forming tissue of pinus koraiensis under inclined conditions. *BioResources*, 7(3):3463–3475.

Shi, J., Xing, D., and Lia, J. (2012). Ftir studies of the changes in wood chemistry from wood forming tissue under inclined treatment. *Energy Procedia*, 16:758–762.

Shirk, M. and Molian, P. (1998). A review of ultrashort pulsed laser ablation of materials. *Journal of Laser Applications*, 10(1):18–28.

Shrotri, A., Kobayashi, H., and Fukuoka, A. (2017). Catalytic conversion of structural carbohydrates and lignin to chemicals. In *Advances in Catalysis*, volume 60, pages 59–123. Elsevier.

SigmaAldrich (2019). Ir spectrum table and chart.

Sim, S. F., Mohamed, M., Lu, N. A. L. M. I., Sarman, N. S. P., and Samsudin, S. N. S. (2012). Computer-assisted analysis of fourier transform infrared (ftir) spectra for characterization of various treated and untreated agriculture biomass. *BioResources*, 7(4):5367–5380.

Sim, S. F. and Ting, W. (2012). An automated approach for analysis of fourier transform infrared (ftir) spectra of edible oils. *Talanta*, 88:537–543.

Sluiter, A., Hames, B., Ruiz, R., Scarlata, C., Sluiter, J., Templeton, D., et al. (2006). Determination of sugars, byproducts, and degradation products in liquid fraction process samples. *Golden: National Renewable Energy Laboratory*.

Tjeerdsma, B. and Militz, H. (2005). Chemical changes in hydrothermal treated wood: Ftir analysis of combined hydrothermal and dry heat-treated wood. *Holz als roh-und Werkstoff*, 63(2):102–111.

Uddin, M. N., Daud, W. W., and Abbas, H. F. (2014). Effects of pyrolysis parameters on hydrogen formations from biomass: a review. *Rsc Advances*, 4(21):10467–10490.

Virtanen, P., Gommers, R., Oliphant, T. E., Haberland, M., Reddy, T., Cournapeau, D., Burovski, E., Peterson, P., Weckesser, W., Bright, J., et al. (2019). Scipy 1.0–fundamental algorithms for scientific computing in python. *arXiv preprint arXiv:1907.10121*.

Wang, G., Luo, Y., Deng, J., Kuang, J., and Zhang, Y. (2011). Pretreatment of biomass by torrefaction. *Chinese Science Bulletin*, 56(14):1442–1448.

Wieser, M. (2015). Source code for irfpy.ica.baseline.

Woittiez, L. S., van Wijk, M. T., Slingerland, M., van Noordwijk, M., and Giller, K. E. (2017). Yield gaps in oil palm: A quantitative review of contributing factors. *European Journal of Agronomy*, 83:57–77.

Wozniak, B. and Dera, J. (2007). *Light absorption in sea water*, volume 33. Springer.

Xie, W., Dai, Y., Wang, R., and Sumathy, K. (2011). Concentrated solar energy applications using fresnel lenses: A review. *Renewable and Sustainable Energy Reviews*, 15(6):2588–2606.

Xu, F., Sun, J.-X., Sun, R., Fowler, P., and Baird, M. S. (2006). Comparative study of organosolv lignins from wheat straw. *Industrial crops and products*, 23(2):180–193.

Yue, P.-P., Hu, Y.-J., Fu, G.-Q., Sun, C.-X., Li, M.-F., Peng, F., and Sun, R.-C. (2018). Structural differences between the lignin-carbohydrate complexes (lccs) from 2- and 24-month-old bamboo (neosinocalamus affinis). *International journal of molecular sciences*, 19(1):1.

Zavala, J. A. and Ravetta, D. A. (2002). The effect of solar uv-b radiation on terpenes and biomass production in grindelia chiloensis (asteraceae), a woody perennial of patagonia, argentina. *Plant Ecology*, 161(2):185–191.

Zhang, H., Baeyens, J., Degrève, J., and Cacères, G. (2013). Concentrated solar power plants: Review and design methodology. *Renewable and sustainable energy reviews*, 22:466–481.

Zheng, Y., Zhao, J., Xu, F., and Li, Y. (2014). Pretreatment of lignocellulosic biomass for enhanced biogas production. *Progress in energy and combustion science*, 42:35–53.

Zhu, Q. (2015). High-efficiency power generation–review of alternative systems. *IEA Clean Coal Centre*.

Zumdahl, S., Zumdahl, S., and DeCoste, D. (2016). *Chemistry*. Cengage Learning.

A APPENDIX A: METHODOLOGY

A.1 ENERGY CALCULATIONS

A.1.1 Energy determination of the CSP-H

The energy input for the CSP-H experiments was determined from the theoretical amount of energy that is required to heat the EFB/H_2O mixture from 17.5^oC (temperature of the sample) to 180^oC under pressurised conditions. This was calculated using the following equation:

$$Q_{total} = Q_{EFB} + Q_{H2O} \tag{A.1}$$

The energy required to heat up the EFB fibres is calculated as follows:

$$Q_{EFB} = m_{EFB} C_{P,EFB} \Delta T \tag{A.2}$$

where, $C_{P,EFB}$ is equal to $1.483kJ/kg.K$ and ΔT is equal to $162.5K$ [Nyakuma et al., 2014].

The energy required to heat up water under pressure was determined from saturated steam tables, based on the enthalpy of saturated liquid at the respective temperatures and is given by the following equation [Sandler, 2017]:

$$Q_{H2O} = m_{H2O}(\hat{H}^L_{180} - \hat{H}^L_{17.5}) \tag{A.3}$$

where, $\Delta\hat{H}^L$ is equal to $689.9kJ/kg$.

The total energy required was determined using a mass of 1g of EFB fibres and 100g of water, this equates to a total theoretical energy input of 69.2kJ. For the CSPL experiments, the mass of EFB fibres was 50mg and 5ml of water was added, this equates to a total theoretical energy input of 3.46kJ.

Duration of CSP and CSPL experiments

The duration of the CSP and CSPL experiments was determined from the solar intensity (at the time of the experiment) and the energy input required (in Joules). The solar intensity (E_e) ranged from $600W/m^2$ to $1100W/m^2$, depending on the angle of the sun. The area of the lens was calculated to be $0.0583m^2$ (from the dimensions of the lens) and an efficiency of 50% was used. This resulted in the following equation to determine the duration of the experiments (in seconds).

$$t_{CSP} = \frac{Q_{total}}{0.5 E_e A_{lens}} \tag{A.4}$$

A.1.2 Energy determination of the PLA experiments

The PLA experiments were performed by investigating a pulse duration of 500 to 4500 pulses (with an interval of 1000 pulses). The intensity of the PLA experiments was determined from the intensity that will be achieved after the concentration of the solar radiation using the Fresnel lens. Based on a concentration factor of 400, an efficiency of 50% and using the average solar intensity of Malaysia ($824W/m^2$) the concentrated intensity is equal to 164 $700W/m^2$.

The power input (P) of the laser is measurable, therefore the intensity was converted to a power input using the area of the laser beam as given by Equation A.5. The area of the laser beam was calculated from the laser diameter which is equal to $9mm$.

$$P = E_a A_{laser} \tag{A.5}$$

The resultant power and intensity values for the three wavelengths is given in Table A.1.

Table A.1: Power and intensity of the laser for the respective wavelengths

	Percentage of solar radiation (%)	Intensity (W/m^2)	Power (W)
UV	5 [1]	8 235	0.52
VIS	43[1]	70 830	4.5
IR	52 [1]	85 650	5.4
Total	100	164 700	10

[1] This data was obtained from the NASA Langley Research Center (LaRC) POWER Project funded through the NASA Earth Science/Applied Science Program.

The energy input for each of the pulse durations was calculated from the pulse duration (10 pulses per second) and the power input (W). For the VIS wavelength, the maximum power available was insufficient, therefore the number of pulses were adjusted to achieve the required energy input. The corresponding energy input for the pulse durations for UV, VIS and IR are given in Table A.2, Table A.3 and Table A.4 respectively.

Table A.2: Corresponding energy and pulse durations for the UV wavelength

Power (W)	Number of pulses	Time (s)	Energy (J)
0.52	500	50	26.2
0.52	1500	150	78.6
0.52	2500	250	131
0.52	3500	350	183

Table A.3: Corresponding energy and pulse durations for the VIS wavelength

Theoretical power (W)	Actual Power (W)	Energy required (J)	Time (s)	Number of pulses
4.5	2.90	225	78	780
4.5	2.90	676	233	2 330
4.5	2.90	1 130	388	3 880
4.5	2.90	1 580	544	5 440
4.5	2.90	2 030	699	6 990

Table A.4: Corresponding energy and pulse durations for the IR wavelength

Power (W)	Number of pulses	Time (s)	Energy (J)
5.5	500	50	272
5.5	1500	150	817
5.5	2500	250	1 360
5.5	3500	350	1 910
5.5	4500	450	2 450

A.2 BIOMETHANE POTENTIAL (BMP)

A.2.1 Volatile solids (VS) content

The volatile solids content of the different substrates and inoculum are given in Table A.5.

Table A.5: Volatile solids content of substrate and inoculum

	VS
Inoculum (g/ml)	0.012
Cellulose (g/g)	0.840
Raw fibres (g/g)	0.898
CSP-H (g/g)	1.000
CSP-N (g/g)	0.908
HT (g/g)	0.960

A.2.2 Calculation of BMP

The BMP of the different substrates and the cellulose was calculated based on the method describe by Hafner [2019] and is calculated based on the volume of CH_4 produced after 27 days of run time.

The variables used in the calculations are described as follows:

- $V_{CH_4,S,i}$, the standardized volume of CH_4 (mL) produced in bottle i with both inoculum and substrate at time t
- $V_{CH_4,I,j}$, the standardized volume of CH_4 (mL) produced in bottle j with only inoculum at time t
- $m_{I,i}$, the mass of fresh inoculum originally added to bottle i
- $m_{VS,S,i}$, the mass of substrate volatile solids (VS) originally added to bottle i
- n, the number of replicate bottles with inoculum and substrate (in this experiment n is equal to 3)
- k, the number of replicate bottles with only inoculum (in this experiment k is equal to 3)

The average productivity of the inoculum (NmL/g) was calculated from the standardised volume of CH_4 produced and the mass of inoculum added, the equation is given below:

$$\overline{v}_{CH4,I} = \frac{\sum_1^k V_{CH4,I,j}/m_{I,j}}{k} \tag{A.6}$$

The net CH_4 production of the substrate is calculated by the following equation:

$$V_{CH4,S,i,net} = V_{CH4,S,i} - \overline{v}_{CH4,I} \cdot m_{I,j} \tag{A.7}$$

The bottle yield for each bottle is calculated by normalizing the net CH_4 production by the VS mass of the substrate as follows:

$$B_i = V_{CH4,S,i,net} / m_{VS,S,i} \tag{A.8}$$

The BMP for a particular substrate is calculated from the mean of these values.

$$B = \sum_{1}^{n} B_i / n \tag{A.9}$$

A.2.3 Calculation of biodegradability

The biodegradability of the BMP was calculated using Buswell's equation for cellulose and the EFB fibres and these two equations are given in Equation A.10 and Equation A.11 respectively.

$$C_6H_{10}O_5 + H_2O \rightarrow 3CH_4 + 3CO_2 \tag{A.10}$$

$$C_{7.4}H_{12.1}O_5.1 + 1.83H_2O \rightarrow 3.94CH_4 + 3.46CO_2 \tag{A.11}$$

Based on these two equations, the theoretical moles and subsequent volume of methane per gram of VS was calculated from the volatile solids of the two substrates (which was $1.2 g_{VS}$) at STP. This resulted in a theoretical methane yield of 414.5 and 484.2 ml/g_VS for cellulose and EFB respectively.

A.2.4 Calculation of relative standard deviation (RSD) in BMP

The two main sources of error found in the BMP is the variation in the apparent inoculum yield in inoculum-only bottles ($s_{\overline{x},2}$) and the variation in apparent yield among substrate bottles ($s_{\overline{x},1}$).

The total relative standard deviation (RSD) is calculated from the two standard errors mentioned and were calculated as follows:

$$s_{\overline{x},BMP} = \sqrt{\sum_{i=1}^{2} s_{\overline{x},i}^2} \tag{A.12}$$

The standard deviation in the substrate is calculated as follows:

$$s_{\overline{x},1} = \sqrt{\sum_{i=1}^{n} \frac{(B_i - \overline{B})^2}{n-1}} \tag{A.13}$$

The standard error from the inoculum-only CH_4 production is calculated by first determining the error from the individual production of CH_4 in mL per g of inoculum for each inoculum-only bottle as follows:

$$s_{\overline{x},I} = \sqrt{\sum_{j=1}^{n} \frac{(v_{CH4,I,j} - \overline{v}_{CH4,I})^2}{k-1}} \tag{A.14}$$

Therefore, for each of the individual bottles $s_{\overline{x},2,i}$ is calculated as follows (assuming the error in the mass is negligible):

$$s_{\overline{x},2,i} = s_{\overline{x},I} \cdot m_{I,i} \tag{A.15}$$

From these values,$s_{\overline{x},2}$ is calculated as follows:

$$s_{\overline{x},2} = \sqrt{\frac{\sum_{j=1}^{n} s_{\overline{x},2,i}^2}{n}} \tag{A.16}$$

A.3 DETAILED METHOD DEVELOPMENT OF FTIR ANALYSIS

The FTIR analysis method was development based on a method described by Sim et al. [2012] for lignocellulosic biomass and which was originally described in a previous paper by the same author to analyse edible oils [Sim and Ting, 2012]. The following sections describe the code developed and the wet experimental condition pretreatment data was used as an example to demonstrate the code.

The first step in the processing of the data was the normalisation of the data, this is due to the observation of vertical shifting of the FTIR plots due to the background noise. This data normalisation was done by vertically translating the entire graph downwards by the average absorbance for wavenumbers $4000cm^{-1}$ to $3980cm^{-1}$. The Python code is given in Figure A.1.

```
import numpy as np
import os
import pandas as pd
import matplotlib.pyplot as plt
import glob
import scipy.stats as stats

from scipy.sparse.linalg import spsolve
from scipy import sparse
import scipy.signal


#%% Normalisation of the data

#Set your path to the folder containing the .csv files
PATH='C:/Users/Julla/Documents/2019/Masters thesis/Experiments/Results/FTIR/max pulses dried/' # Use your path

#Fetch all files in path
fileNames = os.listdir(PATH)

# Filter file name list for files ending with .asc
fileNames = [file for file in fileNames if '.asc' in file]

## Loop over all files
for file in fileNames:
    ### Read .csv file and append to list
    data = pd.read_csv(PATH + file, skiprows=55, delim_whitespace=True, skipinitialspace=True, index_col=0)
    data.rename (columns={'#DATA': 'Abs'}, inplace=True)
    #normalisation of the data, to ensure the absorbance is 0 at a wavenumber 4000cm-1
    avg=np.average(data.iloc[:20,0])
    data= data-avg
    data.to_csv(file)#replaces all files with corrected data (only wavelength and absorbance)

# %% Import all data in one dataframe
os.chdir("C:/Users/Julla/Documents/2019/Masters thesis/Experiments/Results/FTIR/max pulses dried")
extension = 'asc'
all_filenames = [i for i in glob.glob('*.{}'.format(extension))]
#
#combine all files in the list
combined_csv = pd.concat([pd.read_csv(f) for f in all_filenames ], axis=1, ignore_index=True, join='inner')
```

Figure A.1: Python code for the normalisation of the FTIR Data

The next step was the baseline correction of the data and thereafter, the peaks were identified. The normalised data was imported into Python and averaged for for each of the pretreatments and controls and is given Figure A.2.

```
# %% Import all data in one dataframe
os.chdir("C:/Users/Julla/Documents/2019/Masters thesis/Experiments/Results/FTIR/max pulses dried")
extension = 'asc'
all_filenames = [i for i in glob.glob('*.{}'.format(extension))]
#
#combine all files in the list
combined_csv = pd.concat([pd.read_csv(f) for f in all_filenames ], axis=1, ignore_index=True, join='inner')

#combine every second row (delete wavelength to just have absorbance data)
abs data=(combined csv.iloc[:,1::2])
filenames=pd.DataFrame(all_filenames)
abs_data.columns=filenames #label columns

wavenumber=combined csv.iloc[:,0]
wavenumber.columns=["wavenumber"]
x=wavenumber
legend1=['avg_CSPL-H','avg_IR-H', 'avg_UV-H','avg_VIS-H','avg_control']

#average absorbance for each pretreatment
avg_COD=np.mean(abs_data.iloc[:,0:3], axis=1)
avg_CSPLD=np.mean(abs_data.iloc[:,3:6], axis=1)
avg_IRD=np.mean(abs_data.iloc[:,6:9], axis=1)
avg UVD=np.mean(abs data.iloc[:,9:12], axis=1)
avg_VISD=np.mean(abs_data.iloc[:,12:15], axis=1)
avg_control=np.mean(abs_data.iloc[:,15:30], axis=1)

#combine all pretreatments in one DataFrame
avg=pd.concat([avg_CSPLD,avg_IRD,avg_UVD, avg_VISD,
                       avg control], axis=1, ignore_index=True)
```

Figure A.2: Python code for the importing of the normalised FTIR data and for the determination of the average FTIR data for the pretreatments and controls

The averaged data was used for the baseline correction and peak identification analysis. The baseline correction was performed using an asymmetric least squares smoothing Python code developed by Wieser [2015], which is based on the asymmetric least squares smoothing method developed by Eilers and Boelens [2005]. The Python code is given in Figure A.3.

```
#%% Asymmetric Least Squares smoothing
def als(y, lam, p, itermax):

    """
    Implements an Asymmetric Least Squares Smoothing
    baseline correction algorithm (P. Eilers, H. Boelens 2005)

    Baseline Correction with Asymmetric Least Squares Smoothing
    based on https://github.com/vicngtor/BaySpecPlots

    Baseline Correction with Asymmetric Least Squares Smoothing
    Paul H. C. Eilers and Hans F.M. Boelens
    October 21, 2005

    """
    L = len(y)
    #  D = sparse.csc_matrix(np.diff(np.eye(L), 2))
    D = sparse.eye(L, format='csc')
    D = D[1:] - D[:-1]  # numpy.diff( ,2) does not work with sparse matrix. This is a workaround.
    D = D[1:] - D[:-1]
    D = D.T
    w = np.ones(L)
    for i in range(itermax):
        W = sparse.diags(w, 0, shape=(L, L))
        Z = W + lam * D.dot(D.T)
        z = spsolve(Z, w * y)
        w = p * (y > z) + (1 - p) * (y < z)
    return z
```

Figure A.3: Python code for the importing of the normalised FTIR data and for the determination of the average FTIR data for the pretreatments and controls

The following input data was required:

- *y*: input data (absorbance spectra)
- *lam* (λ): smoothness parameter (can be adjusted by user). The larger the λ value is, the smoother the resultant baseline, *z*
- *p*: weighting deviations. 0.5 = symmetric, <0.5: negative deviations are more suppressed and is recommended for signals with positive peaks.
- *itermax*: number of iterations to perform

This results in the output, *z*, which is the baseline correction. As mentioned in Section 4.5.2, a visual inspection is often suitable to find suitable parameters, this resulted in different input data for the different pretreatments. The input data for the different pretreatments is given in Table A.6.

Table A.6: Asymmetric least squares smoothing input data for the different pretreatments

Pretreatment	Input Data
CSP-H, HT, raw fibres, control-H)	z=als(y, $1e^5$, 0.00001, 100)
CSP-N	z=als(y, $1e^5$, 0.000045, 100)
Wet conditions (CSPL-H, UV-H, VIS-H, IR-H, control-h)	z=als(y, $1e^5$, 0.00002, 200)
Wet conditions (CSPL-HE)	z=als(y, $1e^5$, 0.00001, 200)
Wet conditions (CSPL-LIG)	z=als(y, $1e^5$, 0.000025, 200)
Dry conditions (CSPL-N, UV-N, VIS-N, IR-N, raw)	z=als(y, $1e^5$, 0.00002, 200)

The baseline is then subtracted from the normalised FTIR data. Thereafter, the peaks were identified in the averaged final corrected data for each pretreatment

and the control fibres (raw, control-H and control). The peaks were identified using a peak identification function from the Scipy package in Python [Virtanen et al., 2019]. The limitation of this peak identification function is that it is sensitive to noise. To reduce the noise, the final corrected data was also subjected to smoothing before peak identification using a Savitzky-Golay function from the Scipy package in Python [Virtanen et al., 2019]. However, this smoothing can also result in losses of small peaks therefore, conservative smoothing was implemented. The smoothing function parameters are the window length and polyorder. The higher the ratio of these two, the more smoothed the data is. Therefore, a window length of 27 and polyorder of 3 was chosen, which did not result in smoothing of small peaks. However, this did not eliminate all the noise, therefore it was required to compare the identified peaks to visually observed peaks in the FTIR plot and to literature data [Sim et al., 2012; Ishola et al., 2012; SigmaAldrich, 2019]. This resulted in the identified peaks given in the code in Figure A.4.

```
#baseline correction for each of the pretreatments (averaged absorbance)
#loops through FTIR results for each pretreatment
for column in avg:
#Select column contents by column name using [] operator
    y1 = avg[column] #original FTIR data

    plt.figure(31, figsize=(15, 8))
    plt.rc('xtick', labelsize=9)    # fontsize of the tick labels
    plt.rc('ytick', labelsize=9)    # fontsize of the tick labels
    plt.xlabel(r'$Wavenumber(cm^{-1})$', fontsize=10)
    plt.ylabel('Absorbance (Au)', fontsize=10)
    plt.legend(legend1,loc='best', fontsize=8)
    plt.ylim(0, 0.20)


    z1=als(y1, 1e5, 0.00002, 200) #baseline
    final=y1-z1 #corrected FTIR plot

    #smoothing of the FTIR plot
    final = scipy.signal.savgol filter(final, 27 , 3, deriv=0)
    #identification of the peaks
#    peaks,  =scipy.signal.find_peaks(final, height=0.0)
    #print(x[peaks])

    #identified peaks
    xcoords = [695, 770, 897,1032,1103, 1161, 1238, 1319, 1372, 1423, 1461, 1506,1595, 1643, 1730, 2902, 3340]
    for xc in xcoords:
        plt.axvline(x=xc,color='brown', linestyle=':', label=' nolegend ', linewidth=1)
        plt.text(xc,0.188,xc, fontsize=7, rotation=90, rotation_mode='anchor')
    xcoords = [2970]
    for xc in xcoords:
        plt.axvline(x=xc,color='green', linestyle=':', label=' nolegend ', linewidth=1)
        plt.text(xc,0.188,xc, fontsize=7, rotation=90, rotation_mode='anchor')

    plt.plot(wavenumber[200:3900], final[200:3900])
    plt.gca().invert xaxis()
    plt.legend(legend1,loc='best', fontsize=8)
    plt.savefig('FTIRAnalysis_MaxPulses_WetConditions', dpi=1000)
```

Figure A.4: Python code for the baseline correction and peak identification of the average normalised FTIR data for the pretreatments

The T-test comparison was implemented on the second derivative data. Each triplicate, for all the pretreatments (including the controls) was subjected to the above mentioned correction of the data, with the last step being the determination of the second derivative using the same Savitzy-Golay smoothing function. This code is given in Figure A.5.

The second derivative data for the different pretreatments was then compared to the respective 'control' fibres using a T-test. Only the identified peaks were compared using the T-test. For the dry conditions, this was the raw fibres and for the wet conditions, this was control-H for the CSP and HT experiment and control-h for the CSPL wet experiments. The function used for the t-test analysis, was a multi-comparison function from StatsModels. The multi-comparison includes a correction factor for multiple paired comparisons, this however is not necessary for this data. The pretreatments are only compared to the control so uncorrected p-value was taken to observe if there any significant changes ($p<0.05$). The Python code for the T-test is given in Figure A.6.

```
#%% Data processing of all the data for the T-test analysis
data_deriv=pd.DataFrame()
#baseline correction for all the FTIR data (each triplicate)
#loops through FTIR results
for column in abs data:
# Select column contents by column name using [] operator
    y2 = abs_data[column] #original FTIR data
    z2=als(y2, 1e5, 0.00002, 200)  #baseline
    final=y2-z2  #corrected FTIR plot

    #determining the second derivative and smoothong of the data
    # window size 27, polynomial order 3
    y deriv = scipy.signal.savgol filter(final, 27 , 3, deriv=2)
    # Grouping and saving the data in a DataFrame
    y deriv2=pd.DataFrame(y deriv )
    y deriv2=y deriv2.transpose()
    data deriv=data deriv.append(y deriv2)
#final second derivative dataframe for all the pretreatments (for each triplicate)
data_deriv=data_deriv.transpose()
```

Figure A.5: Python code for the correction of the FTIR data and the second derivative determination for each triplicate, for all the pretreatments (including the controls)

```
#%% T-test analysis
#dataframe labeling for Ttest analysis
data_labels=['wavenumber','CSPL-HE',
                    'CSPL-HE',
                    'CSPL-HE',
                    'CSPL-H',
                   'CSPL-H',
                   'CSPL-H',
                   'IR-H',
                   'IR-H',
                   'IR-H',
                   'UV-H',
                   'UV-H',
                   'UV-H',
                   'VIS-H',
                   'VIS-H',
                   'VIS-H',
                   'control',
                   'control',
                   'control',
                   'control',
                   'control',
                   'control',
                   'control',
                   'control',
                   'control',
                   'control',
                   'control',
                   'control',
                   'control',
                   'control',
                   'control',
                   'control']

#wavenumbers that are compared
wn=[695, 770, 897,1032,1103, 1161, 1238, 1319, 1372, 1423, 1461, 1506,1595, 1643, 1730, 2902, 2921, 2970, 3340]
wn=pd.DataFrame(wn)
wn=wn.transpose()

#combining wavenumbers and second derivative data in one DataFrame and labelling columns
data_ttest=pd.concat([wavenumber, data_deriv], axis=1)
data_ttest.columns=data_labels

#looping through each wavenumber FTIR result and performing a ttest analysis
for column in wn:

    wn_data=wn[column]
    print(wn_data, 'wavenumber')
    #specifically analysing the wavenumbers that are relavent for EFB
    data_ttest1=data_ttest.iloc[4000- wn_data,:]
    print(data_ttest1)
    data_ttest1_melt = pd.melt(data_ttest1, id_vars=['wavenumber'], value_vars=['CSPL-HE', 'CSPL-H', 'IR-H', 'UV-H', 'VIS-H', 'control'])

    # replace column names
    data_ttest1_melt.columns = ['wavenumber', 'Treatment', 'Abs']

    #Ttest analysis
    from statsmodels.stats.multicomp import MultiComparison
    mod=MultiComparison(data ttest1 melt['Abs'], data_ttest1_melt['Treatment'])
    rtp = mod.allpairtest(stats.ttest_ind)
    print(rtp[0])
```

Figure A.6: Python code for the T-test analysis for the specific wavenumbers

A.3.1 Particle size distribution

The EFB fibres were shredded to an average particle size range of about 2 to 4*mm*, prior to being analysed using the FTIR spectroscopy. The particle size distribution is given in Figure A.7.

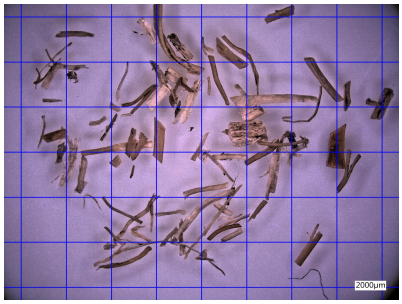

Figure A.7: Particle size distribution of EFB fibres prior to the FTIR analysis

A.4 ADDITIONAL LIQUID HYDROLYSATE ANALYSIS – HPLC

High-performance liquid chromatography (HPLC) was used as additional analysis to determine if there were any sugar compounds as a result of hemicellulose and cellulose degradation. The method used was based on the Laboratory Analytical Procedure(LAP) developed by Sluiter et al. [2006] for the determination of sugars in liquid samples. The following sugar compounds were investigated: $D-(+)$ glucose, D-cellobiose, $D-(+)$ xylose, $L-(+)$ arabinose, $D-(+)$ mannose and $D-(+)$ galactose. A Shimadzu HPLC device equipped with Biorad Aminex HPX-87H column and a refractive index detector was used. The mobile phase was a 0.005M sulphuric acid (H_2SO_4) mixture with a flow rate of $0.6ml/min$. The pH of the samples is required to be below and this was achieved by the addition of $40\mu L$, 2M sulphuric acid. The column temperature was set to 40^oC and the run time was $15min$. A five-point calibration curve was produced for using a concentration range from $50mg/L$ to $1000mg/L$ and the relationship between peak area (from the HPLC analysis) and concentration was used to determine the concentration of the different compounds in the samples.

B APPENDIX B: RESULTS

B.1 STRUCTURAL ANALYSIS OF THE PRETREATED FIBRES

B.1.1 Detailed FTIR analysis CSP pretreatments

A detailed description of the wavenumbers where significant changes were observed for the respective pretreatments(CSP-N, CSP-H and HT) based on a T-test analysis of the second derivative of the FTIR data is given in Table B.1. The functional groups that are associated with the specific wavenumbers and the corresponding component is also given in Table B.1.

B.1.2 Detailed FTIR analysis CSPL and PLA pretreatments for the wet experimental conditions (low energy input)

A detailed description of the wavenumbers where significant changes for the wet experimental conditions at a low energy input is given in this section. A complete list of the observed changes for the respective pretreatments (CSPL-H, UV-H, VIS-H and IR-H) based on a T-test analysis of the second derivative of the FTIR data is given in Table B.2. The pretreatments were compared to the control: control-h. The functional groups that are associated with the specific wavenumbers and the corresponding component is also given in Table B.2. The FTIR results for the intermediate pulse durations, 500 and 2500, (for all experiments) are given in Figure B.1 to Figure B.4 and are mentioned if any significant changes were observed for the other pulse durations.

Significant changes were observed for the wavenumbers 1237 and $1730 cm^{-1}$, with a decrease in the peak absorption. A significant decrease in the absorption for these peaks were also observed for pulses 500 and 2500 for the CSPL-H pretreatment (Figure B.4). These wavenumbers correspond to the LCCs and a decrease in the absorption could be as a result of damage to these ether bonds linking lignin and carbohydrate. Changes in the LCCs linkages could mean that more cellulose is exposed and available for bio-degradation. This is also observed for the UV-H pretreatment for the maximum pulses of 4500 and 2500 pulses for both these wavenumbers (Figure B.1).

A decrease in the absorption for wavenumber $1372 cm^{-1}$ for both CSPL-H and UV-H was observed. This could be as a result of degradation of hemicellulose and cellulose into sugars such as glucose. In the region of wavenumbers 1300 to $1600 cm^{-1}$, it is observed that there is an increase in the absorption for wavenumbers 1423, 1461, 1506 and $1595 cm^{-1}$ for the IR-H pretreatment; wavenumbers 1506 and $1595 cm^{-1}$ are assigned to the aromatic ring vibrations in lignin. The reason for the enhancement of these bands could be due to the accumulation of condensed degraded polysaccharides and breakage of lignin. This results in the original network structure to change from a three-dimensional structure to a linear structure [He et al., 2008]. For the UV-H pretreatment, the absorption decreased, which could mean that the degraded polysaccharides did not accumulate to the same extent as in the IR-H pretreatment. Wavenumber $1423 cm^{-1}$ is assigned to CH_2 scissors vibrations in cellulose and an increase in the absorption for this peak could be as a result of cellulose being more exposed due in the IR-H pretreatment.

Table B.1: Absorption peaks detected, associated functional groups and the corresponding pretreatments where significant changes were observed (based on a T-test analysis of the second derivative of the FTIR data) for the CSP pretreatments

Absorption Peak	Functional group and corresponding component	Corresponding pretreatment ($p<0.05$)
661	-CH bending (cellulose)[1]	HT
692	-CH bending (cellulose)[1]	CSP-N, HT
754	-CH bending (cellulose)[1]	CSP-N
770	CH_2 vibration (cellulose)[1]	CSP-N
811	-CH bending (cellulose)[1]	CSP-N
849	-CH out of plane deformation in position 2, 5, 6 (lignin)[2]	HT
897	*C-O-C* stretching of the asymmetric ring and *CH* rocking vibrations, Glycosidic linkages and breakage degree of intramolecular bonds (cellulose) [3]	CSP-N
1032	Vibrational stretching of *C-O*, *C=O*, *C-C-O*, deformation in primary alcohols (lignin and cellulose I, II)[4,5]	HT
1055	C-OH stretching vibration (cellulose and hemicellulose)[4]	HT
1103	Ring asymmetric stretching (cellulose)[5]	HT
1160	*C-O-C* asymmetric stretching of glycosidic linkages (cellulose I and II, hemicellulose)[4]	HT
1237	*C-O* stretching of ether bonds (lignin and hemicellulose)[5,6,8]	CSP-N
1269	Syringyl ring breathing and *C-O* stretching (lignin and hemicellulose)[7,8]	HT
1372	-CH deformation vibration (cellulose and hemicellulose)[6]	CSP-N
1425	CH_2 bending (cellulose/lignin)[6]	HT
1460	-OH in plane bending (cellulose) and aliphatic part of lignin [1,3]	HT
1511	*C=C* stretching vibrations of aromatic rings of lignin [3]	HT
1644	C=O stretching vibration in conjugated carbonyl of lignin[6]	CSP-N,CSP-H ($p = 0.0566$)
1730	C=O stretching stretch in unconjugated ketone and carboxyl group – ester bonds (lignin and hemicellulose)[5,6,8]	CSP-N, HT
2920	*-CH* stretching (cellulose, hemicellulose, lignin)[4]	CSP-N
3336	*-OH* stretching - intramolecular hydrogen bonded (cellulose, hemicellulose, lignin)[4]	HT, CSP-H ($p = 0.0594$)

[1] Coates [2006], [2] Fackler et al. [2010], [3] Ishola et al. [2012], [4] Shi and Li [2012], [5] Faix and Böttcher [1992], [6] Shi et al. [2012], [7] Yue et al. [2018], [8] He et al. [2008],

B.1.3 Detailed FTIR analysis of the CSPL-HE pretreatment for the wet experimental conditions (high energy input)

A detailed description of the wavenumbers where significant changes for the wet experimental conditions at a high energy input is given in this section. A detailed list of the observed changes for the different energy inputs is given in Table B.3. From Figure 6.4, it is observed that absorbance of the 15kJ is significantly lower than that of the other pretreatments and the specific peaks where changes are observed are given in Table B.3. Changes are observed in the aromatic ring of lignin (1506 and $1595cm^{-1}$), this is most likely due to bond breakages, and a decrease in the cellulose and hemicellulose content of the fibres is also noted due to a decrease in the peak absorbance of wavenumbers 1372 and $1423cm^{-1}$. The only visible change observed is for the 10kJ, where there is an additional peak seen at wavenumber $2935cm^{-1}$. As mentioned previously wavenumbers around $2900cm^{-1}$ are associated with the asymmetrical stretching of *-CH* bond. An additional peak could indicate changes to

Table B.2: Absorption peaks detected, associated functional groups and the corresponding pretreatments where significant changes were observed (based on a T-test analysis of the second derivative of the FTIR data) for the CSPL wet pretreatments

Absorption Peak	Functional group and corresponding	Corresponding pretreatment ($p<0.05$)
1032	Vibrational stretching of *C-O*, *C=O*, *C-C-O*, deformation in primary alcohols (lignin and cellulose I, II)[4,5]	UV-H, VIS-H
1238	*C-O* stretching of ether bonds (lignin and hemicellulose)[5,6,8]	CSPL-H, UV-H,
1372	-CH deformation vibration (cellulose and hemicellulose)[6]	UV-H, CSPL-H
1423	CH_2 bending (cellulose/lignin)[6]	IR-H
1461	-OH in plane bending (cellulose) and aliphatic part of lignin [1,3]	UV-H, VIS-H, IR-H
1506	*C=C* stretching vibrations of aromatic rings of lignin [3]	UV-H, VIS-H, IR-H
1595	C-C (in ring) stretch, aromatic ring vibration (lignin) [3]	UV-H, IR-H, VIS-H (p=0.056), CSPL-H (p=0.065)
1730	C=O stretching stretch in unconjugated ketone and carboxyl group – ester bonds (lignin and hemicellulose) [5,6,8]	UV-H, CSPL-H
2902	-CH stretching (cellulose, hemicellulose, lignin)[4]	UV-H
2970	-CH stretching (cellulose, hemicellulose, lignin)[4]	UV-H, VIS-H

[1] Coates [2006], [2] Fackler et al. [2010], [3] Ishola et al. [2012], [4] Shi and Li [2012], [5] Faix and Böttcher [1992], [6] Shi et al. [2012], [7] Yue et al. [2018], [8] He et al. [2008],

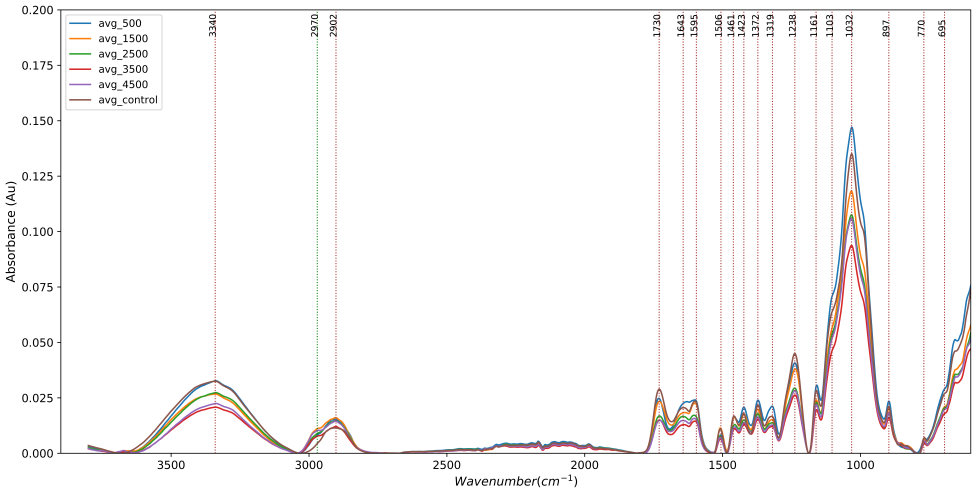

Figure B.1: FTIR analysis of the UV-H wavelength pretreated EFB fibres for pulse durations 0 to 4500 pulses (averaged results)

the hydrogen bonds because blue shifts of the peak around $2902cm^{-1}$ are associated with OH bonded -CH bonds [Selvam et al., 2010].

Peak changes are observed for pretreatments 5kJ, 15kJ and 20kJ for the wavenumber $1730cm^{-1}$. The absorption peak at $1730cm^{-1}$ is associated with the C=O stretching of ester bonds [He et al., 2008]. Therefore, changes in this peak indicate changes to the LCCs, although for 5kJ and 15kJ there is a decrease in the adsorption, indicating the breakages of these bonds. Whilst for 20kJ, there is an increase in the adsorption (possible recondensation of dissolved lignin and other polysaccharides) and no effect is seen for the 10kJ pretreatment [He et al., 2008].

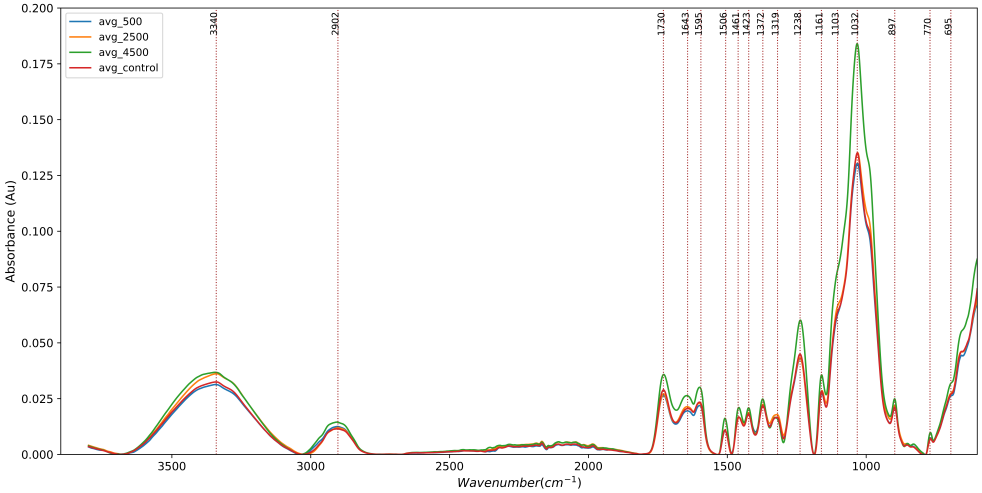

Figure B.2: FTIR analysis of the VIS-H wavelength pretreated EFB fibres for pulse durations 0 to 4500 pulses (averaged results)

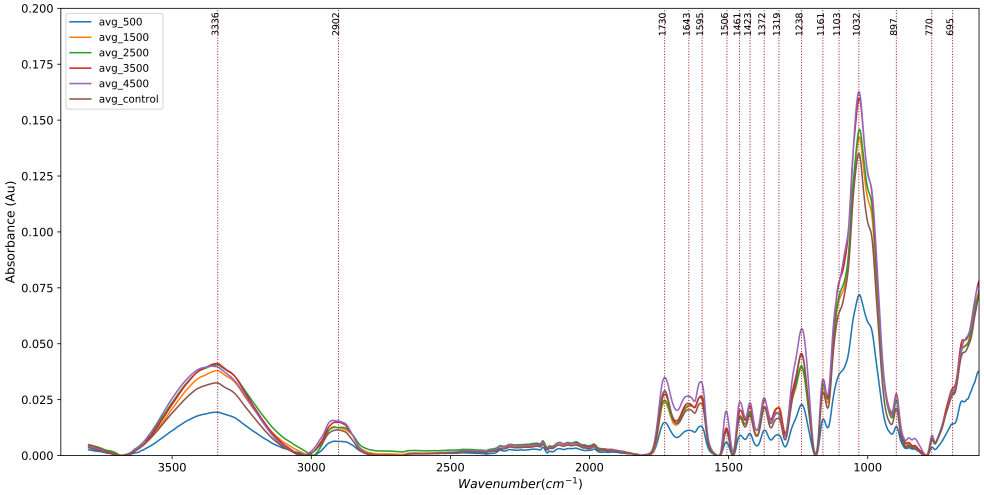

Figure B.3: FTIR analysis of the IR-H wavelength pretreated EFB fibres for pulse durations 0 to 4500 pulses (averaged results)

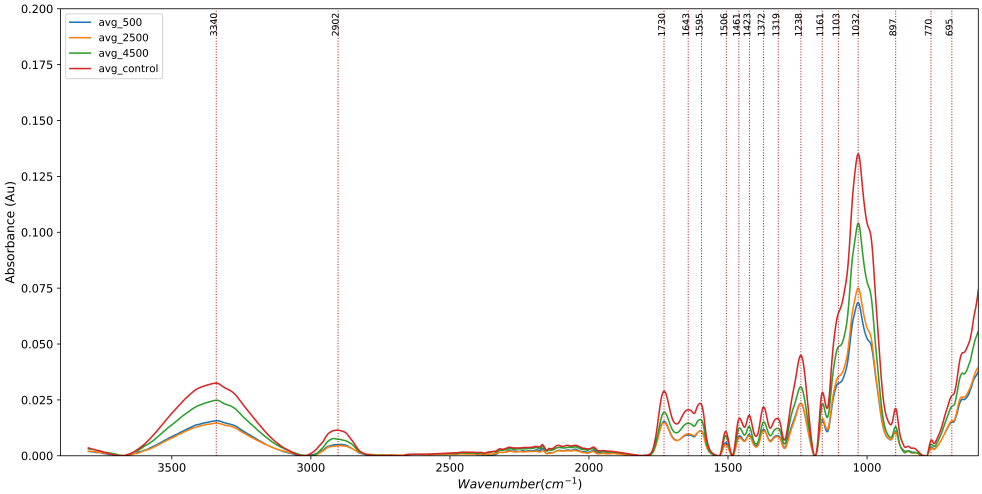

Figure B.4: FTIR analysis of the CSPL-H wavelength pretreated EFB fibres for pulse durations 0 to 4500 pulses (averaged results)

Table B.3: Complete list of significant changes observed in comparing the second derivative results for the CSPL-HE experiment to the untreated blank fibres

Absorption Peak	Functional group and corresponding	Corresponding pretreatment ($p<0.05$)
1032	Vibrational stretching of *C-O*, *C=O*, *C-C-O*, deformation in primary alcohols (lignin and cellulose I, II)[4,5]	15kJ
1238	*C-O* stretching of ether bonds (lignin and hemicellulose)[5,6,8]	15kJ
1372	-CH deformation vibration (cellulose and hemicellulose)[6]	15kJ
1423	CH_2 bending (cellulose/lignin)[6]	15kJ
1461	-OH in plane bending (cellulose) and aliphatic part of lignin [1,3]	15kJ
1506	C=C stretching vibrations of aromatic rings of lignin [3]	15kJ
1595	C-C (in ring) stretch, aromatic ring vibration (lignin) [3]	15kJ
1643	C=O stretching vibration in conjugated carbonyl of lignin[6]	20kJ
1730	C=O stretching stretch in unconjugated ketone and carboxyl group – ester bonds (lignin and hemicellulose) [5,6,8]	5kJ, 15kJ, 20kJ
2935	-CH stretching (cellulose, hemicellulose, lignin)[4]	5kJ,15kJ, 20kJ

[1] Coates [2006], [2] Fackler et al. [2010], [3] Ishola et al. [2012], [4] Shi and Li [2012], [5] Faix and Böttcher [1992], [6] Shi et al. [2012], [7] Yue et al. [2018], [8] He et al. [2008],

B.1.4 FTIR analysis of the CSPL-LIG pretreatment for the wet experimental conditions (high energy input)

The FTIR analysis for the homogeneous lignin powder experiments is given in Figure B.5 and no significant changes were observed for any of the peaks identified.

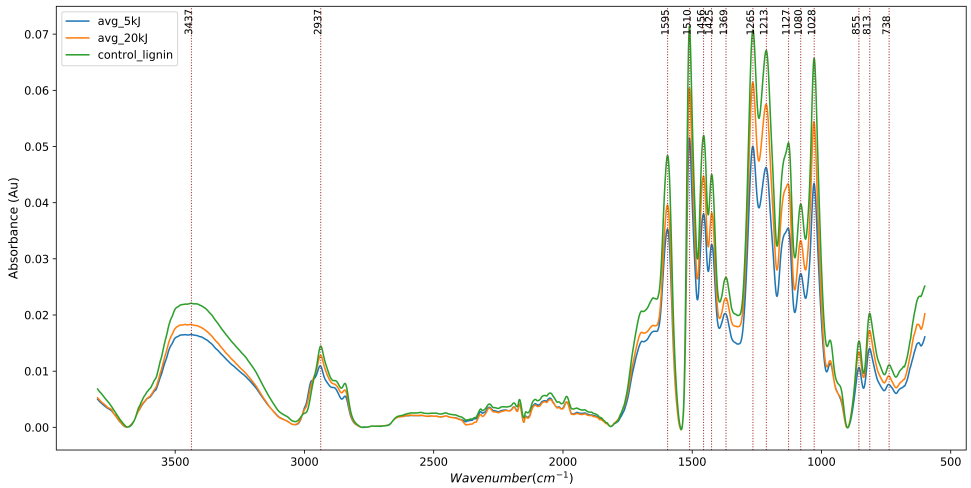

Figure B.5: FTIR analysis of the CSPL-LIG wavelength pretreated EFB fibres for an energy in put of 0 to 20kJ (averaged results)

B.1.5 Detailed FTIR analysis of the CSPL and PLA pretreatments for the dry experimental conditions

A detailed description of the wavenumbers where significant changes were observed for the respective pretreatments (CSPL-N, UV-N, VIS-N and IR-N) based on a T-test analysis of the second derivative of the FTIR data is given in Table B.4.

The pretreatments were compared to the control, the raw fibres. The functional groups that are associated with the specific wavenumbers and the corresponding component is given in Table B.4

Table B.4: Absorption peaks detected, associated functional groups and the corresponding pretreatments where significant changes were observed (based on a T-test analysis of the second derivative of the FTIR data) for the CSPL dry pretreatments

Absorption Peak	Functional group	Corresponding pretreatment
692, 754, 770	CH bending and CH_2 vibration (cellulose)[1]	CSPL-N
811	CH bending (cellulose)[1]	CSPL-N, UV-N, VIS-N
849	-CH out of plane deformation in position 2, 5, 6 (lignin)[2]	CSPL-N
897	*C-O-C* stretching of the asymmetric ring and *CH* rocking vibrations, Glycosidic linkages and breakage degree of intramolecular bonds (cellulose) [3]	CSPL-N
1160	*C-O-C* asymmetric stretching of glycosidic linkages (cellulose I and II, hemicellulose)[4]	CSPL-N
1239	*C-O* stretching of ether bonds (lignin and hemicellulose)[5,6,8]	CSPL-N
1269	Syringyl ring breathing and *C-O* stretching (lignin and hemicellulose)[7,8]	CSPL-N
1319	C-H in plane bending/CH_2 wagging (cellulose, hemicellulose)[3,6]	CSPL-N
1511	*C=C* stretching vibrations of aromatic rings of lignin [3]	CSPL-N
1644	C=O stretching vibration in conjugated carbonyl of lignin[6]	CSPL-N
1730	C=O stretching stretch in unconjugated ketone and carboxyl group – ester bonds (lignin and hemicellulose)[5,6,8]	CSPL-N (1704), VIS-N (1720)
2898, 2920, 2938	CH stretching (cellulose, hemicellulose, lignin)[4]	CSPL-N (2898), VIS-N (2920), VIS-N and UV-N (2938)
3336	*-OH* stretching - intramolecular hydrogen bonded (cellulose, hemicellulose, lignin)[4]	CSPL-N (3395)

[1] Coates [2006], [2] Fackler et al. [2010], [3] Ishola et al. [2012], [4] Shi and Li [2012], [5] Faix and Böttcher [1992], [6] Shi et al. [2012], [7] Yue et al. [2018], [8] He et al. [2008],

FTIR analysis of the CSPL and PLA pretreatments for an increasing pulse duration (dry conditions)

The FTIR analysis for the different wavelengths (UV, VIS and IR) as well as the CSPL-N experiment for the different pulse durations are given in Figure B.6 to Figure B.9.

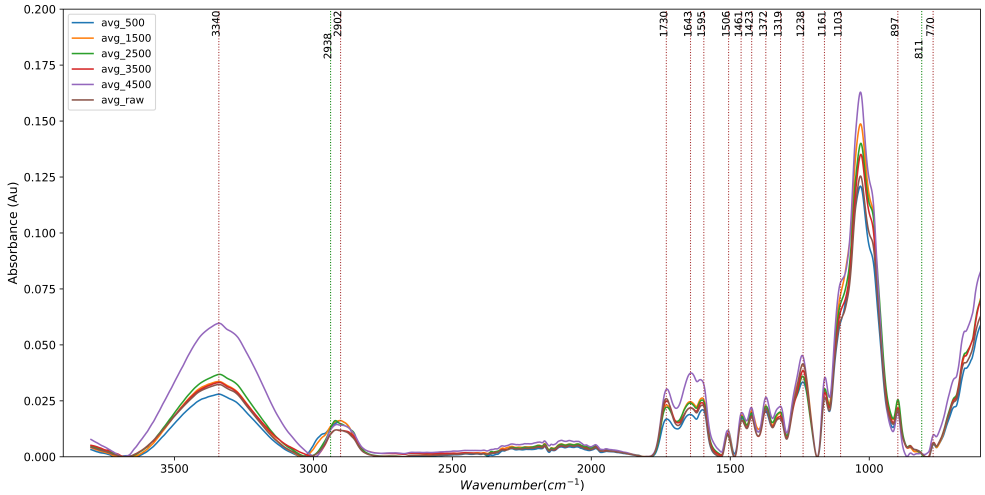

Figure B.6: FTIR analysis of the UV-N wavelength pretreated EFB fibres for pulse durations 0 to 4500 pulses (averaged results)

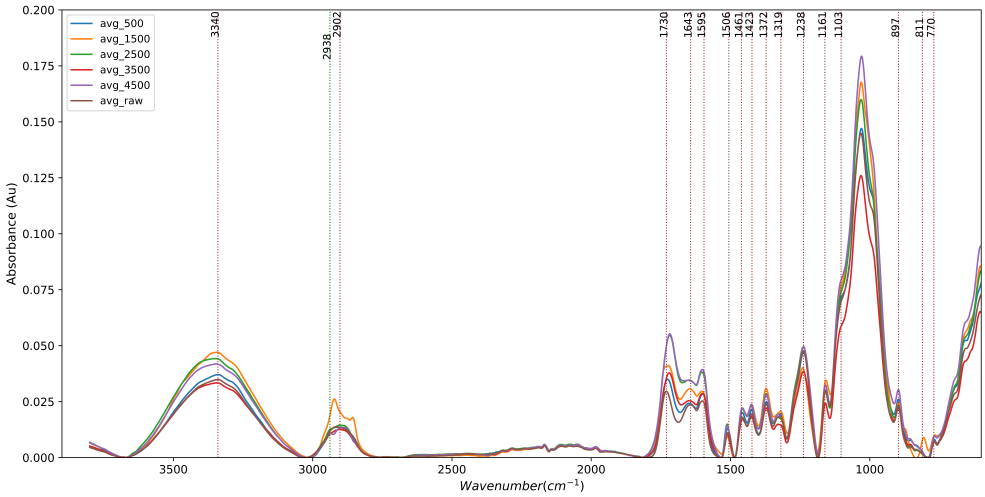

Figure B.7: FTIR analysis of the VIS-N wavelength pretreated EFB fibres for pulse durations 0 to 4500 pulses (averaged results)

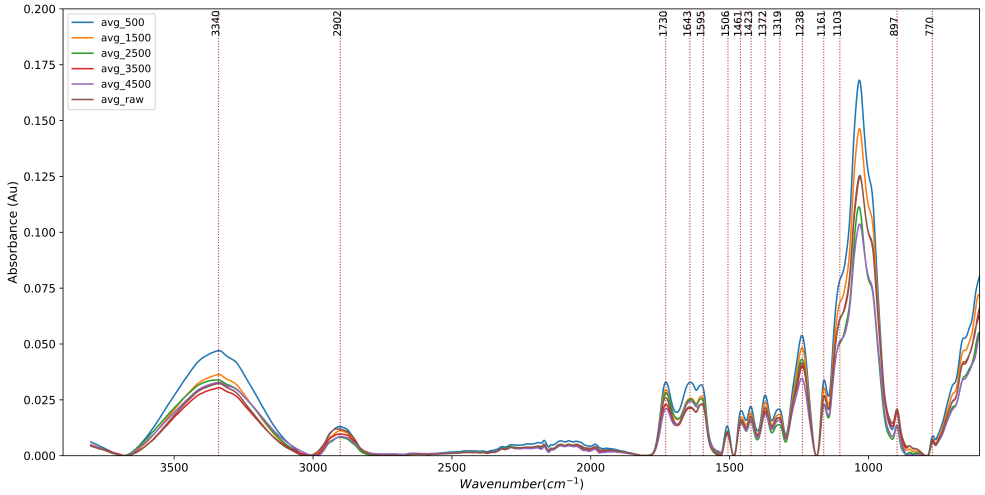

Figure B.8: FTIR analysis of the IR-N wavelength pretreated EFB fibres for pulse durations 0 to 4500 pulses (averaged results)

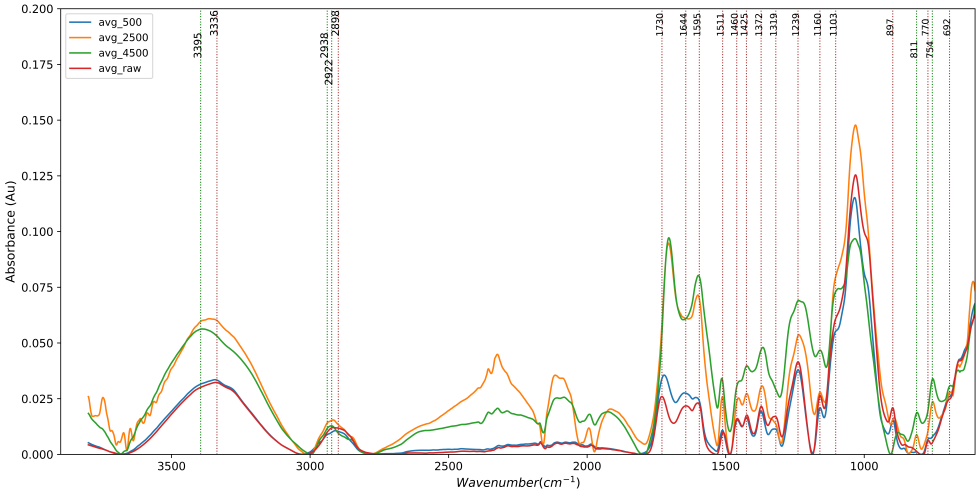

Figure B.9: FTIR analysis of the CSPL-N wavelength pretreated EFB fibres for pulse durations 0 to 4500 pulses (averaged results)

B.2 ADDITION EXPERIMENTAL RESULTS

B.2.1 Analysis results of liquid hydrolysate using HPLC

An HPLC analysis was performed to determine if there was any degradation of hemicellulose and cellulose and the results are given in Table B.5. The galactose peak overlaps with the xylose peak, therefore this concentration could be for either one of these two or a combination of these sugars. Only the HT pretreatment samples measured this peak. Whilst both CSP samples and the HT contained glucose. As a high percentage of the fibres were dissolved in the HT pretreatment, the concentration of sugars is higher. However, there is also a large standard deviation and this is most likely because the samples were old as there were issues with the HPLC and could not be measured while they were fresh. In addition to this, there were other unidentified peaks in the HPLC analysis which indicate that there are other compounds present.

Table B.5: Concentration of sugars in the liquid hydrolysate for the CSP and HT pretreatments

$mg/L.g_{EFB}$	Control-H	CSP-H	HT
Glucose	61.2 ± 4.0	64.8 ± 9.0	116 ± 82
Galactose	0.0	0.0	361 ± 294

B.2.2 Mass analysis results - Dry experimental conditions

The percentage change in mass for the VIS-N and CSPL-N experiments is given in Figure B.10.

B.2.3 Dissolved lignin (CSPL-LIGD) results - Wet experimental conditions

Due to the photochemical effect of UV radiation, it was thought that concentration of dissolved lignin may degrade even further. An experiment was performed, where water was saturated with fibres to dissolve as much lignin as possible into the water. Thereafter, the water as filtered and exposed to solar radiation for a energy input of 5kJ to 20kJ. The results from the experiment are given in Figure B.11.

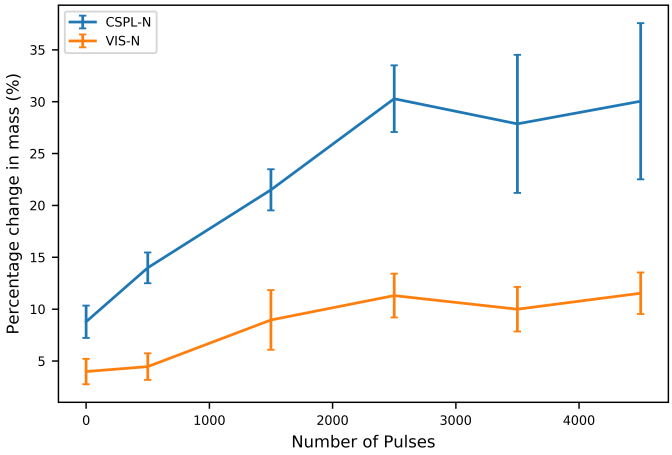

Figure B.10: Percentage change in mass for the VIS-N and CSPL-N experiments

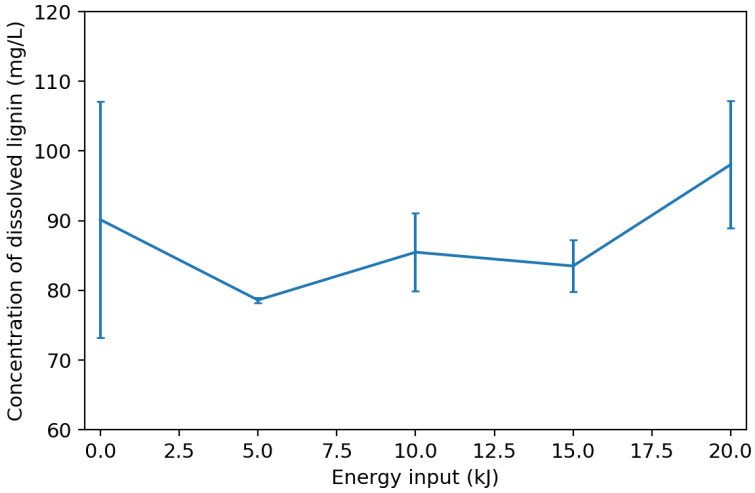

Figure B.11: Concentration of dissolved lignin over an energy input of 5kJ to 20kJ for the CSPL-LIGD

B.3 FUTURE IMPLEMENTATION CALCULATIONS

A rough estimation of the area of land required for the CSP pretreatment was made based on this research. From the CSP pretreatment the following estimations and calculations were made:

- $69kJ$ is required to pretreat 1g of EFB, and this is equivalent to roughly 40min exposure (based on the average solar intensity of Malaysia, $824W/m^2$)
- using the area of the lens, $.0583m^2$, this means that the CSP pretreatment can process $25.7g_{EFB}/m^2 \cdot h$.
- The solar radiation in Malaysia is about 4-6 hours of sunlight (in the rainy season it is 4 hours).
- This means 100 to $150g_{EFB}/m^2$ can be processed a day.
- On average $3.3ton/ha$ of palm oil are produced annually, this results in an annual production of $5ton/ha$ of EFB

- This means that an area of 90 to 140m^2 of CSP is needed per hectare of palm oil plantation.

  Therefore, for a 1000ha plantation, a surface area of 14ha is needed to pretreat the fibres using the CSP pretreatment (based on the rainy season).

COLOPHON

This document was typeset using LaTeX. The document layout was generated using the arsclassica package by Lorenzo Pantieri, which is an adaption of the original classicthesis package from André Miede.